SOLAR ENERGY MANAGEMENT SYSTEM FOR STAND-ALONE APPLICATION: ANALYSIS OF POWER MANAGEMENT STRATEGIES UNDER DIFFERENT SOLAR IRRADIANCE PROFILES

Mr. Chacrit Lerdwithayaprasit

จุฬาลงกรณ์มหาวิทยาลัย
CHULALONGKORN UNIVERSITY

A Thesis Submitted in Partial Fulfillment of the Requirements
for the Degree of Master of Engineering in Chemical Engineering
Department of Chemical Engineering
Faculty of Engineering
Chulalongkorn University
Academic Year 2019
Copyright of Chulalongkorn University

ระบบจัดการพลังงานแสงอาทิตย์สำหรับการใช้งานแบบแยกเดี่ยว: การวิเคราะห์กลยุทธ์การจัดการพลังงานภายใต้รูปแบบของความเข้มแสงที่แตกต่างกัน

นายชาคริต เลิศวิทยาประสิทธิ

วิทยานิพนธ์นี้เป็นส่วนหนึ่งของการศึกษาตามหลักสูตรปริญญาวิศวกรรมศาสตรมหาบัณฑิต
สาขาวิชาวิศวกรรมเคมี ภาควิชาวิศวกรรมเคมี
คณะวิศวกรรมศาสตร์ จุฬาลงกรณ์มหาวิทยาลัย
ปีการศึกษา 2562
ลิขสิทธิ์ของจุฬาลงกรณ์มหาวิทยาลัย

Thesis Title   SOLAR ENERGY MANAGEMENT SYSTEM FOR STAND-ALONE APPLICATION: ANALYSIS OF POWER MANAGEMENT STRATEGIES UNDER DIFFERENT SOLAR IRRADIANCE PROFILES

By   Mr. Chacrit Lerdwithayaprasit

Field of Study   Chemical Engineering

Thesis Advisor   Assistant Professor AMORNCHAI ARPORNWICHANOP, D.Eng.

Accepted by the Faculty of Engineering, Chulalongkorn University in Partial Fulfillment of the Requirement for the Master of Engineering

.... Dean of the Faculty of Engineering
(Professor SUPOT TEACHAVORASINSKUN, D.Eng.)

THESIS COMMITTEE

.... Chairman
(Akawat Sirisuk, Ph.D.)

.... Thesis Advisor
(Assistant Professor AMORNCHAI ARPORNWICHANOP, D.Eng.)

.... Examiner
(Assistant Professor PALANG BUMROONGSAKULSAWAT, Ph.D.)

.... External Examiner
(Assistant Professor Pornchai Bumroongsri, D.Eng.)

จุฬาลงกรณ์มหาวิทยาลัย
CHULALONGKORN UNIVERSITY

ชาคริต เลิศวิทยาประสิทธิ : ระบบจัดการพลังงานแสงอาทิตย์สำหรับการใช้งานแบบแยกเดี่ยว: การวิเคราะห์กลยุทธ์การจัดการพลังงานภายใต้รูปแบบของความเข้มแสงที่แตกต่างกัน. (SOLAR ENERGY MANAGEMENT SYSTEM FOR STAND-ALONE APPLICATION: ANALYSIS OF POWER MANAGEMENT STRATEGIES UNDER DIFFERENT SOLAR IRRADIANCE PROFILES) อ.ที่ปรึกษาหลัก : ผศ. ดร.อมรชัย อาภรณ์วิชานพ

การผลิตพลังงานสะอาดจากแหล่งพลังงานหมุนเวียนได้รับความสนใจอย่างมากเนื่องจากเหตุผลทางด้านสิ่งแวดล้อมและความยั่งยืน เนื่องจากพลังงานหมุนเวียนและความต้องการพลังงานมีความหลากหลายจึงจำเป็นต้องมีระบบพลังงานแบบผสมผสานและการจัดการพลังงานที่เหมาะสม ในการศึกษานี้มุ่งเน้นไปที่การพัฒนาระบบจัดการพลังงาน (EMS) ในระบบพลังงานหมุนเวียนแบบผสมผสานซึ่งประกอบด้วยเซลล์แสงอาทิตย์ (PV), เซลล์เชื้อเพลิงแบบเยื่อเลือกผ่านแลกเปลี่ยนโปรตอน (PEMFC), เซลล์อิเล็กโทรไลซิสแบบเยื่อเลือกผ่านแลกเปลี่ยนโปรตอน (PEMEC) โดยมีแบตเตอรี่แบบมีการไหลของวานาเดียมที่เกิดปฏิกิริยารีดอกซ์ (VRFB) ถูกใช้เป็นแหล่งกักเก็บพลังงานสำหรับการใช้งานระยะยาวถูกรวมเข้ากับระบบพลังงานแบบผสมผสาน แบบจำลองของแต่ละระบบย่อยได้รับการพัฒนาบนพื้นฐานของกฎการอนุรักษ์, ทฤษฎีทางไฟฟ้าเคมีและสมดุลพลังงานซึ่งใช้ในการประเมินประสิทธิภาพของระบบจัดการพลังงานที่พัฒนาขึ้น ในระหว่างกระบวนการทำงานของระบบ พลังงานไฟฟ้าจาก PV จะจ่ายให้กับโหลดและพลังงานส่วนเกินจะถูกใช้เพื่อชาร์จแบตเตอรี่แล้วเรียกใช้ PEMEC สำหรับการผลิตไฮโดรเจน เมื่อเกิดการขาดแคลนพลังงานในระบบ PEMFC จะใช้ไฮโดรเจนที่กักเก็บไว้ หรือจ่ายพลังงานด้วยแบตเตอรี่ให้แก่ระบบ ในส่วนแรกประสิทธิภาพของระบบพลังงานหมุนเวียนแบบผสมผสานที่ใช้แบตเตอรี่วานาเดียมได้รับการตรวจสอบและเปรียบเทียบกับการใช้แบตเตอรี่แบบดั้งเดิมเช่นแบตเตอรี่ตะกั่วกรด ผลการจำลองแสดงให้เห็นว่าภายใต้สถานการณ์พลังงานและความต้องการแบบเดียวกัน ระบบพลังงานแบบผสมผสานที่มี VRFB มีประสิทธิภาพที่สูงกว่าซึ่งทำให้ระยะเวลาการใช้งานแบตเตอรี่ยาวนานขึ้น นอกจากนี้การใช้ VRFB สามารถลดเวลาการทำงานของเซลล์เชื้อเพลิงและเซลล์อิเล็กโทรไลซิสได้ถึง 18.35% และ 14.97% ตามลำดับ จากนั้นผลของการเปลี่ยนแปลงของพลังงานแสงอาทิตย์ตามสภาพอากาศต่อประสิทธิภาพของแต่ละหน่วยในระบบพลังงานแบบผสมผสานถูกวิเคราะห์ในแง่ของปริมาณไฮโดรเจนที่ใช้โดย PEMFC และที่ผลิตโดย PEMEC และปริมาณพลังงานส่วนเกินที่ไม่ถูกใช้งาน (dump load) ในกรณีที่มีการแผ่รังสีแสงอาทิตย์สูงเช่นในฤดูร้อน ระบบพลังงานแบบผสมผสานมีความเสถียรเนื่องจากความสมดุลระหว่างการใช้ไฮโดรเจนและการผลิต รวมถึงพลังงานส่วนเกินที่ไม่ถูกใช้งานต่ำ ในฤดูหนาวและสภาพอากาศแปรปรวนแม้จะมีพลังงานเหลือจากการจัดหาพลังงานให้แก่โหลด แต่ก็ผลิตไฮโดรเจนไม่เพียงพอ การนำไฟฟ้าจากโรงไฟฟ้าหรือการนำเข้าไฮโดรเจนจากแหล่งอื่นจำเป็นสำหรับการทำให้ระบบมีเสถียรภาพในการดำเนินการระยะยาว ในส่วนท้ายกลยุทธ์การจัดการพลังงานสองรูปแบบที่แตกต่างกันที่การปฏิบัติการที่พลังงานขั้นต่ำของ PEMEC ถูกนำเสนอ กลยุทธ์การจัดการพลังงานที่เหมาะสมสำหรับแต่ละสถานการณ์ของความเข้มแสงอาทิตย์ได้ถูกระบุไว้ ในกลยุทธ์การจัดการพลังงานแรกพลังงานส่วนเกินที่ต่ำกว่าพลังงานขั้นต่ำของเซลล์อิเล็กโทรไลซิสจะไม่ถูกนำมาพิจารณา กลยุทธ์นี้เหมาะสมกับฤดูร้อนเนื่องจากปริมาณพลังงานส่วนเกินมาก ในกลยุทธ์ที่สองจะพิจารณาว่ามีพลังงานเพียงพอจากการคายประจุของแบตเตอรี่เพื่อใช้งาน PEMEC ที่จุดพลังงานต่ำสุด ซึ่งพบว่ากลยุทธ์ดังกล่าวเหมาะสมกับสถานการณ์ที่มีพลังงานส่วนเกินต่ำเช่นในฤดูหนาวหรือสภาพอากาศแปรปรวน

จุฬาลงกรณ์มหาวิทยาลัย

CHULALONGKORN UNIVERSITY

สาขาวิชา	วิศวกรรมเคมี	ลายมือชื่อนิสิต ....
ปีการศึกษา	2562	ลายมือชื่อ อ.ที่ปรึกษาหลัก ....

6070160921 : MAJOR CHEMICAL ENGINEERING

Chacrit Lerdwithayaprasit : SOLAR ENERGY MANAGEMENT SYSTEM FOR STAND-ALONE APPLICATION: ANALYSIS OF POWER MANAGEMENT STRATEGIES UNDER DIFFERENT SOLAR IRRADIANCE PROFILES. Advisor: Asst. Prof. AMORNCHAI ARPORNWICHANOP, D.Eng.

Clean power generation from various renewable energy sources has been gaining much attention due to sustainable and environmental reasons. As renewable energy sources and power demand vary, a hybrid power system and proper energy management are required. This study is focused on the development of an energy management system (EMS) in the hybrid renewable energy system consisting of photovoltaic cell (PV), proton exchange membrane fuel cell (PEMFC), and proton exchange membrane electrolysis cell (PEMEC). A vanadium redox flow battery (VRFB) as energy storage for long-term operation is integrated into such a hybrid system. The models of each subsystem are developed based on conservative equations, electrochemistry theory, and power balances used to evaluate the efficiency of the developed EMS. During the system operation, the electric power from PV is supplied to the load, and the excess power is used to charge the battery and then run PEMEC for hydrogen production. When power shortages occur in the system, PEMFC using stored hydrogen or battery is operated. Firstly, the performance of the hybrid energy system using VRFB is investigated and compared with that using a traditional battery (i.e., lead-acid battery). The simulation results show that under the same energy supply and demand situation, the hybrid power system with VRFB outperforms, which leads to a more extended battery operating period. Furthermore, the use of VRFB can decrease the operational time of the fuel cell and electrolysis cell by 18.35% and 14.97%, respectively. Then, the effect of changes in solar energy according to weather conditions on the performance of each unit in the hybrid power system is analyzed in terms of the amount of hydrogen consumed by PEMFC and produced by PEMEC and the amount of dump load power. In the case of high solar irradiance such as in the summer, the hybrid power system is stable due to the balance between hydrogen usage and production, and low dump load power is observed. In the winter and arbitrarily weather, although there is remaining excess power after supplying to the load, it is not sufficient for hydrogen production; taking electricity from the main grid or importing hydrogen from other sources is required to make the system stable for the long-term operation. Finally, the two new energy management strategies of the hybrid power system in which the minimum power of PEMEC operation is differently managed are presented. A suitable energy management strategy for each scenario of the irradiance profiles is identified. In the first strategy, the excess power that is lower than the minimum power for PEMEC operation will distribute to the dump load. This strategy is suitable for the summer scenario due to much excess energy. In the second strategy, it is determined that there is enough power from battery discharging to operate PEMEC at the minimum power point. It is found that this strategy is suitable for the situation with low excess power such as in the winter and arbitrarily weather.

Field of Study:	Chemical Engineering	Student's Signature	....
Academic Year:	2019	Advisor's Signature	....

ACKNOWLEDGEMENTS

Chacrit Lerdwithayaprasit

TABLE OF CONTENTS

Page

LIST OF FIGURES

LIST OF TABLES

Page

NOMENCLATURES

A Cell active area [cm^2]

c'_{O_2} Concentration at the cathode [$\mathrm{mol\,L^{-1}}$]

c_i Concentration of vanadium ions [$\mathrm{mol\,L^{-1}}$]

e_{gap} Energy band gap [eV]

E_{Nernst} Thermodynamic potential [V]

E^o Standard cell potential at equilibrium point [V]

E_{exec} Activation energy for the electrode reaction [$\mathrm{J\,mol^{-1}}$]

E_{pro} Activation energy for proton transport [$\mathrm{J\,mol^{-1}}$]

F Faraday constant [$\mathrm{As\,mol^{-1}}$]

I Current [A]

I_L Light current [A]

I_D Diode current [A]

I_0 Saturation current [A]

I_{mp} Maximum power point current [A]

I_{sc} Short circuit current [A]

I_{mem} Membrane thicknesses [cm]

$j_{0,i}$ Exchange current density [$\mathrm{A\,cm^{-2}}$]

j Current density [$\mathrm{A\,cm^{-2}}$]

k_i Diffusion coefficient [$\mathrm{dm^2\,s^{-1}}$]

p'_{H_2} Partial pressure of hydrogen [atm]

p'_{O_2} Partial pressure of oxygen [atm]

p'_{H_2O} Partial pressure of the vapor [atm]

R_s Series resistance [Ω]

R	Universal gas constant [$\mathrm{J\,mol^{-1}K^{-1}}$]
R_{int}	Internal resistance [Ω]
r_M	Membrane resistivity [$\Omega\mathrm{m}$]
T	Temperature [$^\circ\mathrm{C}$]
T_a	Ambient temperature [$^\circ\mathrm{C}$]
T_c	Cell temperature [$^\circ\mathrm{C}$]
U_L	Overall heat loss coefficient
V	Voltage [V]
V_e	Number of elementary charges

Greek symbols

α	Thermal voltage factor
α_i	Charge transfer coefficients
β	Electrode symmetry factor
ε	Porosity
Φ	Solar irradiance
$\mu_{I,SC}$	Temperature coefficient of the short-circuit current
η	Ideality factor
η_c	Efficiency of the PV cell
$\tau\alpha$	Transmittance-absorption product of PV cell
λ	Function of membrane humidity
σ	Cell conductivity

Subscripts and superscripts

a	Ambient
an	Anode
act	Activation
ca	Cathode
mp	Maximum power point

oc	Open circuit
sc	Short circuit
ohm	Ohmic
con	Concentration

Abbreviations

PV	Photovoltaic cell
PEMFC	Proton exchange membrane fuel cell
PEMEC	Proton exchange membrane electrolysis cell
VRFB	Vanadium redox flow battery
MPPT	Maximum power point tracking

CHAPTER I
INTRODUCTION

1.1 Background and motivation

The smart grid is an intelligent electrical network system for efficient electricity management to control the production, transmission, and distribution of electrical power. There are many challenging technologies involving the smart grid system such as monitoring, analysis, and control [1]. However, the power generation and distribution are complicated systems, and no single entity has complete control of this multi-scale system. The smart grid is also beneficial for the integration of various renewable energy sources. The renewable energy distribution role in the smart grid is very significant. It needs to be combined with an energy management system in order to work efficiently, stably, safely and reliably [2].

Currently, renewable energy usage has grown by 17%, which is above the ten-year average, and the trend is continuously rising [3]. Renewable energy is derived from natural resources such as solar, wind, and water. However, it is generally unpredictable and changes with time and seasons, causing an unbalance of the energy supply and demand. To achieve good energy management, energy storage technology is required. Energy can be normally stored in many forms according to the energy production method such as mechanical, electromagnetic, electrochemical, chemical energy, etc. When considering the operational behavior of energy storage, it can be classified as short-term and long-term energy storage. Battery and supercapacitor act as the short-term energy storage device which can increase the system safety under various constrained conditions, for example, during the start-stop of long-term energy storage with slow dynamic operations. Also, it can supply energy during the lacking energy period but the power supply is unstable and changes with the charge stored in the device[4]. While long-term energy storage will have a slower dynamic but it can provide more stable power. A diesel generator is widely used as long-term energy storage, but this generator requires high maintenance costs and creates environmental pollution. In order to reduce these effects, hydrogen technology is developed to be able to compete with diesel systems due to high performance, lower maintenance, and no

emissions. Both types of energy storage are used together to compensate for the disadvantage of each type of equipment and the energy management system should be systematically designed.

The hybrid renewable energy system is defined as the integration of two or more renewable energy devices. It can be classified according to the system connection, i.e., the stand-alone system [5-7] and grid-connected system [8-11]. The difference between the two topologies was mentioned by Kaundinya and Ravindranath [12]. For the grid-connected system, there will be a power plant as backup energy storage. Thus, ensuring that there is sufficient energy to supply the system. The study of this system will analyze the quality of electricity and the distribution of energy in the energy market. While the stand-alone system will not connect to the grid. The problem with this system is the power supply to meet the load demand. Therefore, unit-sizing should be determined appropriately. In addition, the energy management system used must have good reliability and performance. Consequently, the hybrid renewable energy system for stand-alone applications needs to include a renewable energy system along with a backup energy storage system.

The photovoltaic array (PV) system is a clean energy source powered by solar energy. PV systems directly convert solar energy into electricity. It offers the advantages of long service life with minimal maintenance [13]. In order to enable photovoltaic cells to operate with the highest efficiency, the maximum power point tracking (MPPT) technique is needed to sustain the operating point with maximum performance and power at a particular time [14]. In addition to the renewable energy source, a hydrogen energy storage system using electrolysis cells is used as a long-term application. The generated hydrogen can be used to produce electrical energy through fuel cell technology. Among the various type of electrolysis and fuel cells, the proton exchange membrane (PEMs) fuel cell and electrolysis cell are wisely choices for residential applications due to its low operating temperature and rapid startup time [15].

For short-term energy storage systems, lead-acid batteries and lithium-ion batteries are used in a variety of research relating to renewable energy systems [16-18]. Lead-acid batteries have low energy density and life cycle while lithium-ion batteries have four times the energy density and have twice the lifetime of lead-acid batteries. On the other hand, the charging methods of lithium batteries are more complex, suitable

[19]. It is suitable for the use that requires the quality of the battery, for example, for mobile devices. When considering only the price and capacity, lead-acid batteries are a good alternative for use with energy management systems.

Vanadium redox flow batteries have been studied and developed for decades. It is electrochemical energy storage, which contains an electrolyte flowing through the membrane at the time of operation and returning to the same storage tank. This operating method makes this type of battery system to have a long service life and high efficiency [20]. The energy of vanadium batteries is stored in storage tanks, making it easier to increase the capacity by simply increasing the size of the storage tank. Vanadium batteries have a low operating cost and tend to have lower production costs in the future. Weber and his research team studied the lifespan of vanadium redox flow battery compared with lithium-titanate battery. They concluded that the vanadium redox flow battery has a longer life and can be recycled. In addition, the vanadium redox flow battery is a good choice for stationary battery [21]. Uhrig compared lithium batteries (LiB) with vanadium redox flow batteries for household energy storage. They found that lithium batteries have better performance in energy saving based on the given conditions. However, the vanadium redox flow battery can compete with lithium batteries at high efficiency, and the vanadium redox flow battery has the size flexibility according to the system [22].

In order to efficiently integrate different energy storage types into a renewable energy system with safe operation, it is necessary to have an energy management strategy. The appropriate energy management strategy allows the system to supply enough power to the load, increases the device lifetime, decreases operating costs, and increases the system efficiency both technical and economic aspects. The objective of the power control strategy can be classified into four main topics consists of ensuring the demand, considering by technical decision factor, considering by economic decision factor or both decision factor. The different power management strategies were studied in [23] and decided the best strategy to apply in their work. The impact of seasons on the amount of energy from renewable energy generators was studied to ensure that the energy storage in their system can supply the power to the load with the smooth operation [24, 25]. However, the analysis of seasonal effects includes the use of

different energy management strategies to find a suitable strategy for each season that has not been studied, especially in Thailand.

In this study, the author proposes the use of vanadium redox flow batteries (VRFB) and energy management strategies for hybrid renewable energy management systems that consists of a photovoltaic array (PV), proton exchange membrane fuel cell (PEMFC) and proton exchange membrane electrolysis cell (PEMEC). The simulation of the energy management system is simulated and compared to systems using lead-acid batteries in MATLAB to study the behavior of each device in the system and analyze battery performance. The different control algorithms based on the operating condition of PEMEC with the effect of climate changes affecting the amount of electrical energy produced from a renewable energy source (PV) will be discussed to find the most suitable strategy for each season.

1.2 Research objective

1.2.1 To apply photovoltaic cell, vanadium redox flow battery, proton exchange membrane fuel cell and electrolysis cell to the non-grid-connected application.

1.2.2 To study the effect of solar irradiance profile on a energy management system.

1.2.3. To procure energy management strategies that are appropriate for each situation.

1.3 Scope of research

1.3.1 The simulation of the hybrid renewable energy system is performed in MATLAB which consists of PV, PEMFC, PEMEC, and VRFB. The reference mathematical model on each device is based on this research, including the PV model [26, 27], PEMFC model [28], PEMEC model [29] and vanadium redox flow battery model [30] respectively. For the load demand profile based on Provincial Electricity Authority [31] and solar irradiance profiles are taken from AERONET [32].

1.3.2 Develop and apply two energy management strategies that are managed differently in the minimum power of PEMEC operation with three solar irradiance

profiles (Summer, Winter and Arbitrarily varying weather scenario) to the hybrid renewable energy system.

1.3.3 Analyze simulation results to find suitable strategies for each scenario by using the hydrogen consumption by PEM fuel cell, the production rate of hydrogen in PEM electrolysis cell and the amount of dump load power for decision parameters.

CHAPTER II
THEORIES

2.1 Photovoltaic cell (PV)

A photovoltaic cell or solar cell is an electrical device that converts the light to electricity through the photovoltaic phenomenon. The principle of photovoltaic cells must have 3 basic properties, consisting of the absorption of light to generate electron-hole pairs or excitons, the separation of charge carriers of opposite types and the separate extraction of those carriers to an external circuit. The schematic block diagram of a PV cell is shown in Fig 2.1 [27].
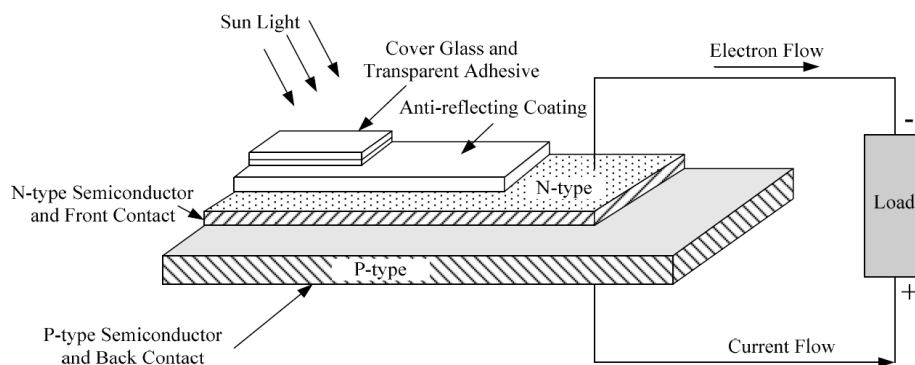
Fig. 2.1 The schematic block diagram of a PV cell [27]

An n-type semiconductor is a silicon sheet that passes through the doping process with phosphorus. Thus, it is able to behave as an electron transmitter when receiving solar energy. The p-type semiconductor is a silicon sheet that passes through the doping process with boron which acts as an electron receptor. The solar energy will transfer light energy to electron and holes. The electrons will move together to the front electrode while holes will move to the back electrode, which makes the system to be fully integrated resulting in electricity generation.

2.2 Proton Exchange Membrane Fuel Cell (PEMFC)

A PEM fuel cell is a hydrogen backup storage system. It can generate electricity using electrochemical reactions according to redox reactions. The substrate of PEMFC consists of hydrogen and oxygen. The hydrogen bond will be broken on the surface of the catalyst at the anode side. The products are protons and electrons based on oxidation reactions. In a fuel cell that uses Nafion as a membrane, only the positive ion can pass. Therefore, the proton can only move through to the cathode. The electrons move away from the electrochemical cell to the cathode through the electrical load. The electrochemical reactions of PEM fuel cells are shown in the equations below (Eqs. (2.1-2.3)) and the corresponding reaction diagram is shown in Fig. 2.2.

Anode: $$H_2 \rightarrow 2H^+ + 2e^- \tag{2.1}$$

Cathode: $$\frac{1}{2}O_2 + 2H^+ + 2e^- \rightarrow H_2O \tag{2.2}$$

Overall: $$H_2 + \frac{1}{2}O_2 \rightarrow H_2O + Heat \tag{2.3}$$
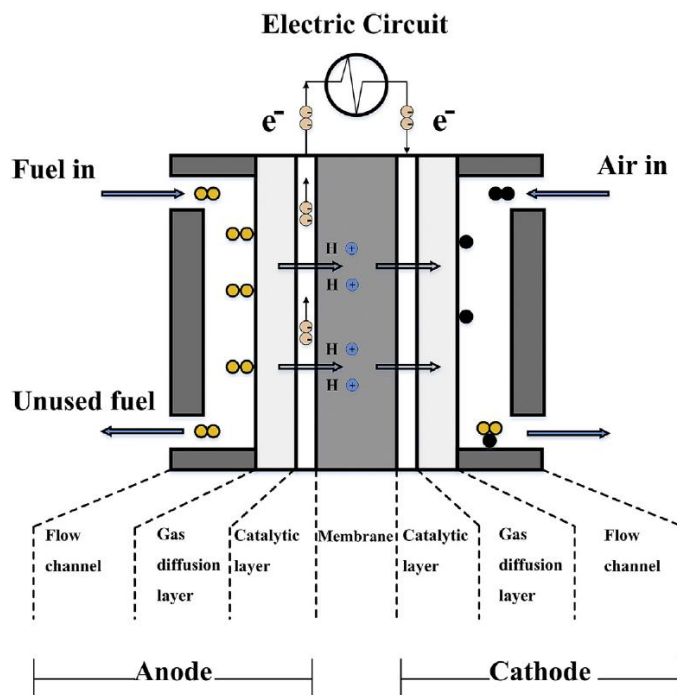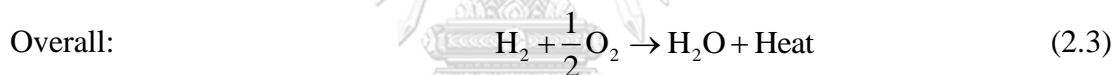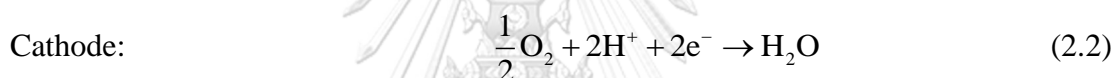
Fig. 2.2 The proton exchange membrane fuel cell diagram [33]

2.3 Proton Exchange Membrane Electrolysis Cell (PEMEC)

PEM electrolysis cell is the reverse process of PEM fuel cell which is the separation of hydrogen and oxygen from water using electricity. The major advantage of the PEM electrolysis cell is its ability flexible to operate at high current densities. The PEMEC diagram is shown in   Fig. 2.3 and the cell reactions are given in (Eqs. (2.4-2.6)).
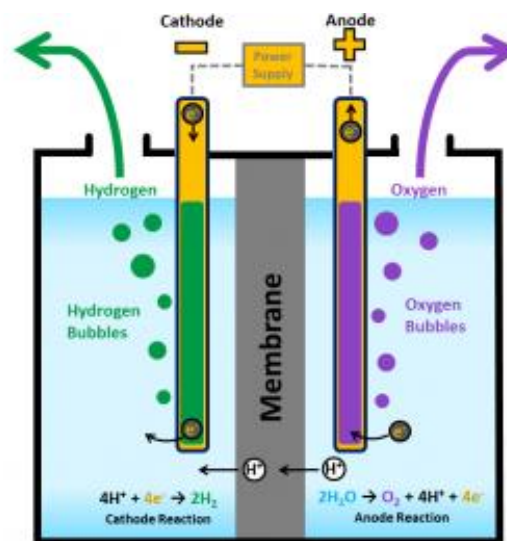
Fig. 2.3 The proton exchange membrane electrolysis cell diagram [34]

At the anode: $\qquad$ $2H_2O \rightarrow O_2 + 4H^+ + 4e^-$ $\qquad$ (2.4)

At the cathode: $\qquad$ $2H^+ + 2e^- \rightarrow H_2$ $\qquad$ (2.5)

Overall: $\qquad$ $2H_2O \rightarrow 2H_2 + O_2$ $\qquad$ (2.6)
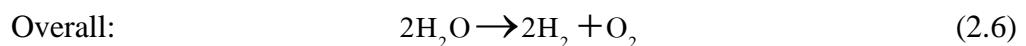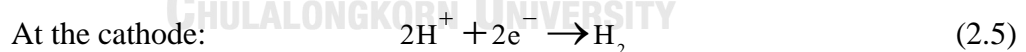
At the anode, the water fed into the cell. The oxidation reaction then occurs which produces oxygen, protons, and electrons. Identically to the PEMFC, the proton transfers through the membrane while electrons move away from the cell. Eventually, the protons and electrons will be combined to produce the hydrogen.

2.4 Vanadium Redox Flow Battery (VRFB)

The vanadium redox flow battery (VRFB) stores energy by using an electrolyte solution which is a vanadium solution in dilute sulfuric acid. The anode contains a vanadium solution with oxidation number +2 and +3, while the cathode has vanadium oxidation number +4 and +5. The electrochemical reactions of the vanadium redox flow battery are shown in the following equations:

At the positive side:

$$VO^{2+} + H_2O \underset{discharge}{\overset{charge}{\rightleftharpoons}} VO_2^+ + 2H^+ + e^- \tag{2.7}$$

At the negative side:

$$V^{3+} + e^- \underset{discharge}{\overset{charge}{\rightleftharpoons}} V^{2+} \tag{2.8}$$
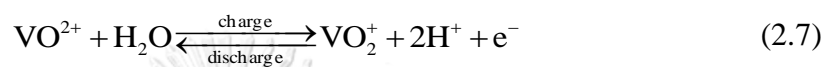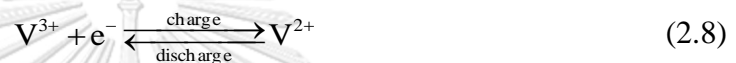
In the charging process, the VO^{2+} ions in the positive half-cell are converted to VO_2^+ ions. The electrons are removed from the positive terminal of the battery. In the same way on the negative side, electrons are converting the V^{3+} ions into V^{2+}. In contrast, the discharging is the reversed process of charging. The schematic of the vanadium redox flow battery is shown in Fig 2.4.
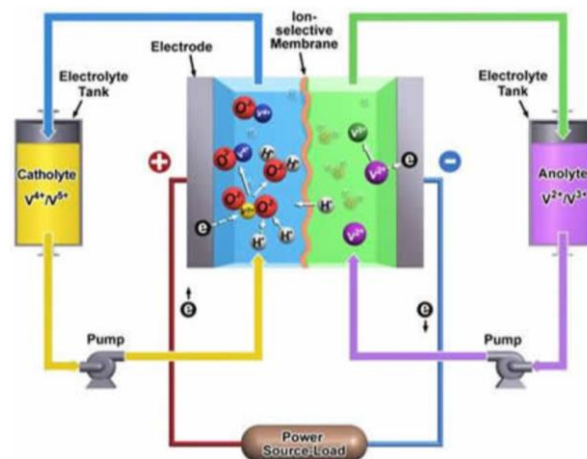
Fig. 2.4 Schematic of a vanadium redox flow battery [35]

In the real operating process, the diffusion of vanadium ions through the membrane cannot be avoided because the diffusion always occurs when the concentrations of vanadium ions are different between the positive and negative half-

cells. This causes self-discharge reactions in each half-cell which degrades the battery efficiency and loses its capacity due to an imbalance of vanadium ions in the two half-cells. In Tang and Bao 's research, they reported the self-discharge reactions following as [30]:

At the positive half-cell:

$$V^{2+} + 2VO_2^+ + 2H^+ \rightarrow 3VO^{2+} + H_2O \tag{2.9}$$

$$V^{3+} + VO_2^+ \rightarrow 2VO^{2+} \tag{2.10}$$

At the negative half-cell:

$$VO^{2+} + V^{2+} + 2H^+ \rightarrow 2V^{3+} + H_2O \tag{2.11}$$

$$VO_2^+ + 2V^{2+} + 4H^+ \rightarrow 3V^{3+} + 2H_2O \tag{2.12}$$
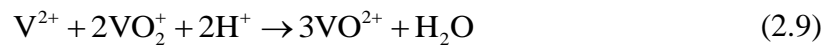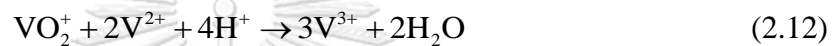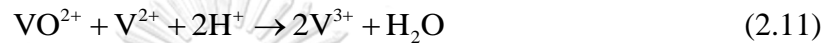
2.5 Energy management system (EMS)

The energy management system is a system that can be monitored and managed the energy consumption to be extremely useful and deal with unnecessary energy to increase efficiency and reduce resource usage. This system consists of various devices that work together, including sensor smart meter and an automatic electrical controller. In this work, we will focus on the energy management of a renewable energy system. The renewable energy systems can be classified in many ways such as topology, integration method and the integrated elements which are described as follows.

2.5.1 The classification by the topology

In this classification, it can be divided into a grid-connected and a stand-alone application. For the on-grid system, the system is connected to the grid. The renewable energy sources in the microgrid can supply to the local loads and feed into the power grid when the power is excess. The power grid will be used as the backup system to ensure that the system can handle the customer load demand. The example of this topology is presented in Fig. 2.5.
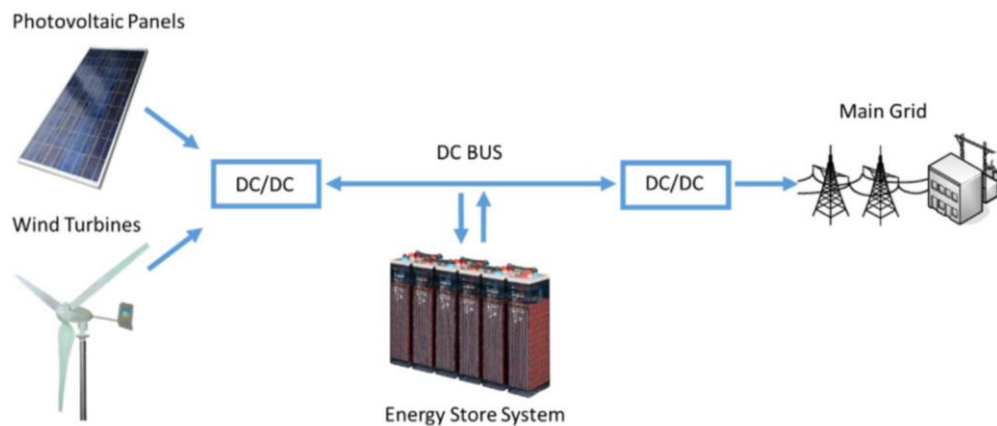
Fig. 2.5 The example of an on-grid configuration [36]

There are two main advantages of grid-tied systems. First, the on-grid system will allow saving the money with renewable energy sources such as solar panels which have good efficiency rates and lower equipment and installation cost. Secondly, the electricity from the power grid can act as the virtual battery in the backup system without the need for maintenance or displacement. Especially, there are no significant losses from the operating of energy storage such as ohmic loss, activation loss, and concentration loss, etc.

Another proposed topology is an isolated system. When there is no connection to the grid, this system can be considered as a complete green power system because the electrical energy is produced from renewable energy sources and energy storage in the system. The isolated system is demonstrated in Fig. 2.6.
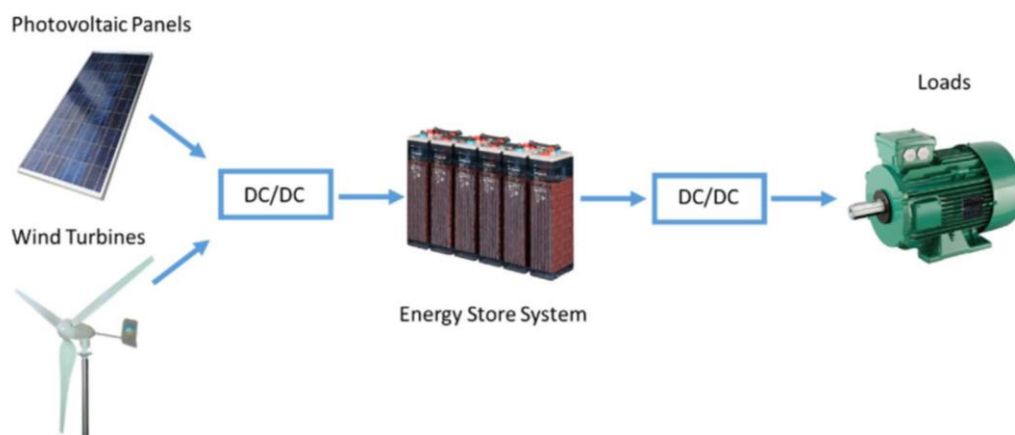
Fig. 2.6 An example of an isolated system configuration [36]

Because it is an off-grid system, there is no power to support when there is a lack of electricity. System reliability and performance are the main problems of this topology. The complete stand-alone system can harm the security of the energy system due to the limited renewable sources available. For these reasons, the sizing of renewable energy devices in the system is important.

2.5.2 The classification by integration method

This classification distinguishes the system depending on the type of internal interconnection bus which is a physical link between all the energy devices. It can be divided into DC, AC and hybrid bus which described below.

DC bus

The DC buses are commonly used in small applications because of the many technical advantages that support its use. We can focus on reducing losses and simplicity of use and avoiding technical power quality problems [37]. This network connection requires a lot of converters because most of the current electrical loads must be supplied with AC. An example of topology based on the DC bus is presented in Fig. 2.7.
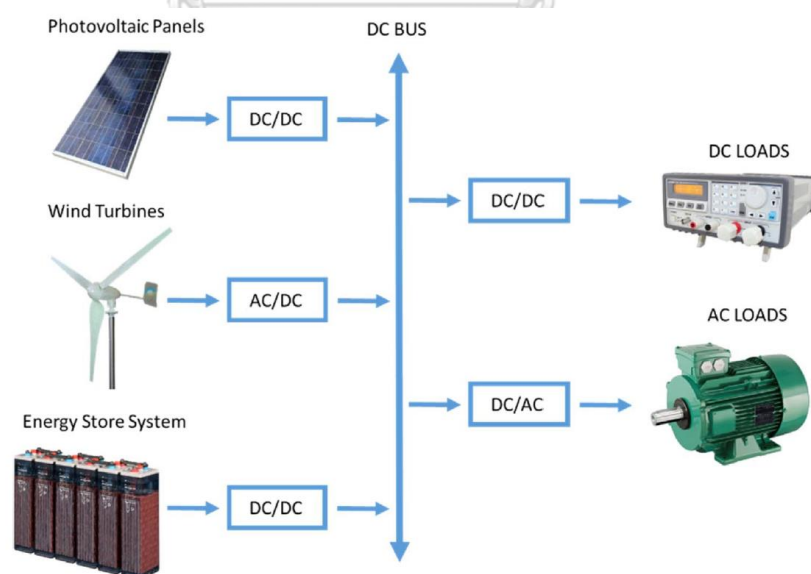
Fig. 2.7 Example of DC bus [35]

AC bus

For the AC bus, it is widely used in medium and large applications due to the higher operating voltages than the voltages of the DC bus. The main disadvantage of this bus is power quality correction. It needs to find electronic loads that can reduce the power factor which can damage the generators. Thus, it needs to use the filtering and compensation for electronic devices that increase the complexity of the system. An example of topology based on the AC bus is presented in Fig. 2.8.
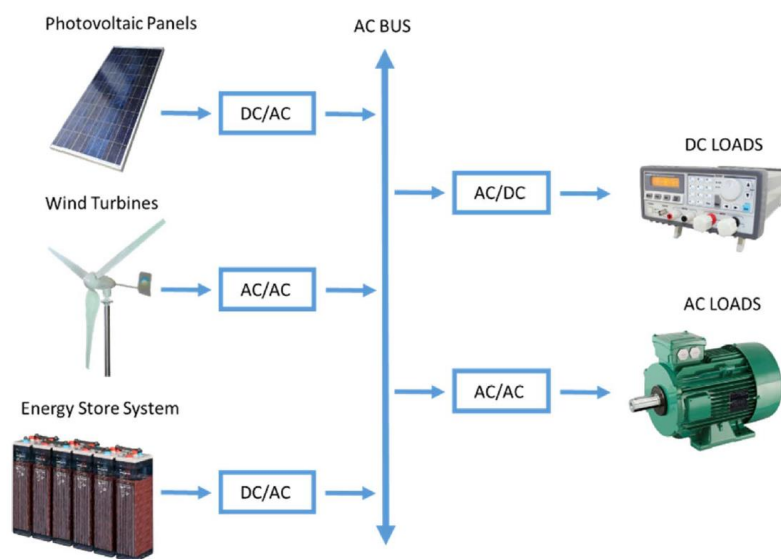
Fig. 2.8 Example of AC bus [35]

Hybrid bus

In the hybrid buses, each type of bus will match with the same nature of the load, thus it can reduce the disadvantages of the previous two bus patterns. In the same way, they must be a more complex control algorithm which works on the different network and ensures the balance of power at all times. An example of topology based on a hybrid bus is presented in Fig. 2.9.
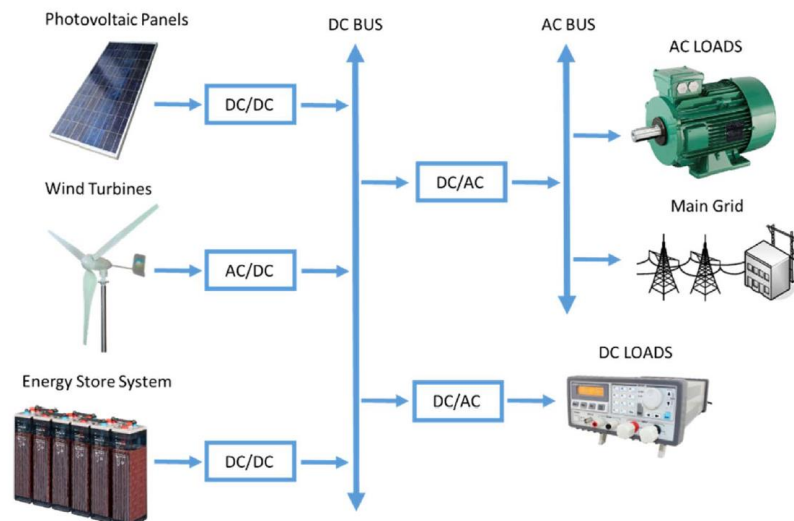
Fig. 2.9 Example of a hybrid bus [35]

2.5.3 The classification by integration elements

The main components in the renewable energy system can be divided into 3 parts which are power generation unit, energy storage unit and energy demand.

Generation unit

The common renewable energy sources such as PV array, wind turbines or hydro turbines. PV arrays can guarantee power during the light which can be predicted [38, 39]. Wind turbines are unstable of energy sources because the behavior of the wind is unpredictable and random, therefore the use of remaining components in the system is necessary to ensure the energy balance. However, the wind flows through the day and becomes more intense at night. Hence, it is important to choose the appropriate location and environment for the operation [40, 41]. According to the above mention, the use of wind turbines as the only energy source is a minority. In most cases, the hybridization of PV arrays and wind turbines is considered an acceptable solution [42, 43].

Energy storage system unit

For medium- and long-term energy storage, the hydrogen storage system is used to supply the demand when the power of short-term energy storage is not enough. The main elements of this type are fuel cell and electrolysis cell. Other non-renewable

storage systems are also used as the last choice. The diesel generators are commonly used which releases environmental pollution [9, 44, 45].

Battery and supercapacitors are often used in short-term energy storage by helping to stabilize the voltage in the system during transients' phase on the generation or load changes. They are conceived as the main component of the system, which determines the operation of the other component in the systems [46-48].

Energy demand

The energy demand will depend on the application in each location. The isolated telecommunication stations, residential uses or office uses are examples of different applications, which have different peak usage periods.

2.6 Energy management control strategy

A good energy management system should have a good control system, a control algorithm to manage the energy. It is necessary for ensuring a safe operating system and facing all limiting conditions. When considering many types of research relating to the power management strategy, it can be summarized into four main topics.

The strategy which ensures the consumer demand

The major objective of this type is to satisfy the power demand, this control algorithm base on power balance, state of charge (SOC) of battery and amount of hydrogen depending on the renewable energy elements which use in the system. A summary scheme of the main characteristic of this strategy is presented in Fig. 2.10.
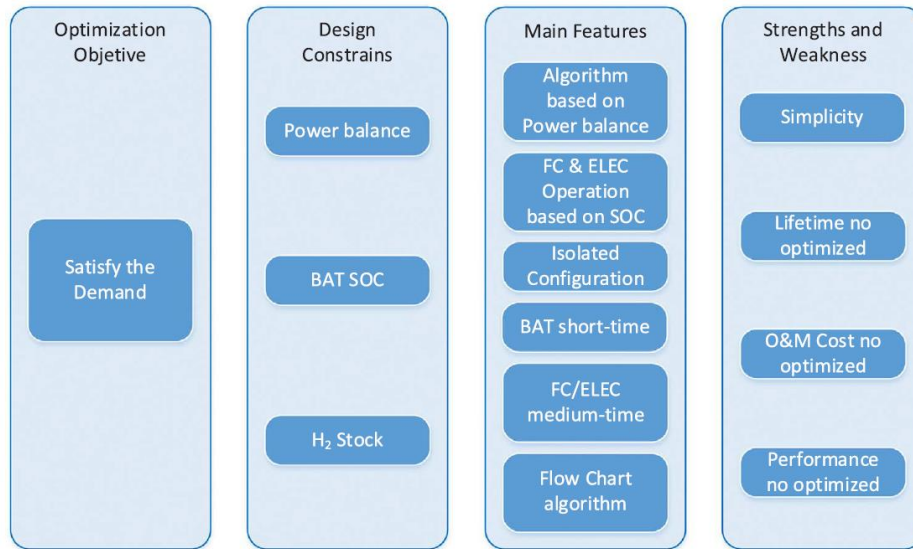
Fig. 2.10 Main characteristics of ensuring-demand strategy [36]

The strategy which considers technical decision factor

These strategies take into account technical criteria to reduce the degradation of the energy device and increase the system's lifetime. The main advantages of this strategy are medium complexity design and control system, and the system performance or other optimization objectives will be considered as the results. A summary scheme of the main characteristic of this strategy is presented in Fig. 2.11.
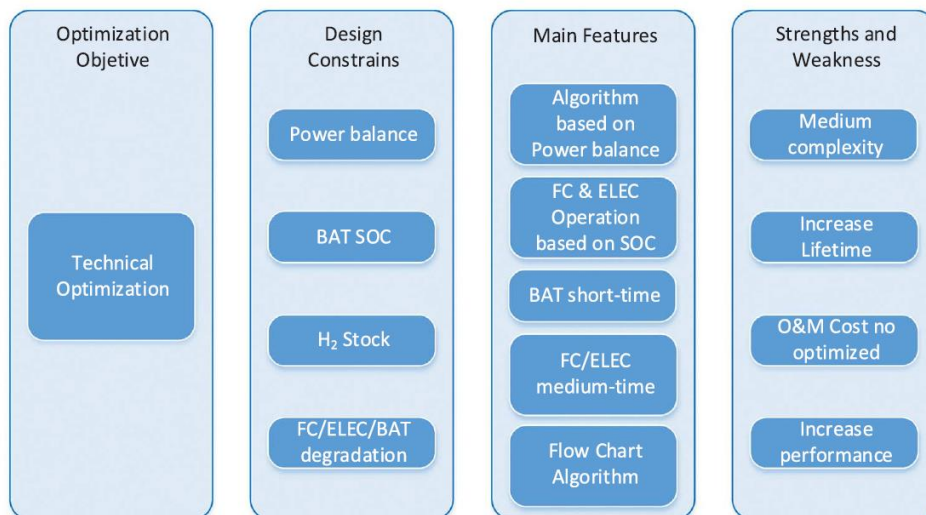
Fig. 2.11 Main characteristics of the strategy with technical decision factors [36]

The strategy which considers economic decision factor

In addition to the basic principle, this strategy considers an economic analysis of the systems such as operating and maintenance costs and sizing of the application. These decision factors help to determine an optimal solution but it does not determine a favorable operation for energy devices because there are no technical criteria to avoid the problems relating to the different operating conditions. A summary scheme of the main characteristic of this strategy is presented in Fig. 2.12.
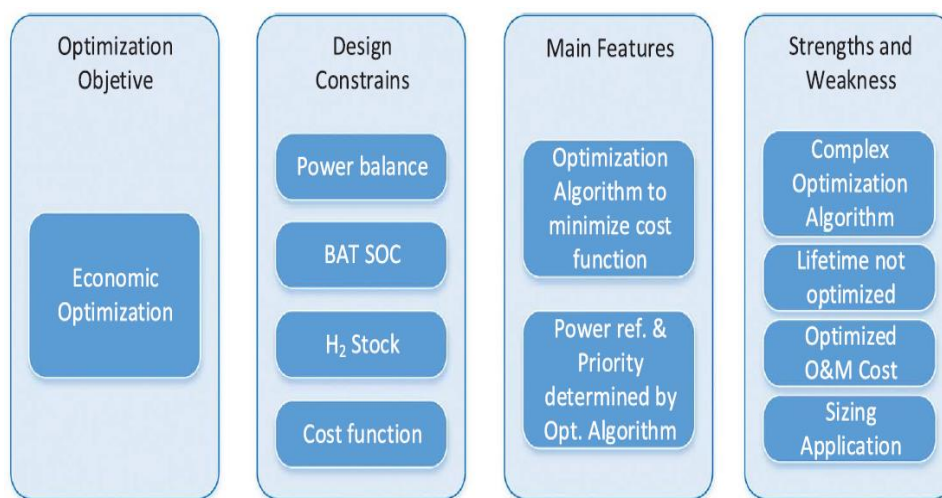
Fig. 2.12 Main characteristics of the strategy with economic decision factor [36].

The strategy which considers both technical and economic decision factor

In the last topic, the technical and economic criteria are integrated to increase equipment lifetime and reduce the operating and maintenance cost. This strategy has an optimal solution, a technical and economic decision factor. The advantage of this strategy covers every aspect and closes to the real application. In order to obtain this realism, the complexity of the optimization algorithm increases too. A summary scheme of the main characteristic of this strategy is presented in Fig. 2.13.
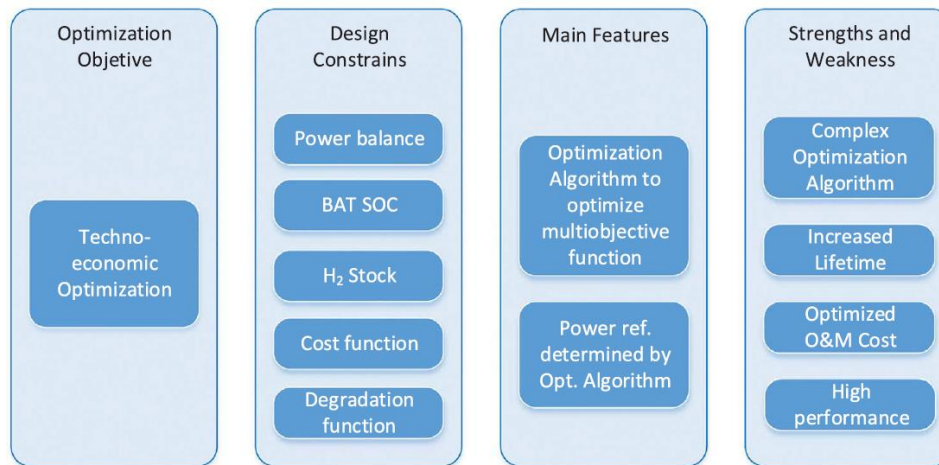
Fig. 2.13 Main characteristics of the strategy with both technical and economic decision factors [36].

CHAPTER III
LITERATURE REVIEWS

3.1 Component model

3.1.1 Photovoltaic cell

The mathematical model based on the equivalent circuit is widely used to simulate photovoltaic cells because it is available for simulation in many types of electrical software. The basic structure of photovoltaic cells is made up of two semiconductor plates with different doping acting as p-n junction diode. It can be divided into two types, consisting of a single diode model and two diode models. The characteristics of simple p-n junction diode were governed by Shockley diode equation [49]. Kumari and Babu [50] reported the simulation of photovoltaic cells using the ideal single diode model. It can be described with three parameters, namely the light current, saturation current, and ideality factor but this model is only used to explain the basic concept of photovoltaic cell modeling. The model that takes into account the loss from the resistance between semiconductor and electrodes surfaces or series resistance have been proposed in a variety of researches. This resistance is determined by the value of the reciprocal of the derivative of the circuit model at open-circuit voltage condition in Walker's research [51], while Weidong et al. [52] and Ulapane et al. [53] derived by rearranging the equation and using the voltage and current value at maximum power. Bellini et al. [54] proposed the photovoltaic model derived from Weidong et al. [52] which did not require a numerical method to calculate the output. In a situation of temperature variation, the accuracy of the series resistance model decreases due to the temperature coefficient is calculated. The accuracy of the model is improved by integrating shunt resistance resulting in reduced temperature sensitivity. The five parameters model which combining both types of resistors is the most popular. Hadji et al. [55] proposed the estimation of shunt resistance by the reciprocal of the slope at short circuit current and De blas et al. [56] recalculates the shunt resistance every time from the difference between the two resistors at the previous value. Lineykin et al [57]. using Kirchoff's laws and Lambert-W function to explain the relationship between the output current and voltage. The assumption of single diode models neglected the effect

of recombination in the depletion layer between two different semiconductors which causes current loss. The two-diode model is a more precise solution. Two new parameters in the equation are saturation current and ideal factor for the second diode. This photovoltaic model is still an attractive option due to its high accuracy in low radiation conditions. However, the model used in the aforementioned research will predict the output current and voltage by using the reference value at standard condition (1000 W/m², 298 K) but Zhang et al. [58] proposed a solution to the problem in the absence of references data at standard conditions. They referring to the reference values from the measured conditions, which it actually works.

3.1.2 Proton exchange membrane fuel cell

The types of models fall into three categories consist of analytical, semi-empirical, and theoretical. Analytical models are estimates and limited to predicting voltage losses for simple designs. Mass, Momentum, and energy conservation are described in mathematics. The examples of analytical modeling are reported by Standaert et al. [59, 60]. The isothermal and non-isothermal models were developed by using the first-order boundary value problems (1st-BVP) to estimate the current density. This method makes a quick calculation for a simple system. The semi-empirical model combines theoretical and algebraic equation with empirically to determine the relationships. The empirical model is performed when the physical phenomena are complex to the calculation or still do not understand all that. Springer et al. [] developed a semi-empirical model for a partially hydrated membrane that is related to membrane conductivity, electrode porosity and water content in Nafion membrane. Amphlett et al. [61] developed the activation overpotential and ohmic overpotential estimation to predict the characteristic of the cell. These parameters were correlated with temperature, partial pressure and current density. The semi-empirical model of concentration overpotential was developed by Maggio et al. [62]. However, the semi-empirical models have limitations according to the narrow operating condition range. It only correlates output with input, so it cannot be used to predict the performance of a new innovative design. Mechanistic modeling or theoretical modeling the dynamic and cell voltage equation are derived from physics and electrical chemistry the control of the phenomenon within cells. Gurau et al. [63] developed a two-dimensional to

determine concentration of each species and the effect of gas diffuser porosity on fuel cell performance. The three domains that are considered consist of gas diffusers, gas flow channels, catalyst layers, and membrane. The gas diffusers and gas flow were combined into one domain by writing the governing equations for each region in a similar form. The result was able to accommodate both regions into one domain.

3.1.3 Proton exchange membrane electrolysis cell

The cell voltage modeling of the electrolysis cell of each author has a similar starting point. It is caused by the sum of the four-term voltage. The first term is the open-circuit voltage. It can be explained in two forms according to the Nernst equation and Gibb's Free Energy. These methods are theoretically identical. However, different methods exist in the literature review in determining the temperature dependent value of open-circuit voltage. The using the Nernst equation-based models have a difference in finding reversible cell potential term. Awasthi et al. [64] and Biaku et al. [29] use this potential value from the proportion between the product of the change in entropy and the temperature and Faraday constant which is multiplied by two because there are two moles of electrons. Dale et al. [65] define the temperature dependent term as enthalpic voltage causing different forms of the equation which correspond to Garcia-Valverde et al. [66]. Marangio et al. [67] use the application of Gibb's Free Energy-based model and applied the non-standard temperature and pressure term. It is evaluated at both sides of the electrolysis cell, so the specific temperature dependent term of both species is calculated. The advantage of this method is its reliance on acceptable empirical data for enthalpy and entropy as opposed to using only the fitting parameter. However, this method is complicated to calculate because there is the use of large thermodynamic lookup tables. The using the Nernst equation-based model is more computational efficiency and the temperature dependent model was developed to reduce the errors that can replace the Gibb's Free Energy approach.

The second term is the activation overpotential term. The Butler-Volmer expression is widely used to predict this value. The important parameters in this equation are the charge transfer coefficient and the exchange current density. In most cases, the charge transfer coefficient of both sides is set to be equal to 0.5 according to assumption. The effect of the temperature dependence of the charge transfer coefficient

was reported by Biaku et al [29]. They indicated the charge transfer coefficient and another parameter at varying temperatures. A good estimation is important in predicting the precise of the characteristics of electrolysis cells. The exchange current density is determined by many physical parameters based on the catalyst which are difficult to quantify. This is an important problem as the polarization curves are heavily sensitive to the exchange current density. There are values of exchange current density which are different in each research [68]. Due to the variable exchange current density is a wide range, most researchers select values that are fit to the experimental data. Garcia-Valverde et al. [66] apply an Arrhenius expression to the temperature dependence of the exchange current density model which increases the effective range of a model.

The ohmic overpotential is mainly caused by membrane resistance. The proton conductivity through the membrane is the main parameter for determining the resistance. Many approaches exist to modeling, most of these models have been developed for the fuel cell modeling which consists of conductivity term that takes into account the water content and temperature dependent term. The value of the water content is disputed because of the possibility of Schroeder's paradox which reported in Bass et al. [69] and Onishi et al. [70]. Choi et al. [71] developed a membrane conductivity model based on Grotthuss diffusion which relied only on the physical parameter of the membrane. The water content is a major issue on fuel cells but in the electrolysis cell, it can be neglected because the membrane can be considered fully hydrated [66]. For concentration overpotential, this term can be described by Fick's law but it occurs when the current density high enough to hinder the reaction by the number of molecules that react too much. It can be avoided by operating below the limit of current density [65].

3.1.4 Vanadium redox flow battery

The mathematical model of vanadium redox flow battery can be divided into 2 types which are a multi-dimensional model and a zero-dimensional model. You et al. [72] developed a two-dimensional stationary model based on universal conservation law. The effect of current density, electrode porosity, and mass transfer coefficient was studied through the single cell. They reported that a decreasing porosity will lead to a rapid decline in the concentration of the precursor with a higher average value of the

transfer current density and overpotential. Al-Fetlawi et al. [73] studied the non-isothermal with a two-dimensional model and combined it with a kinetic model. The variation electrolyte flow rate and heat loss to the environment is simulated at different conditions to observe the charge/discharge characteristics. The rise of temperature decreases the deviation of cell voltage from the equilibrium value. Ma et al. [74] developed a three-dimensional model for negative half-cell with isothermal. The simulation result is shown that the distribution of electrolyte velocity in the electrode has significant on the concentration, overpotential and transfer current density.

The complexity of the multi-dimensional model leads to reduced computational efficiency and increased time spent. To study factors other than those mentioned above, for example, capacity, life cycle, etc., zero-dimensional models were developed which in which each model has different parameters depending on the assumption of the authors. Tang et al. [30] proposed the dynamic model that is considered the effect of ion diffusion and side reaction which causes the self-discharge phenomenon and capacity loss. Three different types of membranes are used to study the effects of imbalances and reduced capacity of the battery. The efficiency of the capacity depends on the diffusion property of the membrane which a high rate of diffusion will increase the capacity performance after 200 cycles. Bhattacharjee and Saha [75] proposed the self-discharge voltage model by a controlled current source and a shunt resistance. This resistance is a variable parameter which varies with the concentration of each species. The proposed model is applied for investigating the system performance with a dynamic optimal flow rate. They show the proper flow rate for each SOC range which helps maximize overall efficiency.

3.2 The operation of the equipment

To increase the system performance, designing suitable control methods and reduce degradation during the normal operation, it is necessary to consider the proper operating condition of the subsystem.

3.2.1 Photovoltaic operation

In solar power sources, the maximum power point tracking (MPPT) is allowed to improve performance and production at a particular time. Husain et al. [76] reviewed

the methods for maximum power based on different parameters. Faisal et al. [77] using fractional short circuit current method to determine the maximum power from the linear relationship between the maximum current and the open-circuit current. The maximum current can be determined from the fixed percentage of short circuit current which is a constant of proportionality and is called the current factor. Another major technique is voltage-based maximum power point. This technique is used in Ahmed's research [78]. It is based on a similar idea to the fractional short circuit current method. Measuring the open-circuit voltage of the solar panel will help to find the operation point at a constant of proportionality of open-circuit voltage. The Perturb-and-Observe (P&O) is the most commonly used in this research area. The working voltage is perturbed by a power converter which will change the value of power to find a maximum point. The range of voltage perturbation is very important. The large range gives fast-tracking but it makes a large fluctuation nearly the peak. On the other hand, a small range will make slow tracking but make a few noises in the control scheme. Ahmed and Salam [79] improve the efficiency of this algorithm by reducing the steady-state oscillation and develop the algorithm to eliminate the wrong tracking direction. The proposed algorithm can increase the tracking performance by 2%. When considering the accuracy and speed of prediction, the first two techniques have a low accuracy due to the use of a single constant parameter for estimation in all situations and the speed is at a medium level. While the P&O algorithm has higher accuracy and speed depending on the rang of voltage interference. If taking the operation cost into consideration, the computational or lookup table method is most suitable. It is formulated based on the experimental data or predefined equation to find the maximum power point. Scarpa et al. [80] applied this method and compare with fractional open circuit voltage method. The simulation results were shown the higher tracking efficiency and suitable for low-cost PV system. However, it is not true maximum power point but the tacking is near to the exact maximum power.

3.2.2 Fuel cell and electrolysis cell operation

The degradation in the start-stop cycles of the equipment is an important issue for both systems. Lin et. al. [81] are studied the effect of start-up and shut-down cycle on the performance of proton exchange membrane fuel cells (PEMFC). The reverse

current between cathode and anode causes a potential voltage and the oxidation of carbon in the plates, decreasing active surface area, which results in increasing of ohmic loss as shown in Fig.3.1. The decreasing of the electrochemical area leads to the increase charge transfer coefficient of the oxygen reduction reaction.
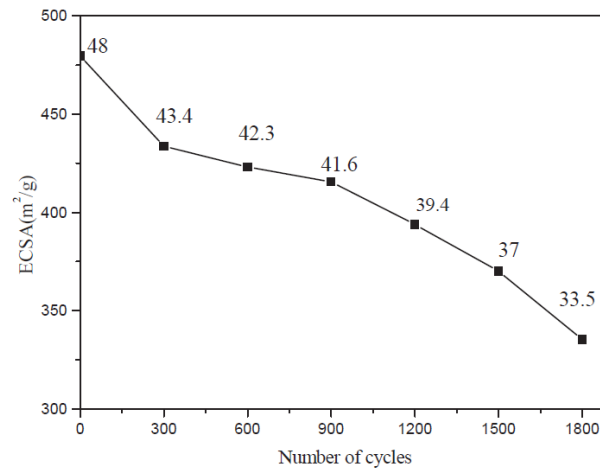
Fig. 3.1 Electrochemical surface area of cathode after start-up and shut-down cycles [81]

Haruni et al. [82] studied the operation of a standalone hybrid renewable power system. Fuel cells are defined to perform in the ohmic region, which has linear behavior in the polarization curve. The operation range is consistent with Bizon et al. [83]. The maximum efficient point (MEP) has been chosen as an operation point as Fig.3.2, which is in the ohmic region.
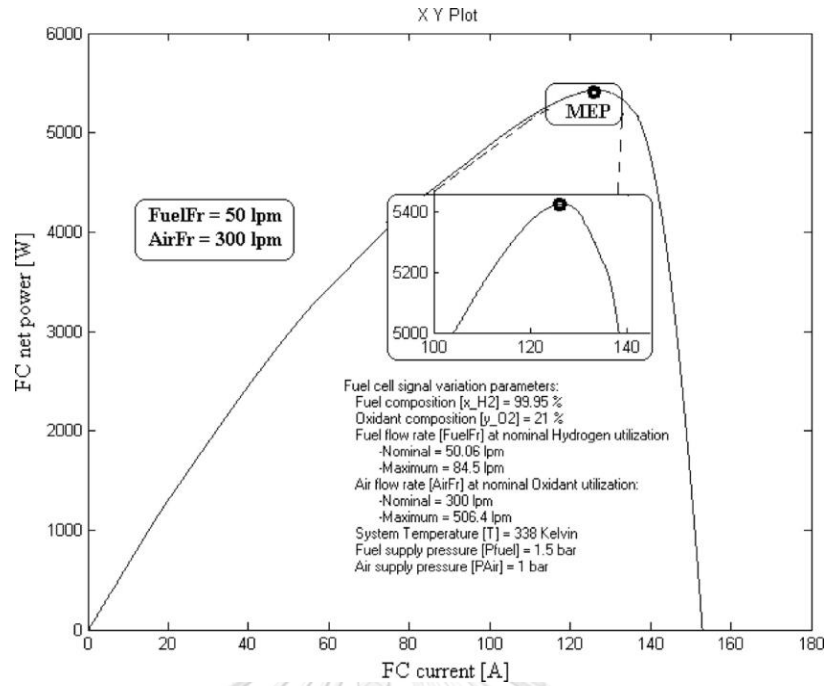
Fig. 3.2 The fuel cell net power characteristic [83].

For electrolysis cells, the low power operation can cause pressures drop between the anode and cathode resulting in a low purity product due to the crossover flow from one electrode to another [84]. While the operating at high power, hydrogen and oxygen gas bubbles evolve at the anode and cathode respectively, thus the bubble resistance increases and reduce the system performance. Zeng and Zhang [85] illustrated all species of energy losses as Fig. 3.3.
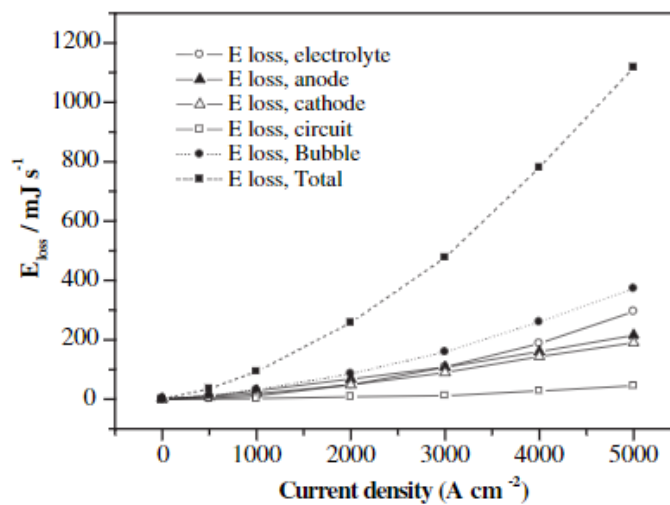
Fig. 3.3A comparison of all species of energy losses [85].

The operating range should be between the two-point mentioned earlier. For use in the energy management system, Ulleberg [86] reported the different operation of the electrolysis cell by comparing the constant and variable power modes. The simulation results were shown the benefit of variable power mode rather than the fixed mode. The operation in variable power mode is less operation time and frequency of switch on/off time than fixed power mode.

3.2.3 Battery operation

For lead-acid battery, the battery degradation on the use of high discharge depths. In Rodolfo et. Al. research [87], they compare the different lead-acid battery lifetime prediction models and study some parameters that affect the battery lifetime. The state of charge that disable supplying energy to the load and the state of charge to reconnect to the load is determined at different conditions to predict the service life of the device. The simulation results show that the determination of the minimum state of charge increase, the battery lifetime also increase too. These results are consistent with Crossland et. al. research [88]. The maximum capacity has fallen to 80% of nominal capacity is an optimum condition. The charging process is another important process as well. The fast charging method requires high voltages and high current. It causes inefficient charging processes, which may cause overcharging if not controlled. However, a slow charging process is a safer and more efficient charge but takes a long time. In addition, other factor needs to be considered, for example, the charge imbalance, etc [89].

For the vanadium redox flow battery, Jirabovornwisut [90] studied the effect of the operating condition on battery performance. In the study of the effect of current density on battery voltage, the charging and discharging take less time at high current but the SOC range at the upper and lower limit is also narrow. Likewise, the total overpotential increases when the current is increased and the ohmic overpotential has the highest change. The optimal condition for battery capacity and power design is 120 mA/cm^{-2}. The effect of vanadium concentration at different initial concentrations was investigated according to the concentration range 1.4-2.0 M. The simulation results were shown the higher initial concentration has a long charging and discharging time due to the increased battery capacity. The SOC upper- and lower-limitation were

expanded. For the long-term operation, the high vanadium concentrations still had greater capacities than lower concentrations throughout 200 cycles.

3.3 Energy management strategies

Ahmed [78] has proposed a grid-connected energy management system to ensure demand with the goal of focusing on the algorithm design to control the power converter to connect various components in the system and determine the appropriate operating point for each device. The main sources of energy are wind and solar. If the production of energy exceeds the demand, it will sell energy to the grid. If there is a shortage of energy, the fuel cell will provide energy to the system. If not enough, electricity will be used from the grid. Xiafeng et al. [91] studied isolated micro-grid systems which are low-voltage power systems that combine the power generation, electrical loads and energy storage systems to work together as on system. The main objective is the study of different control algorithms for power converter to ensure an optimum operating point. The energy that is not being used will be discarded by dumping load. The electrolysis cells are used to absorb excess energy and Haruni et al. [82] reported the renewable energy system consisting of wind turbines, fuel cells, electrolysis cells, and batteries. The energy management strategies are based on wind and load demand forecasts. Determining the maximum amount of acceptable load, including equipment priority and operation of each subsystem depends on the different operating points of the battery state of charge (SOC) and the system response depends on the accuracy of the wind forecasting.

From the above researches, the short-term energy storages are responsible for absorbing energy during the interaction of each device in the system and stabilizing the power balance between a maximum and minimum state of charge and reducing the occurrence of excess energy (dump load). Short-term energy storage applications can limit the use of hydrogen energy storage, which helps the components in the system to have a lower rate of degradation. Fuel cells and electrolysis cells are used in cases where there is a power deficit or too much excess energy respectively. In some studies, there is no indication of the state of charge of battery or ultracapacitor as a system design parameter. The conditions for enabling and disabling the hydrogen energy storage system are only determined by power balance. This causes frequent shutdowns of the

system which will reduce the lifetime of the device. It can be seen that the limitations that will determine the operating point of each device to support different purposes, such as increasing lifetime or system optimization, are not considered.

In order to increase the system lifetime, the different systems being used to reduce the deterioration caused by the start-stop cycles of fuel cells and electrolysis cells have been studied. Zhou et al. [92] proposed the solutions for the degradation of fuel cells and electrolysis cells in a system that uses solar resources as the primary electricity source and batteries will be used as a last resort. The implement a strategy based on hysteresis band operation for battery SOC is developed. This strategy will determine the start-stop cycles of hydrogen energy storage. Fuel cells will operate in a constant mode to avoid the power transient operation. The electrolysis cell in variable power mode is more efficient. This strategy outlines possible solutions to extend equipment lifetime, reduce operating cost and avoid faults related to incorrect operations of the system. Like Tesfahunegn et al. [93], the state of charge is a parameter that determines the start-stop conditions of electrolysis cells and fuel cells but this research focuses on reducing the size of batteries to avoid the deterioration caused by overcharging. Bulk charging and bulk discharging are determined as a special operation mode of the battery. The fuel cells and electrolysis cells are being used at full power so the batteries are in safe operation. The genetic algorithm is applied in Carapellucci and Giordano [94]. It can solve problems in terms of size, cost and lifetime of each component. Diesel power generators are used in Ziogou et al. [95] and Giannakoudis [96] in the case of severe energy shortages to ensure a power balance in the system.

There are a variety of researches that focus on weather and load demand forecasting to consider the need for hydrogen energy storage systems in the next iteration steps, which will improve system performance. Brka et al. [97] proposed the using of artificial neural networks (ANN) for load demand and weather forecasting in an interval of fewer than two minutes. With the results of forecasting and current state of charge of the system, which will determine the operation to allow the battery to charge and discharge or the operating of fuel cells with reference energy of each device. This strategy will be able to determine the efficiency of fuel cells and avoid unnecessary start-stop cycles, which help reduce degradation. In Miland and Ulleberg [98].The amount of hydrogen stored is determined as a key decision variable for the system,

including the generation and load forecasting, which will consider three different strategies. The first strategy has a minimum power of electrolysis cells along with the discharge of the battery if it was necessary. The second strategy will specify the operating point of the fuel cell in the most efficient range, which will specify the minimum and maximum energy which can support form fuel cells. The third strategy will focus on reducing the number of operating cycles in the equipment, which will cause the reducing of overall start-stop cycles.

When considering the economic aspect, the complexity of optimization problems will be raised due to the limitations of economics that have an effect on the choice of operating strategies. The parameters related to the lifetime and expense for deterioration of the device will be calculated in multi-objective optimization [99]. Garcia-Trivino et al. [100] applied particle swarm optimization to different three strategies to demonstrate the correct operation. The algorithm response has different values depending on the goals, which include cost reduction, increase system performance and lifetime of the devices, respectively. The priority of the operation of each device depends on the results of each strategy for each use.

จุฬาลงกรณ์มหาวิทยาลัย

CHULALONGKORN UNIVERSITY

CHAPTER IV
COMPONENT MODELING AND MODEL VALIDATION FOR HYBRID RENEWABLE ENERGY SYSTEM

4.1 Mathematical model and model validation for Photovoltaic cell

4.1.1 Model assumptions

The mathematical model of PV which used in this research is based on a single diode equivalent circuit consisting of the diode, shunt resistance, and series resistance [26]. Since the shunt resistance is large enough, it can be neglected. The simplified equivalent circuit can be explained by the four-parameter model that shown in Fig 4.1.
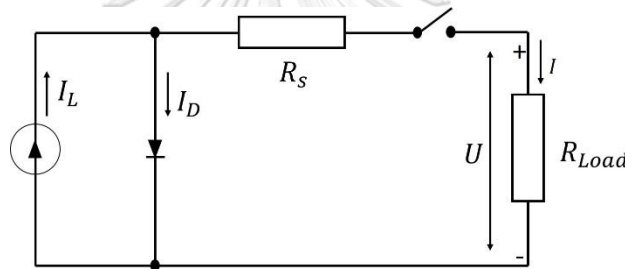
Fig. 4.1 The simplified equivalent circuit.

4.1.2 Mathematical model

From Fig. 4.1, The relationship between the output voltage (V) and load current (I) can be expressed as Eq. (4.1)

$$I = I_L - I_D = I_L - I_0 \left[\exp\left(\frac{V + IR_s}{\alpha} \right) - 1 \right] \qquad (4.1)$$

The four parameters consisting of light current (I_L), saturation current (I_0), series resistance (R_s) and thermal voltage factor (α). In Eq. (4.1), it is only the last step to define the I-V characteristic. Actually, the above four parameters are functions of solar irradiance and temperature with the following calculation procedures as Eqs. (4.2-4.11)

$$I_L = \frac{\Phi}{\Phi_{ref}} \left[I_{L,ref} + \mu_{I,SC} \left(T_c - T_{c,ref} \right) \right] \qquad (4.2)$$

The light current (I_L) can be determined based on the light current ($I_{L,ref}$) and solar irradiance (Φ_{ref}) at the reference point with the temperature coefficient of the short-circuit current ($\mu_{I,SC}$). Similarly, the saturation current (I_0) can be expressed in terms of the value that the reference condition in Eq. (4.3)

$$I_0 = I_{0,ref} \left(\frac{T_{c,ref} + 273}{T_c + 273} \right)^{\frac{3}{\eta}} \exp\left[\frac{-q e_{gap}}{\eta k N_s} \left(\frac{1}{T_c + 273} - \frac{1}{T_{c,ref} + 273} \right) \right] \quad (4.3)$$

where q is the number of elementary charge, e_{gap} is energy band gap of the materials (1.12 eV for crystalline silicon and 1.75 eV for Amorphous silicon), η is the quality factor for the diode (n=2 for crystalline and less than 2 for amorphous material), k is Boltzmann constant and N_s is the number of cells in series of the PV module. The saturation current at the reference point can be calculated as Eq. (4.4)

$$I_{0,ref} = I_{L,ref} \exp\left(-\frac{V_{oc,ref}}{\alpha_{ref}} \right) \quad (4.4)$$

The thermal voltage timing completion factor is a function of temperature and it can be determined from the value at the reference point (α_{ref}) as Eq. (4.5). This value can be calculated in two ways:

$$\alpha = \frac{T_c + 273}{T_{c,ref} + 273} \alpha_{ref} \quad (4.5)$$

In the case that there is a manufacturer datasheet, this factor at reference condition can be determined by maximum power point voltage ($V_{mp,ref}$), maximum power point current ($I_{mp,ref}$) and short circuit current ($I_{sc,ref}$) as Eq. (4.6).

$$\alpha_{ref} = \frac{2V_{mp,ref} - V_{oc,ref}}{\dfrac{I_{sc,ref}}{I_{sc,ref} - I_{mp,ref}} + \ln\left(1 - \dfrac{I_{mp,ref}}{I_{sc,ref}} \right)} \quad (4.6)$$

In the other case, the raw materials used for PV are known. The equation was expressed as Eq. (4.7)

$$\alpha_{ref} = \frac{N_s \cdot \eta \cdot k \cdot (T_{c,ref} + 273)}{q} \tag{4.7}$$

The last parameter is a Series resistance (R_s). This resistance value is usually provided by a manufacturer. If not provided, it can be estimated as Eq. (4.8)

$$R_s = \frac{\alpha_{ref} \ln\left(1 - \dfrac{I_{mp,ref}}{I_{sc,ref}}\right) + V_{oc,ref} - V_{mp,ref}}{I_{mp,ref}} \tag{4.8}$$

The operating temperature can be estimated from a simple lumped thermal model [101]. In this work, the relationship of PV cell temperature (T_c) ambient temperature (T_a) and solar irradiance (Φ) can be expressed as Eq. 3.8

$$T_c = T_a + \left[\Phi(\tau\alpha / U_L)\right]\left[1 - (\eta_c / \tau\alpha)\right] \tag{4.9}$$

Where U_L is the overall heat loss coefficient, η_c is the efficiency of the PV cell and $\tau\alpha$ is the transmittance-absorption product of PV cell (0.9). The ratio between $\tau\alpha$ and U_L depends on nominal operating cell temperature (NOCT) conditions [102].

4.1.3 Model validation

From Zhang et al. [58], They studied I-V characteristics using single-diode combined with an explicit analytical model. Normally, the determination of the current value of the solar cell requires the reference data at standard reference condition (SRC) at solar irradiance 1000 Wm^{-2} and 298 K. However, the reference conditions obtained from the measurement (measured reference condition: MRC) at solar irradiance of 398 Wm^{-2} and 296 K are used in this research. The research model will be examined with the real test using solar panel LNPV-125*125-F/C monocrystalline silicon, by data at MRC as table 4.1.

Table 4.1 Parameters for a single diodes model at MRC (398 Wm^{-2} and 296 K)

Parameters	Symbols	Value
Short-circuit current	I_{sc}	1.55 A
Open-circuit voltage	V_{oc}	40.15 V
Light current	I_L	1.5504 A
Diode saturation current	I_0	2.42×10^{-7} A
quality factor	η	1.395

In order to apply this information to the simplified single-diode solar cell model used in this thesis, it needs to calculate backward by using the Eqs. (4.2-4.8) to get the parameters at standard reference condition (SRC). All parameters used are shown in Table 4.2.

Table 4.2 Model parameters used in the simulation of PV

Parameters	Symbols	Value
Short-circuit current, (A)	$I_{sc,ref}$	3.99
Open-circuit voltage, (V)	$V_{oc,ref}$	42.84
Light current, (A)	$I_{L,ref}$	3.98
Diode saturation current, (A)	$I_{0,ref}$	2.4478×10^{-7}
Ideality factor	η	1.395
Series resistance, (Ω)	R_s	0.56
Thermal voltage factor, (V)	α_{ref}	2.58
The energy bandgap of the materials, (eV)	e_{gap}	1.17
number of elementary charges, (C)	q	1.602×10^{-19}
Boltzmann constant, (J K^{-1})	k	1.38065×10^{-23}
Temperature coefficient of the short-circuit current	$\mu_{I,SC}$	0.06 %
Number of cells in series	N_s	72

To calculate the load current according to Eq. (4.1), the Newton Raphson method is used to find the answer rearranged the PV model as Eqs. (4.10-4.13).

$$f(\mathrm{x}) = I - I_L - I_0\left[\exp\left(\frac{U + IR_s}{\alpha}\right) - 1\right] \tag{4.10}$$

$$f'(\mathrm{x}) = -1 - I_0\,\frac{R_s}{\alpha}\left[\exp\left(\frac{U + IR_s}{\alpha}\right) - 1\right] \tag{4.11}$$

$$f(\mathrm{x}_1) = I - \frac{\left[I_L - I - I_0\left[\exp\left(\dfrac{U + IR_s}{\alpha}\right) - 1\right]\right]}{-1 - I_0\,\dfrac{R_s}{\alpha}\left[\exp\left(\dfrac{U + IR_s}{\alpha}\right) - 1\right]} \tag{4.12}$$

The test of the model is divided into 6 cases as shown in Table 4.3. The simulation results compared with the real operation are shown in Fig. 4.2. From the simulation results, it shows the consistency of the model with the behavior of photovoltaic cells as well.

Table 4.3 Experiment conditions including date, time solar irradiance and temperature

	Date	Time	Φ (Wm^{-2})	T(K)
C1	April 10	1:15 p.m.	790	316
C2	May 30	1:45 p.m.	1135	345
C3	April 11	8:40 a.m.	389	296
C4	May 25	3:30 p.m.	82	302
C5	March 20	11:20 a.m.	737	298
C6	March 20	2:10 p.m.	635	322
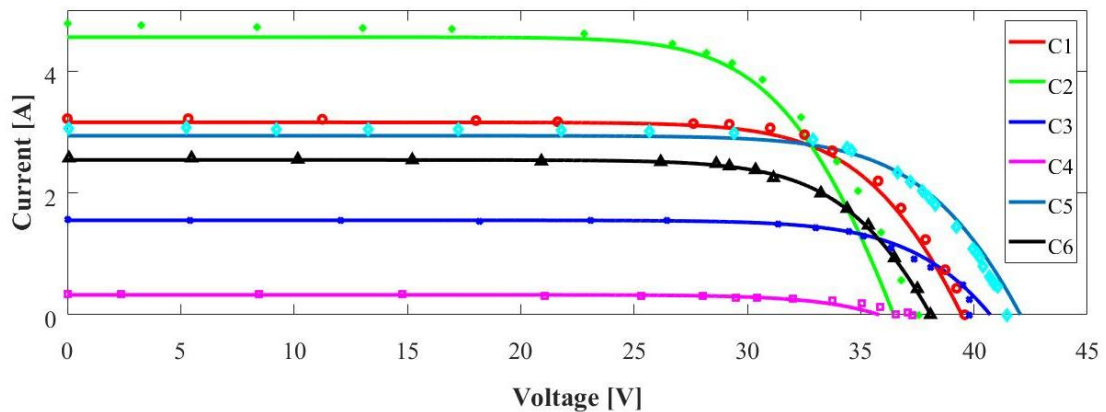
Fig. 4.2 I-V characteristic obtained from the simulation compared to the experiment.

4.2 Mathematical model and model validation for Proton Exchange Membrane Fuel Cell (PEMFC)

4.2.1 Model assumptions

The behavior of PEMFC depends on the range of operating factors, such as pressure, membrane water content, and temperature, resulting in high nonlinearity. To simplify the model, the assumptions based on previous similar research [33] are shown below.

1. The model is described by the one-dimensional and lumped model.
2. The reactants are saturated vapor.
3. All gases behave as ideal gases.
4. The membrane is fully saturated with water
5. Pure hydrogen is fed into the anode side and the air is fed into cathode side with 21% oxygen.
6. The system is isothermal and the temperature is uniform throughout the stack.

4.2.2 Mathematical model

In general, the characteristic of PEMFC can be explained by the polarization curve, which shows the relationship between the output voltage and current density. The output voltage of the PEM fuel cell can be explained by the summation of 4 terms of the voltage, i.e., electric potential according to the thermodynamic theory (E_{Nernst}),

overpotential from chemical reactions (V_{act}), overpotential from electrical resistance (V_{ohm}) and overpotential from concentration (V_{con}). The equation can be expressed as Eq. (4.13) [28].

$$V_{PEMFC} = E_{Nernst} - V_{act} - V_{ohm} - V_{con} \qquad (4.13)$$

The thermodynamic potential $\left(E_{Nernst}\right)$ is the open circuit condition at thermodynamic balance. It can be calculated by the Nernst equation as Eq. (4.14) [28].

$$E_{Nernst} = E^o + \frac{RT}{nF} \ln\left[p'_{H_2} \left(p'_{O_2}\right)^{0.5} \right] \qquad (4.14)$$

where E^o is the standard overpotential, p'_{H_2} is the partial pressure of hydrogen, p'_{O_2} is the partial pressure of oxygen, R is the universal gas constant, F is the Faraday constant, T is the fuel cell temperature. The deviation from the standard condition can be determined in a temperature dependent expression for E^o as given in Eq. (4.15)

$$E_{Nernst} = 1.229 - 8.5 \times 10^{-3}\left(T - 298.15\right) + \frac{RT}{nF} \ln\left[p'_{H_2} \left(p'_{O_2}\right)^{0.5} \right] \qquad (4.15)$$

The activation overpotential (V_{act}) is caused by a low chemical reaction rate which may occur at any stage in the reaction such that the anode reaction as Eq (4.16)

$$A \leftrightarrow A^+ + e^- \qquad (4.16)$$

While the open circuit has no current flowing through the cell, the reaction rate according to Eq. (4.16) from the left to right side and from the right to left side is equal due to the equilibrium condition. When electricity flows out of the cell, the reaction rate from left to right is more than one and the electric potential is reduced to constant. The empirical model [61] is widely used in this term.

$$V_{act} = -\left[\xi_1 + \xi_2 T + \xi_3 T \left[\ln\left(c'_{O_2}\right) \right] + \xi_4 T \left[\ln\left(I\right) \right] \right] \qquad (4.17)$$

where c'_{O_2} is the oxygen concentration at the cathode, I is the cell current and $\xi_1, \xi_2, \xi_3, \xi_4$ are the parameter coefficients. The more generalized steady-state model is given in [61] can be adopted as

$$\xi_1 = -0.948$$

$$\xi_2 = 0.00286 + 0.0002 \ln(A) + 4.3 \times 10^{-5} \ln(c'_{H_2})$$

$$\xi_3 = 7.6 \times 10^{-5}$$

$$\xi_4 = -1.93 \times 10^{-4}$$

where A is the cell active area and c'_{H_2} is the hydrogen concentration at the anode.

The concentration of oxygen and hydrogen at the electrode can be determined by Henry's law as

$$c'_{O_2} = p'_{O_2} \times 1.97 \times 10^{-7} \exp\left(\frac{498}{T}\right) \tag{4.18}$$

$$c'_{H_2} = p'_{H_2} \times 9.174 \times 10^{-7} \exp\left(\frac{-77}{T}\right) \tag{4.19}$$

In fuel cells that use acid or base solutions as electrolytes, the internal resistance is low because this electrolyte has good electric conductivity. In the case of the proton exchange membrane as the electrolyte of the fuel cell will make the overpotential from electrical resistance (V_{ohm}) is high value because the proton exchange membrane uses fewer ions than acid or base solution. The ohmic voltage term is given by Eqs. (4.20-4.22).

$$V_{ohm} = -IR_{int} \tag{4.20}$$

where R_{int} is the internal resistance is expressed as [61].

$$R_{int} = \frac{r_M I_{mem}}{A} \tag{4.21}$$

$$r_M = \frac{181.6\left[1 + 0.03j + 0.062\left(\frac{T}{303}\right)^2 (j)^{2.5}\right]}{[\lambda - 0.634 - 3j]\exp\left[4.18\left(\frac{T-303}{T}\right)\right]} \tag{4.22}$$

where j is the current density, r_M is the membrane resistivity, I_{mem} is the membrane thickness, A is the effective cell area and λ is a function of membrane humidity $(10-23)$.

The overpotential from concentration V_{con} is caused by the fuel or oxidizing agent being used too much, and the effect of the reaction that occurs at the electrode can cause the reduction of concentration or pressure of the substrate according to the Nernst equation. This problem often occurs with fuel cells using air as an oxidizing agent. The mathematical model can be expressed as Eq. (4.23)

$$V_{con} = \frac{RT}{2F} \ln\left(1 - \frac{j}{j_{\max}}\right) \tag{4.23}$$

where $j_{\max}$ is the maximum current density (1000-1500 $mA cm^{-2}$).

The reactant flow rates at the anode and cathode base on the ideal gas law and molar conservation while the dynamic model of the partial pressure of hydrogen is simplified by assuming that pure feed flowing into the channel as follows

$$\frac{dp_{H_2}}{dt} = \frac{RT}{V_{an}}\left(\dot{m}_{H_2,in} - k_{an}\left(p_{H_2} - p_{atm}\right) - \frac{jA}{2F}\right) \tag{4.24}$$

4.2.3 Model validation

From Mueller et al. [103], they studied a quasi-three-dimensional dynamic model of PEMFC compared with the experiment and design in the operating area of 25 cm^2. The membrane used in the fuel cell is Nafion 112. At the anode, the reactant is high purity hydrogen and the cathode is dry air which is humidified by the transmission of external bubble humidifier in each gas line. The flow rates of hydrogen and air are controlled and measured by two mass flow controllers. The humidity temperature of the substrate is controlled by the humidity modifier. In this experiment, the specified fuel cell temperature is 70 ºC and the pressure is 1.1 bar. The model parameters used for PEMFC simulation are given in Table 4.3, and the result compared with the experimental data is shown in Fig. 4.4. The simulation result shows good consistency with experimental data.

Table 4.4 Model parameters used in the simulation of PEMFC

Parameters	Symbols	Value
Reference potential, (V)	E^o	1.229
The partial pressure of hydrogen, (atm)	p'_{H_2}	1.086
The partial pressure of oxygen, (atm)	p'_{O_2}	1.086
Universal gas constant, ($J\,mol^{-1}K^{-1}$)	R	8.314
Faraday constant, ($C\,mol^{-1}$)	F	96485
Fuel cell temperature, (K)	T	343
Cell active area, (cm^2)	A	25
Membrane water content	λ	14
Membrane thickness (Nafion 117), (cm)	I_{mem}	0.0178
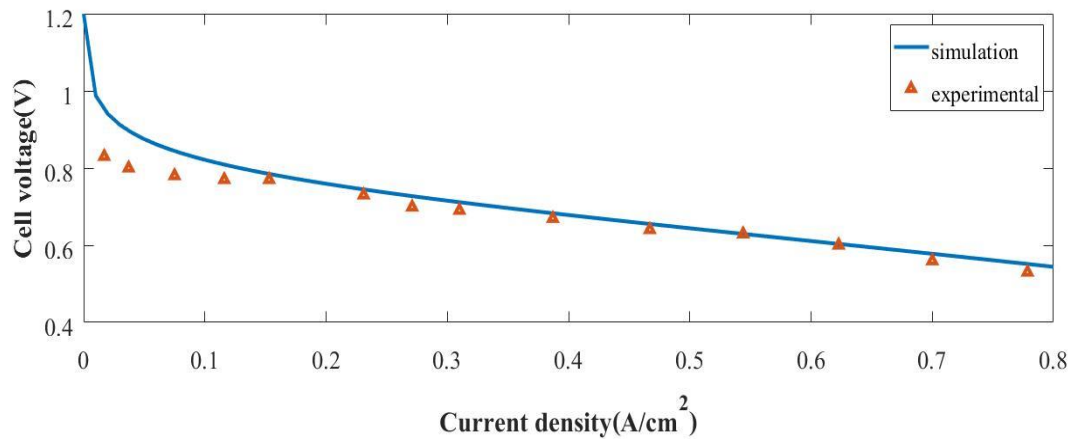
Fig. 4.3 The polarization curve of PEMFC at the experimental condition

4.3 Mathematical model and model validation for Proton Exchange Electrolysis Fuel Cell (PEMEC)

4.3.1 Model assumptions

In this work, the electrochemical model is based on the following assumptions [29]:

1. All gases are ideal gases.
2. The pressure at the anode side is at atmospheric pressure.
3. The diffusion of hydrogen and oxygen through the membrane is not considered.

4. The solubility of hydrogen and oxygen in water is negligible.

5. The PEM electrolysis cell system is isothermal and uniform throughout the stack.

6. The liquid water exerts its saturated vapor pressure at both the cathode and anode at the prevailing conditions.

7. The CTC of the hydrogen electrode is the same as the symmetry factor (0.5).

8. The symmetry factor at the oxygen electrode is 0.5.

9. The membrane is completely saturated with water; therefore, the conductivity is only depending on temperature and water management in PEMEC.

4.3.2 Mathematical model

The behavior of PEMEC can be explained by the polarization curve like PEMFC. Due to the above assumption, the total operating voltage of PEM electrolysis cell can be described in the summation of Nernst potential (E_{Nernst}), activation overpotential (V_{act}), ohmic overpotential (V_{ohm}) [104] as:

$$V_{PEMEC} = E_{Nernst} + V_{Act} + V_{Ohmic} \qquad (4.33)$$

The value of the Nernst potential is related to the concentration of the products and reactants as

$$E_{Nernst} = E^o + \frac{RT}{V_e F} \ln\left(\frac{P_{H_2} P_{O_2}^{0.5}}{P_{H_2O}}\right) \qquad (4.34)$$

where E^o is the cell potential at equilibrium point regardless of the effect of pressure which can be expressed as [65]:

$$E^o = 1.5241 - 1.2261 \times 10^{-3} T + 1.1858 \times 10^{-5} T \ln(T) + 5.6692 \times 10^{-7} T^2 \qquad (4.35)$$

In this work, the partial pressure of hydrogen and oxygen is calculated from the total pressure at the cathode and anode as:

$$p'_{H_2O} = \frac{610}{10^5} \exp\left(\frac{t}{t + 238.3} \times 17.2694\right) \qquad (4.36)$$

$$p'_{O_2} = p'_{an} - p'_{H_2O} \tag{4.37}$$

$$p'_{H_2} = p'_{ca} - p'_{H_2O} \tag{4.38}$$

Where p'_{H_2O} is the partial pressure of the vapor, p'_{O_2} is the partial pressure of oxygen, p'_{H_2} is the partial pressure of hydrogen and T is cell temperature in celsius degree.

When current flows through the electrolysis cell, charge-transference and mass-transport phenomena at the electrodes must be considered. Assuming no transport limitations, the Butler-Volmer expression [101] relates the current density to the activation overpotential V_{act} at each electrode as:

$$j = j_0 \left[e^{\frac{\beta n F}{RT} \eta} - e^{\frac{(1-\beta)nF}{RT} \eta} \right] \tag{4.39}$$

The β value is defined as the electrode symmetry factor, which represents the physical ratio of additional energy towards the reduction (β) and the oxidation $(1-\beta)$. It can form the expression of the overpotential voltage at the anode and cathode as follows:

$$V_{act} = V_{act,an} + V_{act,ca} = A_{an} \ln\left(\frac{j}{j_{0,an}} \right) + A_{ca} \ln\left(\frac{j}{j_{0,ca}} \right) \tag{4.40}$$

$$A_{an,ca} = \frac{RT}{2\alpha_{an,ca}F} \tag{4.41}$$

where α_{an} and α_{ca} are charge transfer coefficients and $j_{0,an}$, $j_{0,ca}$ are exchange current density at the anode and cathode respectively. The value of exchange current density can be modeled using an Arrhenius form as described by Eq. (4.42). A value for exchange current density at the reference point obtained by the polarization curve fitting from experimental data.

$$j_0 = j_{0,ref} e^{\left[-\frac{E_{exec}}{R}\left(\frac{1}{T} - \frac{1}{T_{ref}} \right) \right]} \tag{4.42}$$

where E_{exec} is the activation energy for the electrode reaction.

The ohmic overpotential is caused by the resistance of the membrane while the hydrogen ion moves through it. The mathematical model is shown as Eq. (4.43).

$$V_{ohm} = \frac{I_{mem}}{\sigma} j \qquad (4.43)$$

where I_{mem} is the membrane thickness and σ is cell conductivity. The water content of the membrane is a major problem for PEMFC. However, in the case of PEMEC, the membrane can be assumed to be fully moist. The electrical conductivity depends on the temperature and can be modeled by using the reference temperature with the Arrhenius model as in the Eq. (4.44).

$$\sigma = \sigma_{0,ref} e^{\left[-\frac{E_{pro}}{R} \left(\frac{1}{T} - \frac{1}{T_{ref}} \right) \right]} \qquad (4.44)$$

where E_{pro} is temperature-independent parameters showing the activation energy for proton transport in selective membranes.

4.3.3 Model validation

Garcia-Valverde et al. [66] had proposed a simple model for PEMEC at atmospheric pressure or low pressure which helps to accurately reproduce the behavior of electrochemistry, temperature and the amount of hydrogen production for engineering use. The effect of temperature is used to calculate in the range of 20-80 $^{\circ}C$. The model parameters used for PEMEC simulation are given in Table 4.5.

จุฬาลงกรณ์มหาวิทยาลัย

CHULALONGKORN UNIVERSITY

Table 4.5 Model parameters used in the simulation of PEMEC

Parameters	Symbols	Value
The partial pressure of hydrogen, (atm)	p'_{H_2}	1 atm
The partial pressure of oxygen, (atm)	p'_{O_2}	1 atm
Universal gas constant, ($J\,mol^{-1}K^{-1}$)	R	8.314
Faraday constant, ($C\,mol^{-1}$)	F	96485
Membrane thickness (Nafion 115), (cm)	I_{mem}	0.0127
Reference temperature, ($^o C$)	T_{ref}	55
Reference exchange current density, ($A\,cm^{-2}$)	$j_{0,ref}$	10^{-6}
Reference membrane conductivity, ($S\,cm^{-1}$)	$\sigma_{0,ref}$	0.05
The activation energy of the water oxidation, ($J\,mol^{-1}$)	E_{exc}	53990.065
The activation energy of proton transport, ($J\,mol^{-1}$)	E_{pro}	18912.42

The simulation result is compared with the experimental data at the temperature of 30, 40 70 and 80 ^{o}C are shown in Fig. 4.5. The simulation result shows good consistency with experimental data.
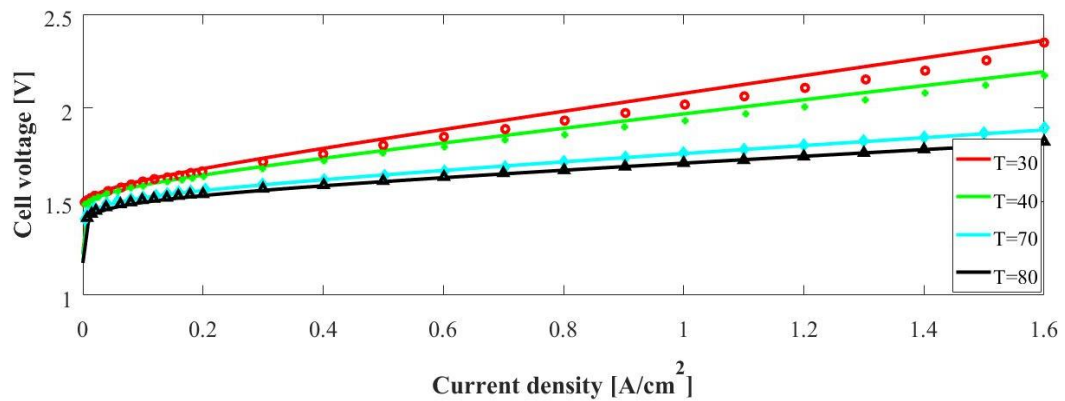
Fig. 4.4 The polarization curve of PEMEC at each experimental condition

4.4 Mathematical model and model validation for Vanadium Redox Flow Battery (VRFB)

4.4.1 Model assumptions

In this work, the electrochemical models and the dynamic model with diffusion terms of all vanadium ions can be described based on these assumptions to simplified the model [30].

1. The room temperature is constant.
2. The electrolyte flow rate is not taken into account
3. The physical properties of electrode, electrolytes properties are constant
4. The volume of electrolytes in each half cell is constant
5. The electrolytes are perfectly mixed
6. The side reactions caused by the diffusion of vanadium ions across the membrane are instantaneous
7. The charge transfer coefficient (CTC) of the anode and cathode is equal to 0.5.
8. The upper and lower cell voltage limits are 1.7 V and 1.1 V respectively for the end of the charge and discharge process.

4.4.2 Mathematical model

As with general electrochemical energy storage, the output voltage of the cell explained by the sum of the 4 voltage terms open-circuit voltage (E_{Nernst}), activation overpotential (V_{act}), and resistance overpotential (V_{ohm}). For concentration overpotential ($V_{conc,i}$), it will not be calculated due to the above assumption that the electrolyte flow rate is not taken into account.

The open-circuit voltage could be described by the Nernst equation according to Eq. (4.45) by calculating the difference between the positive and negative voltage.

$$E_{Nernst} = V_p - V_n = E^0 + \frac{RT}{nF} \ln\left(\frac{C_{V^{2+}} C_{V^{4+}}}{C_{V^{3+}} C_{V^{5+}}} \right) \qquad (4.45)$$

The activation overpotential can be represented by the Butler-Volmer expression as Eq. (4.39). The activation loss of each half-cell can be expressed as Eq. (4.46).

$$V_{act,i} = \frac{RT}{\alpha_i nF} \ln\left(\frac{j}{j_{0,i}}\right) \tag{4.46}$$

where α_i is the charge transfer coefficient of each side which is equal to 0.5 as specified in the above assumptions. n is the number of electron transfer which is equal to 1 according to Eq. (2.7) in chapter 2. Therefore, it can be simplified to form the following equation.

$$V_{act,i} = \frac{2RT}{F} \ln\left(\frac{j}{j_{0,i}}\right) \tag{4.47}$$

The resistance overpotential or ohmic loss consists of resistance from the membrane, electrode and electrolyte as shown in Eqs. (4.48-4.51) [105].

$$V_{ohm} = j\left(\frac{I_e}{\sigma_e} + \frac{I_{mem}}{\sigma_{mem}} + \frac{I_{elec}}{\sigma_{elec}}\right) \tag{4.48}$$

$$\sigma_{mem} = 7.3e^{\left(1268\left(\frac{1}{T_{ref}} - \frac{1}{T}\right)\right)} \tag{4.49}$$

$$\sigma_{elec} = \frac{F^2}{RT}\sum_i z_i^2 D_i^{eff} c_i \tag{4.50}$$

$$D_i^{eff} = \varepsilon^{3/2} D_i \tag{4.51}$$

The electrolyte resistance model is complicated in the calculation and has very little effect on ohmic overpotential, so it can be neglected. Therefore, the term resistance over potential is calculated only from the membrane and electrode resistance.

In order to find the concentration of each vanadium ion at any time, molar mass balance dynamic equation associated with the diffusion term according to the chemical reactions shown in chapter 2 is shown as Eqs.(4.52-4.55).

$$V_s \frac{dc_{V^{2+}}}{dt} = \pm \frac{jA}{zF} - k_2 \frac{C_2}{d} S - 2k_5 \frac{C_5}{d} S - k_4 \frac{C_4}{d} S \tag{4.52}$$

$$V_s \frac{dc_{V^{3+}}}{dt} = \pm \frac{jA}{zF} - k_3 \frac{C_3}{d} S + 3k_5 \frac{C_5}{d} S + 2k_4 \frac{C_4}{d} S \tag{4.53}$$

$$V_s \frac{dc_{V^{4+}}}{dt} = \pm \frac{jA}{zF} - k_4 \frac{C_4}{d} S + 3k_2 \frac{C_2}{d} S + 2k_3 \frac{C_3}{d} S \tag{4.54}$$

$$V_s \frac{dc_{V^{5+}}}{dt} = \pm \frac{jA}{zF} - k_5 \frac{C_5}{d} S - 2k_2 \frac{C_2}{d} S - k_3 \frac{C_3}{d} S \tag{4.55}$$

where $c_{V^{2+}}$ is the concentration of V^{2+} ions ($molL^{-1}$)

$c_{V^{3+}}$ is the concentration of V^{3+} ions ($molL^{-1}$)

$c_{V^{4+}}$ is the concentration of V^{4+} ions ($molL^{-1}$)

$c_{V^{5+}}$ is the concentration of V^{5+} ions ($molL^{-1}$)

k_2 is the diffusion coefficient for V^{2+} across the membrane ($dm^2 s^{-1}$)

k_3 is the diffusion coefficient for V^{3+} across the membrane ($dm^2 s^{-1}$)

k_4 is the diffusion coefficient for V^{4+} across the membrane ($dm^2 s^{-1}$)

k_5 is the diffusion coefficient for V^{5+} across the membrane ($dm^2 s^{-1}$)

V_s is the volume of half-cell solution (L)

A is electrode surface area (cm^2)

z is the number of electrons transferred in the reaction

d is the membrane thickness (dm)

S is the membrane area (dm^2)

4.4.3 Model validation

Ngamsai and Arpornwichanop [106] analyzed and measured the electrolyte imbalance level in the vanadium battery. During the electrolyte preparation process, vanadium pentoxide powder is dissolved in the sulfuric acid solution. The concentration of the prepared vanadium solution is 1.6 $molL^{-1}$ which fits with a half-cell battery of $10 \times 10 \times 3$ cm in a system that uses an electrolyte with a volume of positive 260 ml. and negative 250 ml. The process of charging and discharging is done in constant current mode (CC) with 3 current adjustments, 10A, 15A, and 20A. The membrane used in the research is Selemion APS-4. Due to lack of diffusion coefficient data, the

selemion AMV is also chosen, which is the same type of membrane. The data of the diffusion coefficient are shown in Table 4.5 [30]. In the simulation, there are variables used to adjust the coefficient so that the simulation result is consistent with the experimental results with an approximate value of 3.5-3.9 times of Selemion AMV. The model parameters used for VRFB simulation are given in Table 4.6. The simulation results of the open-circuit voltage are shown in Fig. 4.6 and the VRFB cell voltage are shown in Fig. 4.7.

Table 4.6 The diffusion coefficient of vanadium ion in different membrane

Membrane	k_2 ($\mathrm{dm\ s^{-1}}$)	k_3 ($\mathrm{dm\ s^{-1}}$)	k_4 ($\mathrm{dm\ s^{-1}}$)	k_5 ($\mathrm{dm\ s^{-1}}$)
Selemion CMV	3.17×10^{-7}	30.716×10^{-7}	2×10^{-7}	1.25×10^{-7}
Selemion AMV	3.53×10^{-8}	2.18×10^{-8}	10.91×10^{-8}	2.57×10^{-8}
Nafion 115	6.9×10^{-7}	2.54×10^{-7}	5.37×10^{-7}	4.64×10^{-7}

Table 4.7 Model parameters used in the simulation of PEMEC

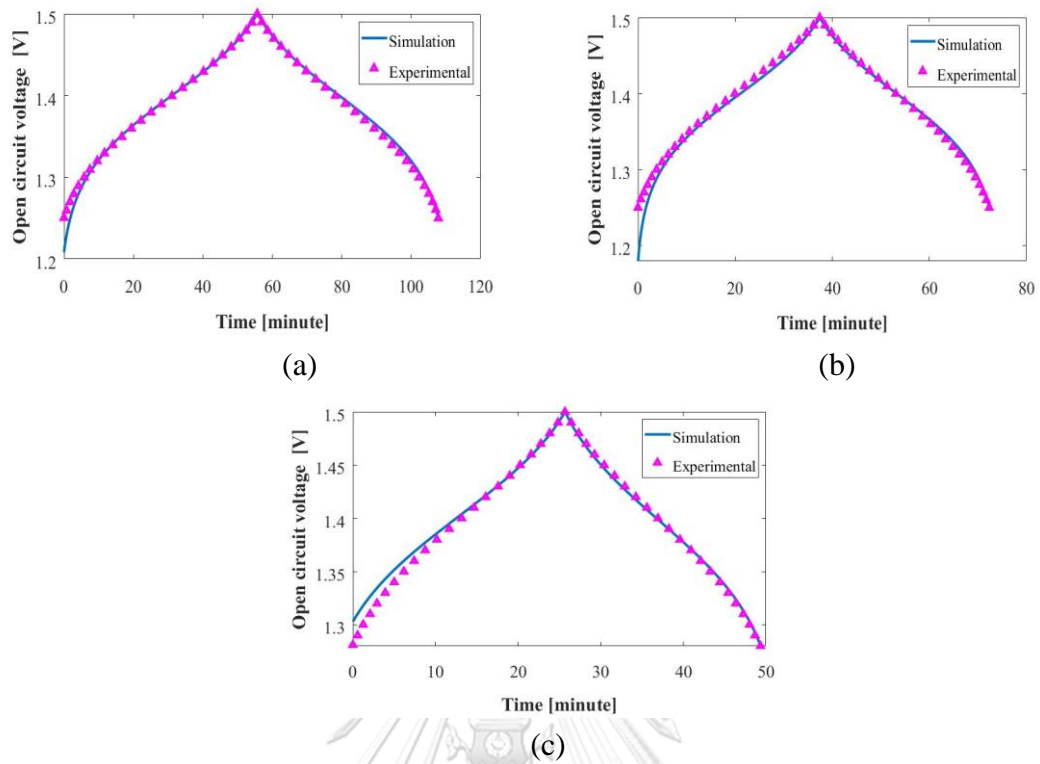| Parameters	Symbols	Value
Membrane thickness, (μm)	I_{mem}	30
Membrane area, ($\mathrm{m^2}$)	A_{mem}	0.081
Thickness of electrode, (m)	I_e	0.003
The volume of half-cell solution, (L)	V_s	0.25
Electrode conductivity, ($\mathrm{Sm^{-1}}$)	σ_e	363
Standard cell potential, (V)	E^o	1.4

Fig. 4.5 Comparison the open-circuit voltage of the simulation result with experimental data in different current. (a) 10A (b) 15A (c) 20 A.
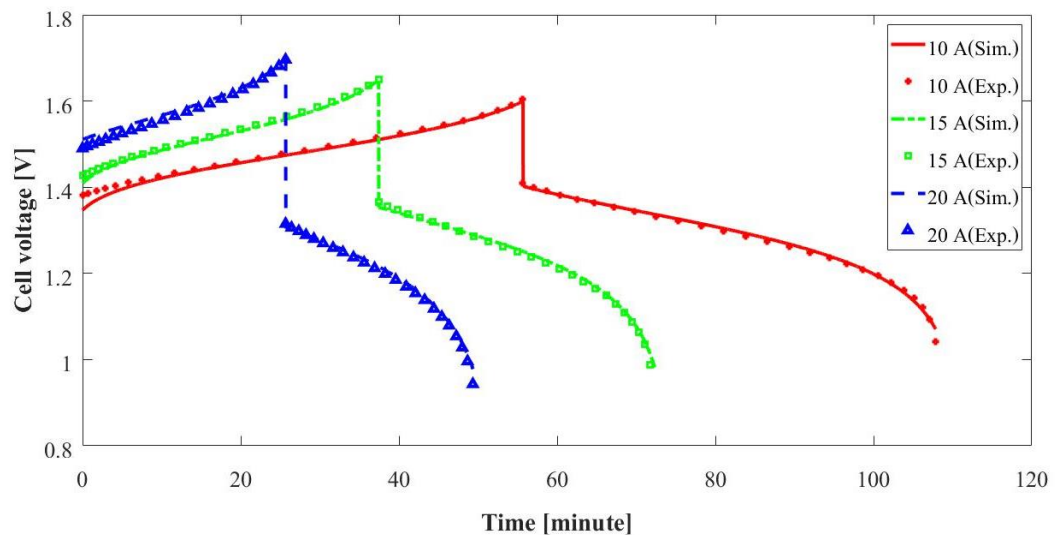

Fig. 4.6 Comparison the VRFB cell voltage of the simulation result with experimental data.

CHAPTER V
THE VANADIUM REDOX FLOW BATTERY USAGE IN THE SOLAR ENERGY MANAGEMENT SYSTEM

Batteries are an important part of energy management systems that have high investment benefits at present which are characterized by modularization and rapid response. The battery system is associated with flexible installation and short construction time. Therefore, it has been successfully applied to energy storage systems. For solar power sources, suitable batteries are nickel-metal hydride (NiMH), lead-acid and lithium-ion battery. In deciding which type of battery depends on the primary needs of use. For example, lead-acid or NiMH batteries should be selected when considering the price and capacity. While lithium-ion batteries have the benefit of high energy density and small size.

This chapter presents the usage of vanadium batteries in comparison to the traditional batteries commonly used in this research area which are lead-acid batteries. The power control algorithm, system size, solar irradiance profile, and load demand profile are based on Dash and Bajpai research [24].

5.1 Specification of the model of the hybrid renewable energy system

In Dash and Bajpai's research [24], they studied alternative energy systems combined with photovoltaic cells (PV), proton exchange membrane fuel cell (PEMFC), proton exchange membrane electrolysis cell (PEMEC) and lead-acid battery. The goal of their research is to establish an energy management system and integrating the output power from the electrical devices described above with a provision for the hydrogen production process from PEMEC and hydrogen tank. The parameters used for modeling of the renewable energy system components are shown in Table 5.1-5.4.

Table 5.1 PV module specification at STC (1000 Wm^{-2}, 25 $^{\circ}C$)

Parameters	Value
Nominal power, (W)	165
Voltage at MPP, (V)	35
Current at MPP, (A)	4.7
Open-circuit voltage, (V)	40.15
Short-circuit current, (A)	1.55
No. of solar cells in series in a module	72
Short-circuit current cell temperature coefficient	0.007%
Number of modules in each string	3
Number of strings in parallel	10
Maximum voltage at STC, (V)	105
Maximum current at STC, (A)	47

Table 5.2 PEMFC module specifications

Parameters	Value
Rated capacity, (W)	500
Number of cells	48
Operating pressures, (atm)	1.5
Number of modules in series	5
Rated power, (kW)	2.5
Maximum voltage, (V)	108
Maximum current, (A)	21.3

Table 5.3 PEMEC module specifications

Parameters	Value
Number of cells	10
Operating pressures, (atm)	1
Rated power, (kW)	2.75
Maximum voltage, (V)	24
Maximum current, (A)	110

Table 5.4 Lead-acid battery specification

Parameters	Value
Ampere hour rating, (Ah)	400
Nominal voltage, (V)	48
Fully charged voltage (No load), (V)	55.2
Charging rate	C/10

In Table 5.1, the PV array of 4.95 kW consists of 10 strings in parallel and 3 modules in each string (30 modules of 165 W each). For PEMFC stack (Table 5.2), there are a total of 5 modules and each module has a capacity of 500 W delivers a maximum of 464 W at 21.38 A and 21.69 V. In Table 5.3, the rated power of the PEMEC is 2.75 kW at 110 A and 24 V. The battery bank has a 400Ah rated, nominal voltage of 48V and has a maximum current of 40A, which means can charge 400 Ah batteries at constant current at 40A in 10 hours (C/10) (Table 5.4).

Since the model using in the reference research is based on electrical theory than chemistry, some parameters are neglected, such as the active area in the cell and water content. Therefore, in this thesis, additional parameters need to be calculated in the model. From Table 5.2, it is found that the voltage in each cell is 0.4519 V at the maximum voltage of PEMFC. Considering the polarization curve, the current density is 0.7756 A cm^{-2}. Thus, the active area should be 27.57 cm^2. In the case of PEMEC, the calculation provides that the active area is approximately 57.53 cm^2.

The mathematical models of PV, PEMFC, and PEMEC have already been described in chapter 4, but the data for the parameters using in the lead-acid battery

model is not sufficient. Consequently, the lead-acid battery model is based on the research of Blaifi et al. [107]. It consists of a model of the voltage of charging and discharging the battery and the state of charge (SOC) at that time, as shown in Eqs. (5.1-5.3) respectively.

$$V_{dc}(t) = n_s \left[V_{bodc} - K_{bodc}(1 - SOC(t)) \right] - n_s \frac{\left| I_{bat}(t) \right|}{Q} \left(\frac{P_{1dc}}{1 + \left| I_{bat}(t) \right|^{P_{2dc}}} + \frac{P_{3dc}}{SOC(t)^{P_{4dc}}} + P_{5dc} \right)$$

$$\cdot \left(1 - \alpha_{rdc} \Delta T(t) \right) \tag{5.1}$$

$$V_c(t) = n_s \left[V_{boc} - K_{boc} SOC(t) \right] - n_s \frac{\left| I_{bat}(t) \right|}{Q} \left(\frac{P_{1c}}{1 + I_{bat}(t)^{P_{2c}}} + \frac{P_{3c}}{\left(1 - SOC(t) \right)^{P_{4c}}} + P_{5c} \right)$$

$$\cdot \left(1 - \alpha_{rc} \Delta T(t) \right) \tag{5.2}$$

$$\Delta SOC(t) = \frac{\left(\int_{t-1}^{t} I_{bat}(t) \cdot dt \right)}{Q} \times 100 \tag{5.3}$$

where V_{bodc} and V_{boc} are charging and discharging voltage respectively, K_{bodc} and K_{boc} are the voltage coefficient that changes according to SOC and P_1, P_2, P_3, P_4, P_5 are the value of the loss associated with the internal resistance which depends on the operating point, α_r is the temperature coefficient. For the battery's module referenced from TECHNO SUN 2V-OPzS-TCH2765 (Techno Sun, Valencia, Spain), each cell has a nominal voltage equal to 2V. In order to have the same size of battery used in this research, a series of 24 cells are connected. The parameters using for the model are shown in Table 5.5.

Table 5.5 Model parameters of lead-acid battery

Parameters	Discharge	Parameters	Charge
V_{bodc}, (V)	2.147	V_{boc}, (V)	1.98
K_{bodc}, (V)	0.284	K_{boc}, (V)	0.149
P_{1dc}, (VAh)	4.083	P_{1c}, (VAh)	5.923
P_{2dc}	-6.634	P_{2c}	0.024
P_{3dc}, (Vh)	0.27	P_{3c}, (Vh)	0.048
P_{4dc}	1.5	P_{4c}	1.2
P_{5dc}, (Vh)	0.02Vh	P_{5c}, (Vh)	0.036
α_{rdc}, ($^{\circ}C^{-1}$)	0.007	α_{rc}, ($^{\circ}C^{-1}$)	0.025

5.2 Power management strategy algorithm

The power management strategy is adopted from Dash and Bajpai's algorithms [24], which will be simplified to reduce the complexity of calculations as follows:

1. The converter is not calculated in the system.
2. No battery charging in constant voltage (CV) mode but will stop charging at SOC equal to 99.5 %
3. The precursor flow of PEMFC and PEMEC are instantaneously reached to the set point.
4. The mathematical model of each component will be used according to the model mentioned in this thesis.

The simplified power management strategy used in the thesis is shown in Fig. 5.1. In the power management algorithm, the electrical energy produced by PV will always be distributed to the load first $P_{excess} = P_{Pv} - P_{load}$ in the first step measures. After that, the operations can be divided into sub-modes as follows:
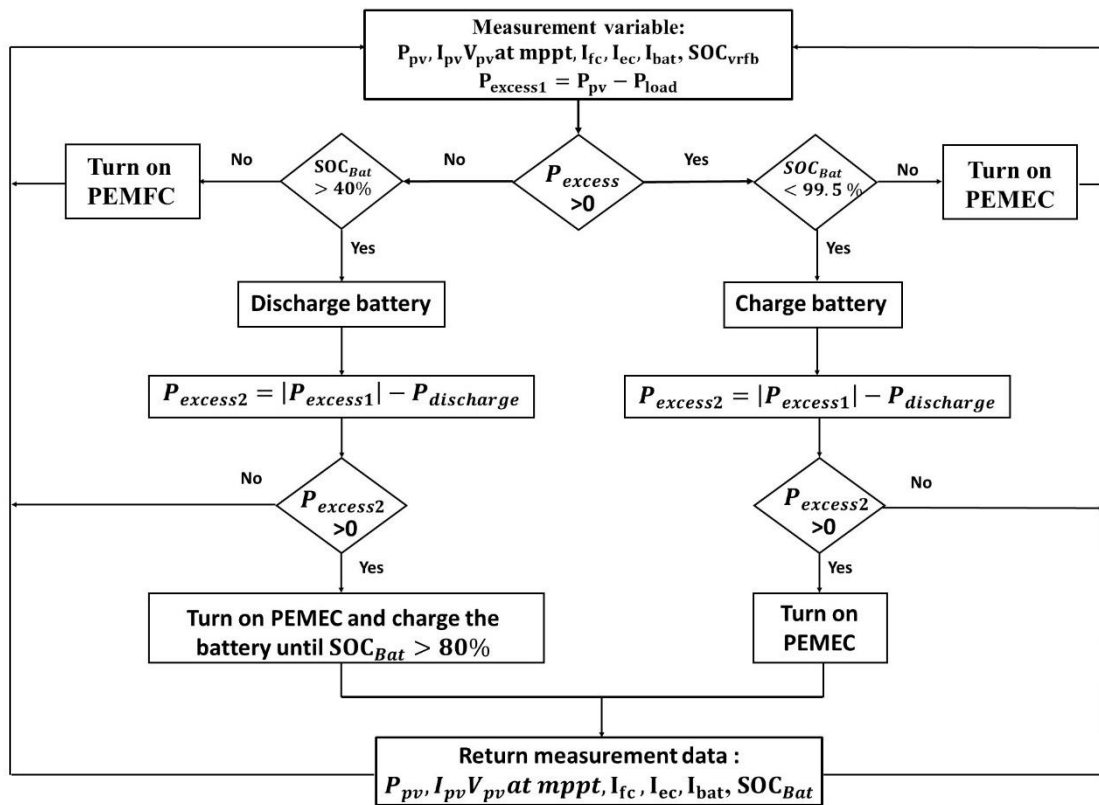
Fig. 5.1 Block schematic of the power management strategy algorithm for the renewable system

Mode 1: $P_{excess} < 0$ and $\mathrm{SOC} > \mathrm{FC_{on}}$

In the case that the electrical power produced from the PV is less than the required load power, the SOC of the battery will be checked. If there is more than the minimum SOC, it will discharge from the battery to load according to the power deficit ($P_{excess} = P_{Bat\_dc}$). Due to the requirement that the battery can supply a maximum current of 40A, the PEMFC will turn on when the required power is greater than the supplied power of the battery ($P_{excess} = P_{Bat\_dc} + P_{FC}$).

Mode 2: $P_{excess} < 0$ and $SOC < FC_{on}$

After the battery continuously discharges the electricity, the SOC decreases until it is below the minimum SOC of 40% (FC_{on}). The battery will stop working and enable PEMFC. The PEMFC usually operates at a maximum power point (MPP) to reduce the loss of electrical energy. If PEMFC can supply more power than the deficit

power required by the load ($P_{FC} > P_{excess}$), the remaining excess power will be used to charge the battery ($P_{FC} = P_{excess} + P_{Bat\_dc}$). PEMFC will be used to charge the battery and will charge the battery continuously until the SOC exceeds the minimum battery activation ($FC_{off} = 0.8$).

Mode 3: $P_{excess} > 0$ and $SOC < 99.5\%$

In the case of excess energy remaining from supplying to the load, it will be used to charge the battery with SOC less than 99.5% to reduce the wear of the battery ($P_{excess} = P_{Bat\_c}$). Same as the discharging of the battery, the battery will able to charge at the maximum current equal to 40A. If there is more power than the power which the battery can accept, PEMEC will be enabled ($P_{excess} = P_{Ec} + P_{Bat\_c}$).

Mode 4: $P_{excess} > 0$ and $SOC > 0.995$

If the battery has been charged until the SOC is approximately 95%, it will stop the charging process and use the remaining excess energy for the hydrogen production using PEMEC for use with fuel cells ($P_{excess} = P_{Ec}$).

In the situation that the battery is discharging and there is still a deficit of power, the PEMFC will be used according to the desired power. The power and voltage of the fuel cell are a function of current density, thus the Newton Raphson method can be used to solve the equation to find the operation point by the following equations.

$$j_{n+1} = j_n - \frac{f(j_n)}{f'(j_n)} \tag{5.4}$$

$$f(j_n) = P_{Fc} - \left(A \times j_n \times V_{cell}(j_n) \times n_{Fc}\right) \tag{5.5}$$

$$f'(j_n) = -\left(\left(A \times V_{cell}(j_n) \times n_{Fc}\right) + \left(j_n \times A \times n_{Fc} \times \left(V'_{cell}(j_n)\right)\right)\right) \tag{5.6}$$

$$V'_{cell}(j_n) = \left(\xi_4 \frac{T}{j_n}\right) + \left(\left(\frac{RT}{2F} \times \frac{1}{j_{max} - j_n}\right)\right) - \left(A \times R_{int}(j_n) + R'_{int}(j_n) \times j_n \times A\right) \tag{5.7}$$

$$R_{int}(j_n) = \frac{181.6I_{mem}\left[1+0.03j+0.062\left(\frac{T}{303}\right)^2(j_n)^{2.5}\right]}{A[\lambda-0.634-3j_n]\exp\left[4.18\left(\frac{T-303}{T}\right)\right]}$$ (5.8)

$$R'_{int}(j_n) = \frac{\left(181.6I_{mem}\left(0.03+\left(0.062\left(\frac{T}{303}\right)^2\right)\times(2.5j_n^{1.5})\right)\right)\left(A[\lambda-0.634-3j_n]\exp\left[4.18\left(\frac{T-303}{T}\right)\right]\right)}{\left(A[\lambda-0.634-3j_n]\exp\left[4.18\left(\frac{T-303}{T}\right)\right]\right)^2}$$

$$-\frac{\left(181.6I_{mem}\left[1+0.03j+0.062\left(\frac{T}{303}\right)^2(j_n)^{2.5}\right]\right)\left(-3A\exp\left(4.18\frac{T-303}{T}\right)\right)}{\left(A[\lambda-0.634-3j_n]\exp\left[4.18\left(\frac{T-303}{T}\right)\right]\right)^2}$$ (5.9)

In the case of PEMEC, the equation can be forming the following equations.

$$f(j_{Ec}) = P_{Ec} - \left(A\times j_{Ec}\times V_{cell}(j_{Ec})\times n_{Ec}\right)$$ (5.10)

$$f'(j_{Ec}) = -\left(\left(A\times V_{cell}(j_{Ec})\times n_{fc}\right)+\left(j_{Ec}\times A\times n_{Ec}\times\left(V'_{cell}(j_{Ec})\right)\right)\right)$$ (5.11)

$$V'_{cell}(j_{Ec}) = -\left(\frac{RT}{n\times F\times j_{Ec}}+\frac{I_{mem}}{\sigma}\right)$$ (5.12)

The hybrid renewable system is simulated in the summer scenario. The simulation is considered for 48 h. FC_{on} and FC_{off} are considered as 40% and 80% respectively and the initial SOC of battery is 85%. The simulation results will provide the profile of solar irradiance, load, battery current, battery voltage, battery SOC, PV power, PEMFC power, and PEMEC power as shown in the following figures.
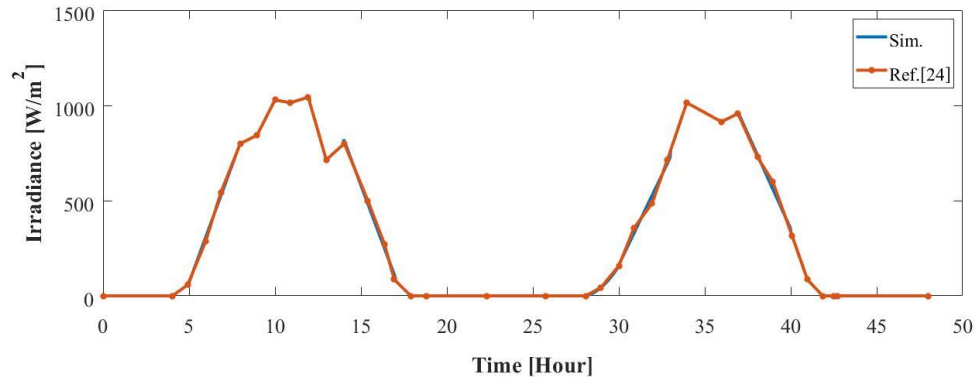
Solar irradiance profile:

Fig. 5.2 Solar irradiance of PV array in a summer scenario
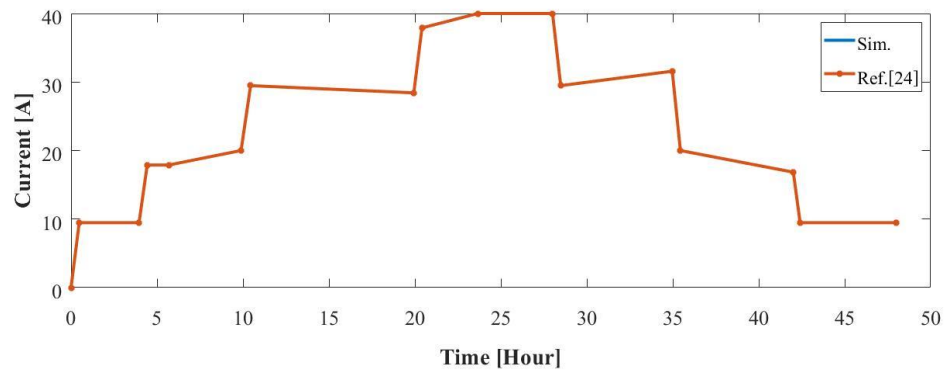
Load current profile:

Fig. 5.3 Load current in a summer scenario
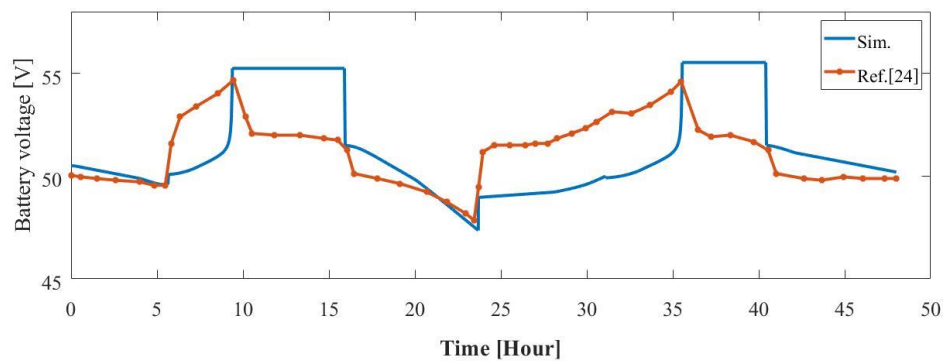
Lead-acid battery operation:

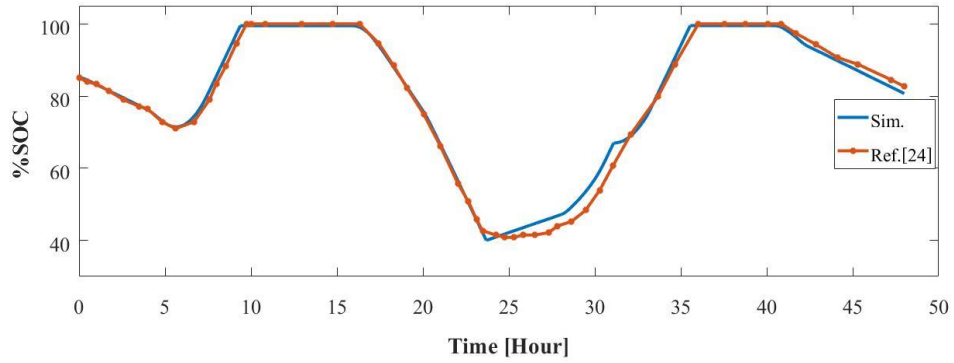Fig. 5.4 Battery voltage in summer scenario at 85% SOC initial

Fig. 5.5 Battery SOC in summer scenario at 85% SOC initial
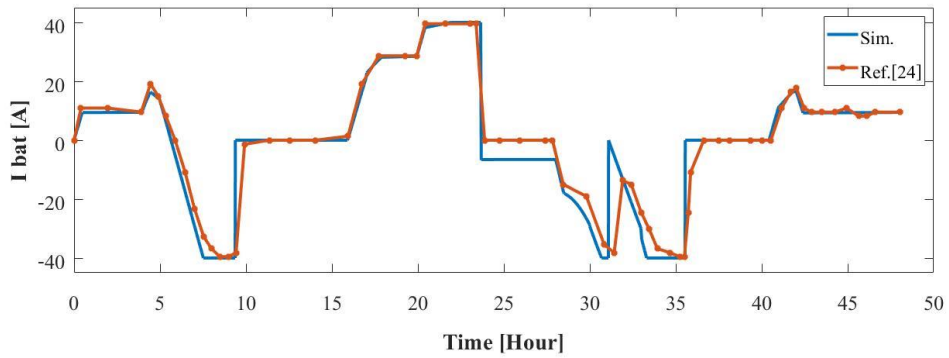

Fig. 5.6 Battery current in summer scenario at 85% SOC initial
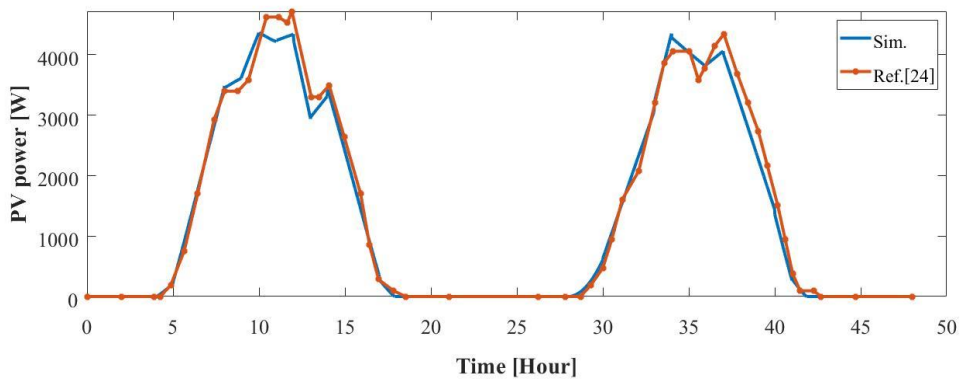
PV power:

Fig. 5.7 PV power in summer scenario at 85% SOC initial
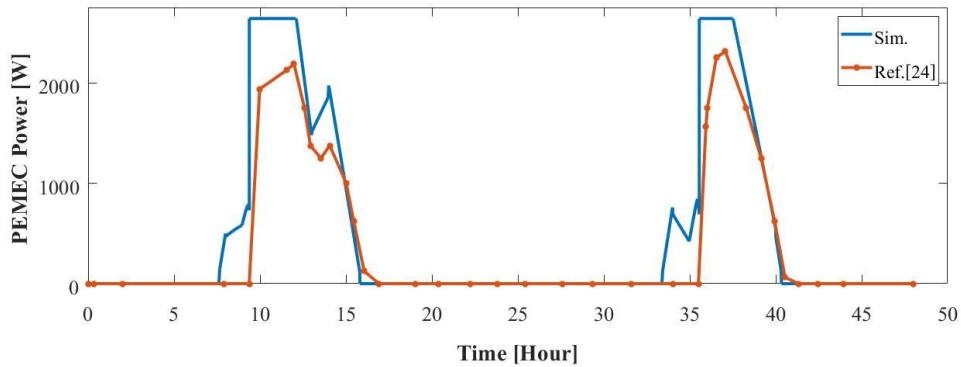
PEMEC power:

Fig. 5.8 PEMEC power in summer scenario at 85% SOC initial

PEMFC power:
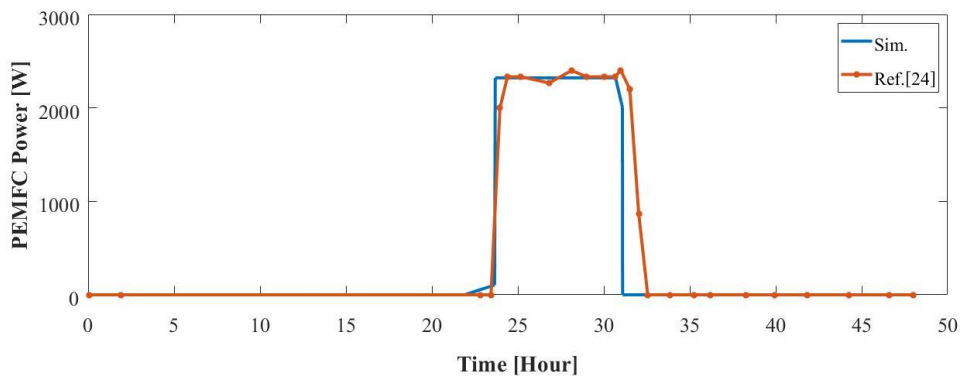
Fig. 5.9 PEMFC power in summer scenario at 85% SOC initial

The simulation results show that although the power management strategy is simplified, it still tends to be in the same direction as reference research and can still manage the system overview. The most inaccurate part is the battery voltage since there is no charge in CV mode but the energy usage during that period is low, almost equal to zero, therefore it does not affect the system much. Since the converter is not simulated, therefore, the energy loss from this equipment is not calculated, resulting in more energy usage in the electrical power produced from PEMFC and the use of energy to produce hydrogen by PEMEC than that of the reference research.

5.3 Using vanadium redox flow batteries instead of lead-acid batteries

In order to test whether VRFB can be used instead of lead-acid batteries and which are better. VRFB models are simulated in the same system. The parameters used in the simulation are shown in Table 5.6.

Table 5.6 VRFB specification

Parameters	Value
Ampere hour rating, (Ah)	400
Number of cells	35
Charging rate	C/10
The volume of half-cell solution, (L)	9.32

The ion imbalance in the VRFB model will be ignored in this part because the lead-acid model is not mentioned in terms of deterioration. This battery is charged and discharged until the battery voltage reaches the upper and lower limits of 1.7 and 1.1 V, respectively. For this reason, the maximum SOC will be fix equal to 87.5% when compared with the operation of the lead-acid battery, causing the operation points are changed as shown in Table 5.7.

Table 5.7 The operation point of VRFB

Parameters	Lead-acid	VRFB
Initial SOC	85 %	72.55%
Maximum SOC	99.95%	87.5%
Minimum SOC	40%	27.55%

The simulation results show the behavior of each component in the system as follows:
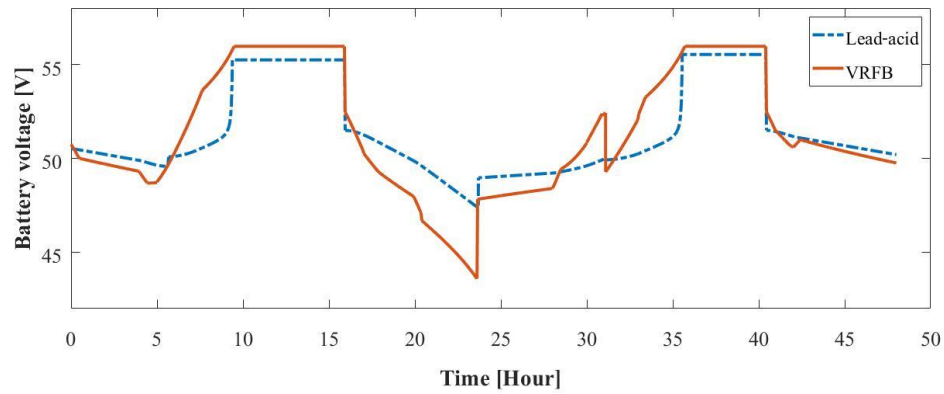

Fig. 5.10 Battery voltage comparison between lead-acid and VRFB in the same condition
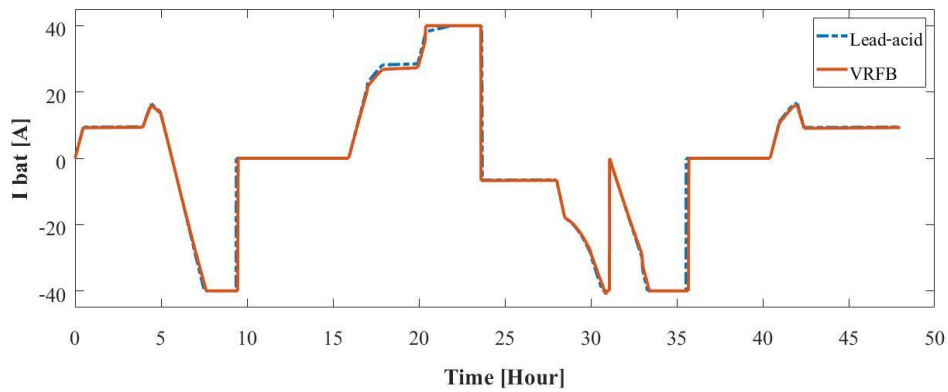

Fig. 5.11 Battery current comparison between lead-acid and VRFB in the same condition
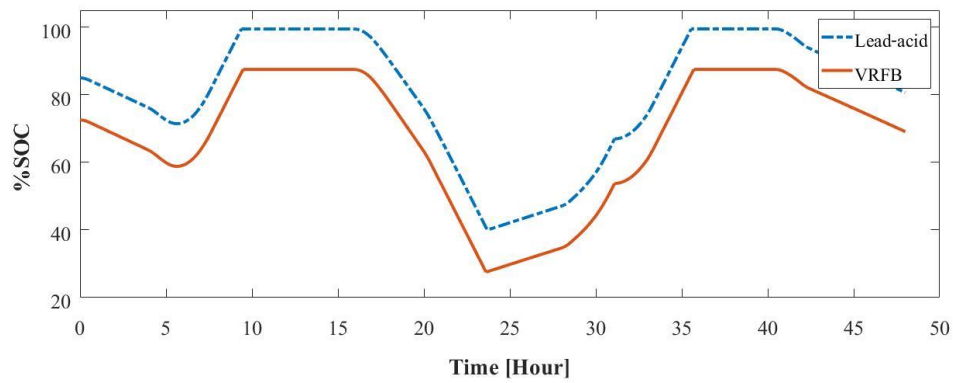
Fig. 5.12 SOC of battery comparison between lead-acid and VRFB in the same condition

Due to the same condition, both types of batteries have similar behavior, which shows that vanadium redox flow batteries can be used instead of lead-acid batteries. But in reality, vanadium batteries can do more than that. VRFB can be used around 90% or more, while lead-acid batteries have a depth of discharge (DoD) around 50-60%. This means that in lead-acid batteries can use only 50-60% of its capacity. Therefore, if compared to the true performance of the vanadium battery, the battery will be able to use longer. The simulation results of energy management systems using VRFB at 80% DoD show the following system behavior.

Battery operation:

Fig. 5.13 Battery voltage comparison between lead-acid and VRFB

Fig. 5.14 Current-voltage comparison between lead-acid and VRFB

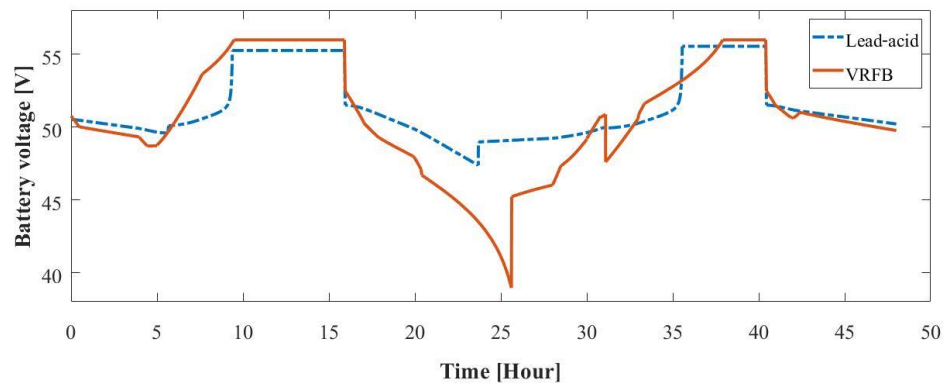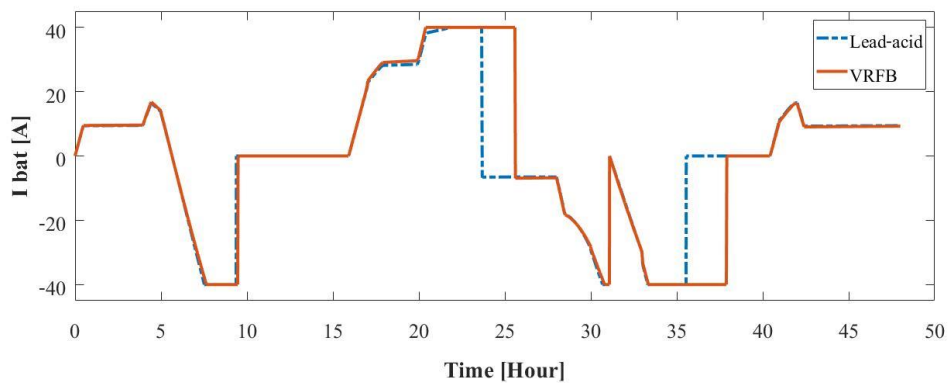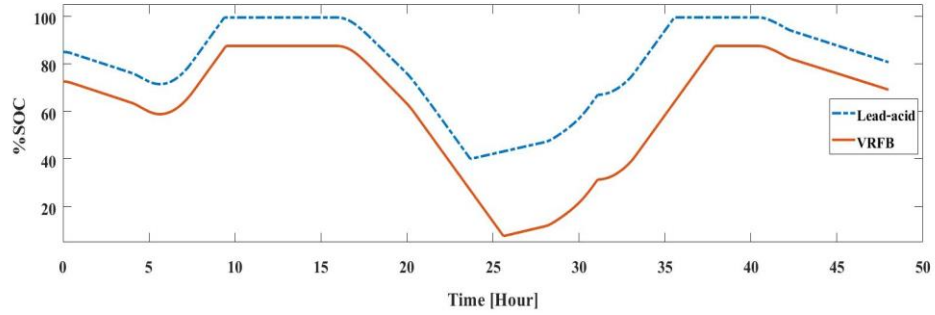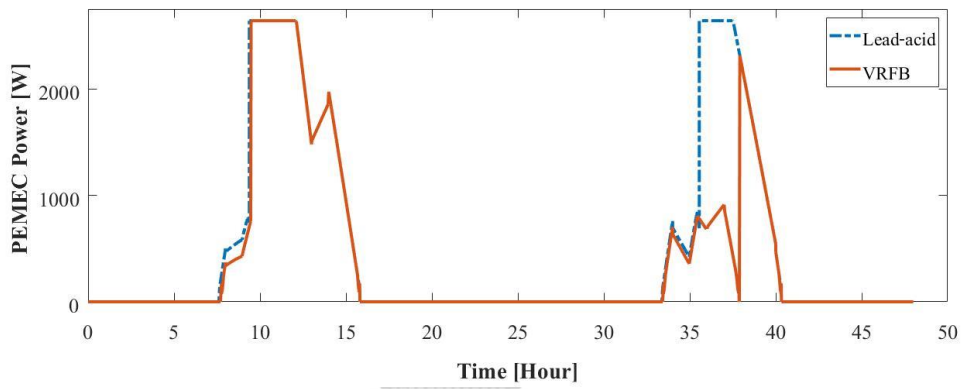Fig. 5.15 SOC of battery comparison between lead-acid and VRFB

PEMEC power:

Fig. 5.16 Power consumed from PEMEC comparison between lead-acid and VRFB

PEMFC power:
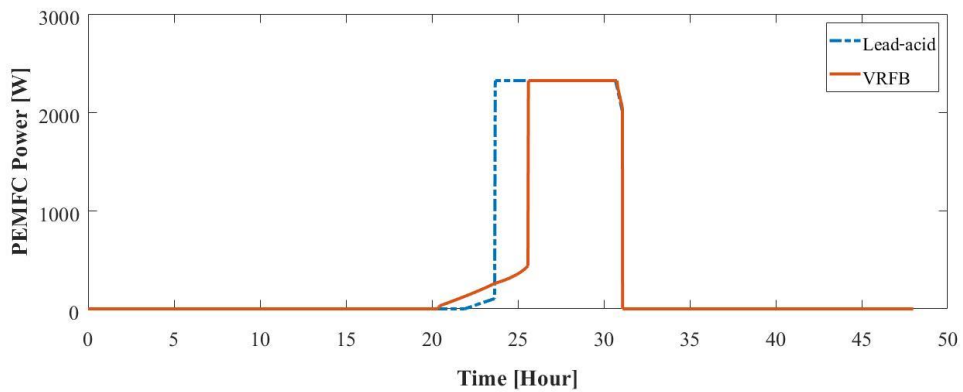
Fig. 5.17 Power produced from PEMFC comparison between lead-acid and VRFB

Table 5.8 Power data for the operation of the comparison energy management system between using lead-acid and vanadium redox flow battery

	Lead-acid system	VRFB system
Battery		
Total charge time (hrs.)	15.61	16.14
Total battery charge power (kWh)	17.64	22.64
Total discharge time (hrs.)	20.98	22.91
Total battery discharge power (kWh)	18.29	21.04
Percentage of operating time	76.22%	81.35%
PEMEC		
Total power (kWh)	23.99	18.83
H_2 production (m^3)	3.58	2.91
PEMFC		
Total power (kWh)	17.22	13.76
H_2 consumption (m^3)	2.86	2.21
Dump load		
Total power (kWh)	1.31	0.75

At the same operating condition, the application of vanadium redox flow battery is almost no difference with the use of lead-acid batteries because we define the exact limits of the equipment. This is a limitation in the operation of lead-acid batteries but the vanadium battery has a wider operating range. This is one of the advantages of vanadium batteries that demonstrate better performance under the same battery specification.

The simulation results at a different operating range of battery show better VRFB performance results in longer service life than lead-acid batteries as a result, the use of PEMEC and PEMFC decreased significantly. The fuel cell usage decreased by 18.35% and electrolysis cell usage decreased by 14.97%. Dump load is the excess

energy produced by PV that exceeds the device limits. From table 5.8 show that systems using vanadium batteries can manage energy in the system more efficiently than using lead-acid batteries.

The number of cycles in the use of lead-acid batteries depends on the depth of discharge (DoD). Considering the battery capacity used in the system, the number of cycles to failure and the amount of lifetime energy throughput are shown in Fig 5.18.

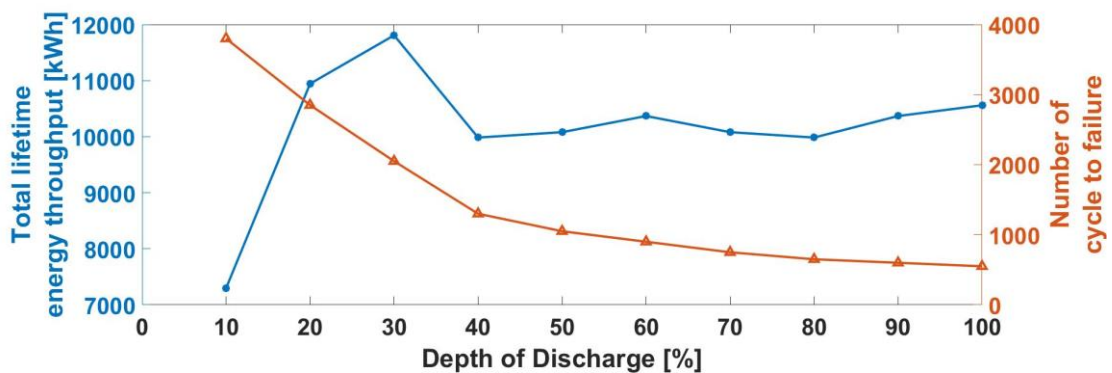Fig. 5. 18Cycles to failure and total energy throughput for lead-acid battery based on reference research

In Dash and Bajpai's research [24], the limit of the lead-acid battery operation is 60% DoD, therefore there are around 900 cycles, while vanadium batteries can operate at 90% DoD and have cycle durability more than 12,000 cycles, which shows that technically, vanadium batteries clearly have better performance.

CHAPTER VI

ANALYSIS OF ENERGY MANAGEMENT SYSTEM UNDER DIFFERENT SOLAR IRRADIANCE PROFILE AND POWER MANAGEMENT STRATEGIES

The effective manage energy management systems is a challenging issue and the solution is developed all the time. The power input from renewable energy generation and the control algorithm used in energy management is the main factors affecting system stability. The first factor arises from the uncertainty of the amount of natural energy that is changing according to the season. As a result, the amount of energy is uneven. The design of the energy distribution system should be consistent with the amount of energy produced. This is the second factor in planning the system for optimal performance. In addition, to the factors mentioned above, the topology used also affects the design of the system. In this study, the isolated topology will be used. Therefore, determining the size of the equipment in the system is another problem that should be considered.

In this chapter, the hybrid power system including PV, PEMFC, PEMEC, and VRFB is used to determine the size of each component to be consistent. This study proposes two types of energy management strategies that are simulated under three different scenarios of solar irradiance. The simulation results will be analyzed for the operating system behavior and the efficiency of the equipment will be discussed.

6.1 Unit-sizing design

The unit-sizing of the hybrid renewable power system method proposed in Wang and Nehir's research [108]. The purpose of unit-sizing is to properly size the components to guarantee reliable power distribution. Hence, an economic perspective is not considered in this work. This hybrid power system is designed for one household resident in Nakhon Pathom province, Thailand, according to sources of solar irradiance data. In determining the size of the components, it is based on the load demand profile shown in Fig 6.1.
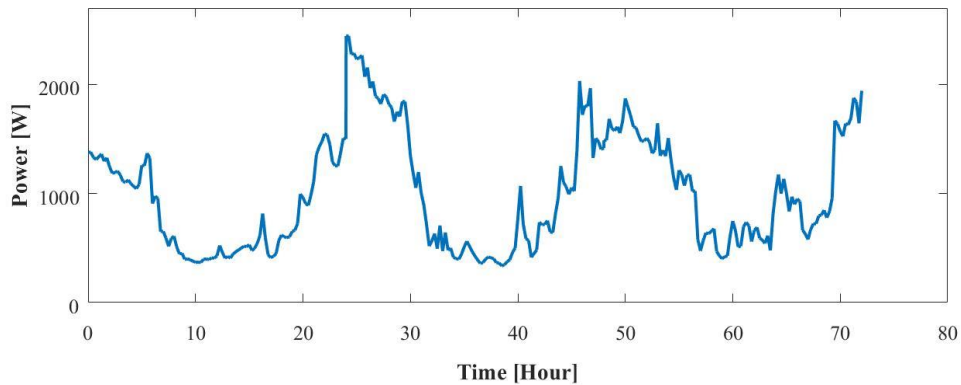
Fig. 6.1 load demand for one household resident

The peak power of load demand is approximately 2.5 kW. The following sizing procedure is used to determine the size of the PV arrays, which will design the power of the PV in twice the peak load. PEMFC must be designed to be able to support during peak loads in the even that electricity cannot be generated from PV arrays, so 2.5 kW of PEMFC is used. Then, the size of PEMEC can be calculated from the difference between available excess power and load demand. It is about 4 kW. The last unit is vanadium redox flow batteries. it must have sufficient power in the case of deficit power where the average power is less than 2 kW. The design for a battery capable of supplying 2kW of power is sufficient to meet the load requirements. The other information about each unit other than PEMEC can be shown in the previous chapter as Table 5.1,5.2 and 5.4. For PEMEC, data specification will be changed form Table 5.3 slightly, by increasing the number of cells to 15 cells.

6.2 Power management strategies

The basic objective of an energy management strategy is to be able to supply the energy according to the energy balance requirements. The algorithm used is simple as shown in Fig. 6.4. In the first step, the user will measure the power produced by PV and electrical load power. The availability of excess power will always charge the battery first if the state of charge (SOC) is between the minimum and maximum values. If there is more power than the battery can charge, it will be dump load to avoid overcharging. In the case of $SOC > SOC_{max}$, the algorithm checks that the excess power is between the minimum and maximum power, the system will supply excess

power to enable PEMEC. If $P_{excess} < P_{elec\_min}$ the available power is used to charge the battery or take to dump load. If $P_{excess} > P_{elec\_max}$ the electrolysis cells will operate at its maximum power. In the case of an energy shortage, the battery will discharge to the system. If the required power is more than the battery can supply, it will activate the PEMFC to compensate for the lack of power. If the state of charge (SOC) is lower than the minimum value, the power from the fuel cells will be supplied to meet the demand.

The example of simulation results shown in Fig 6.2. It shows that the algorithm can supply electrical power according to power balance. However, when considering the behavior of PEMFC, it can be seen that there is an irregular operation and the performance is not fully effective as shown in Fig 6.3.
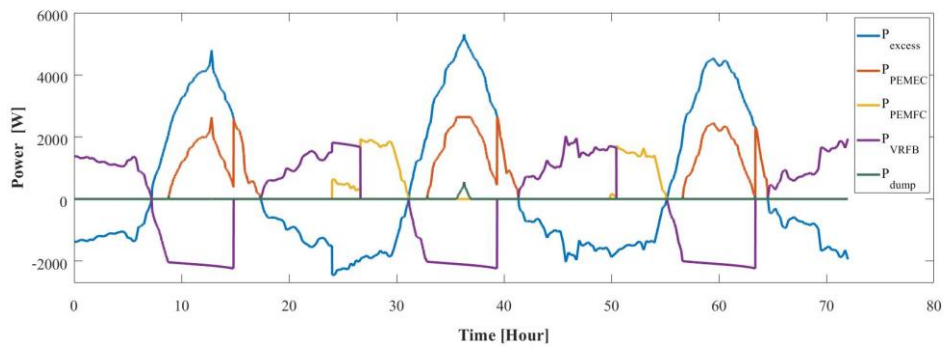

Fig. 6.2 System response for three-day simulation with simple strategies
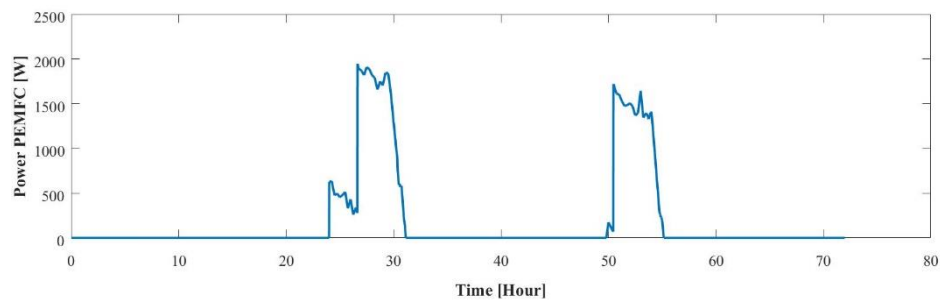

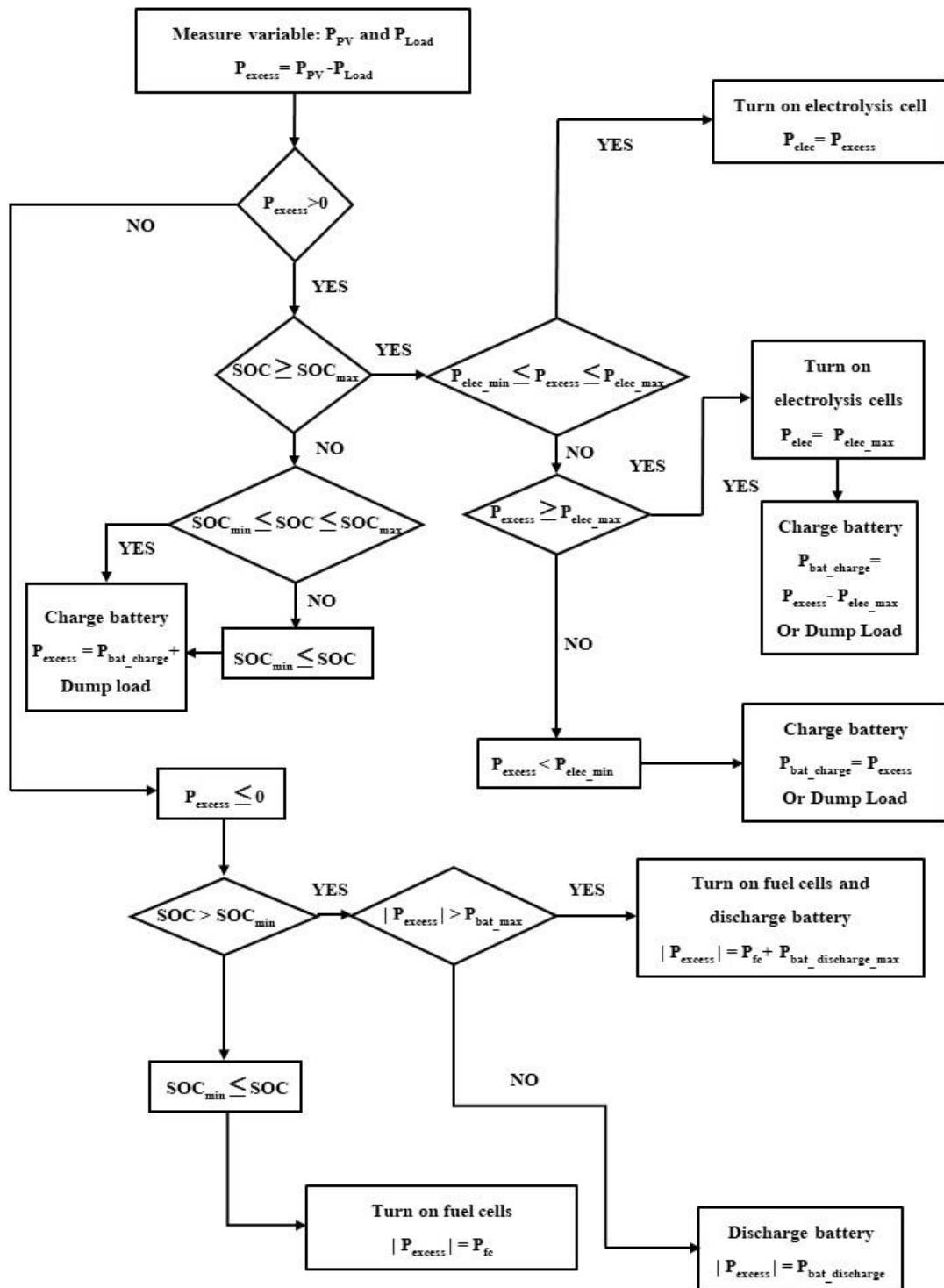Fig. 6.3 Operating behavior of PEMFC with simple strategies

Fig. 6.4 The simple energy management strategies

PEMFC operations at low power are difficult to control due to the nonlinear behavior of the fuel cell and the excess power that is not being used remains (dump

load). Therefore, leads to the development of energy management strategies to make the system more efficient and with less dump load.

To reduce the mentioned problems can be done by adding an algorithm related to fuel cell operations and eliminating dump load. The first energy management strategy proposed is shown in Fig. 6.5. PEMFC will operate with constant power at the maximum power point (MPPT). If $P_{excess} < 0$ and $SOC > SOC_{min}$, the algorithm will predict the maximum power discharge form battery. If there is more power required than maximum discharge power and maximum rated power from PEMFC, the fuel cell will be enabled and the battery will supply the power to compensate for the missing part. If less, then the remaining power from PEMFC will be used to charge the battery. If $SOC < SOC_{min}$, then the fuel cell provides the power to meet the load demand and will be charged the battery if there is excess power. The fuel cell will be operated until the SOC is greater than the specified value (70%).

The minimum power for PEMEC is determined at approximately 25% of the maximum capacity, so there is a chance that the excess power remaining is below the minimum. This will cause this energy part which is not used (dump load). The battery will provide the power that is required to reach the electrolysis cell to operate at the lowest available power, P_{elec_min}. The second energy management strategy is developed to increase the power consumption of electrolysis cells by discharge the battery in the case of excess power less than the minimum power of the electrolysis cell. The control scheme is shown in Fig. 6.6.
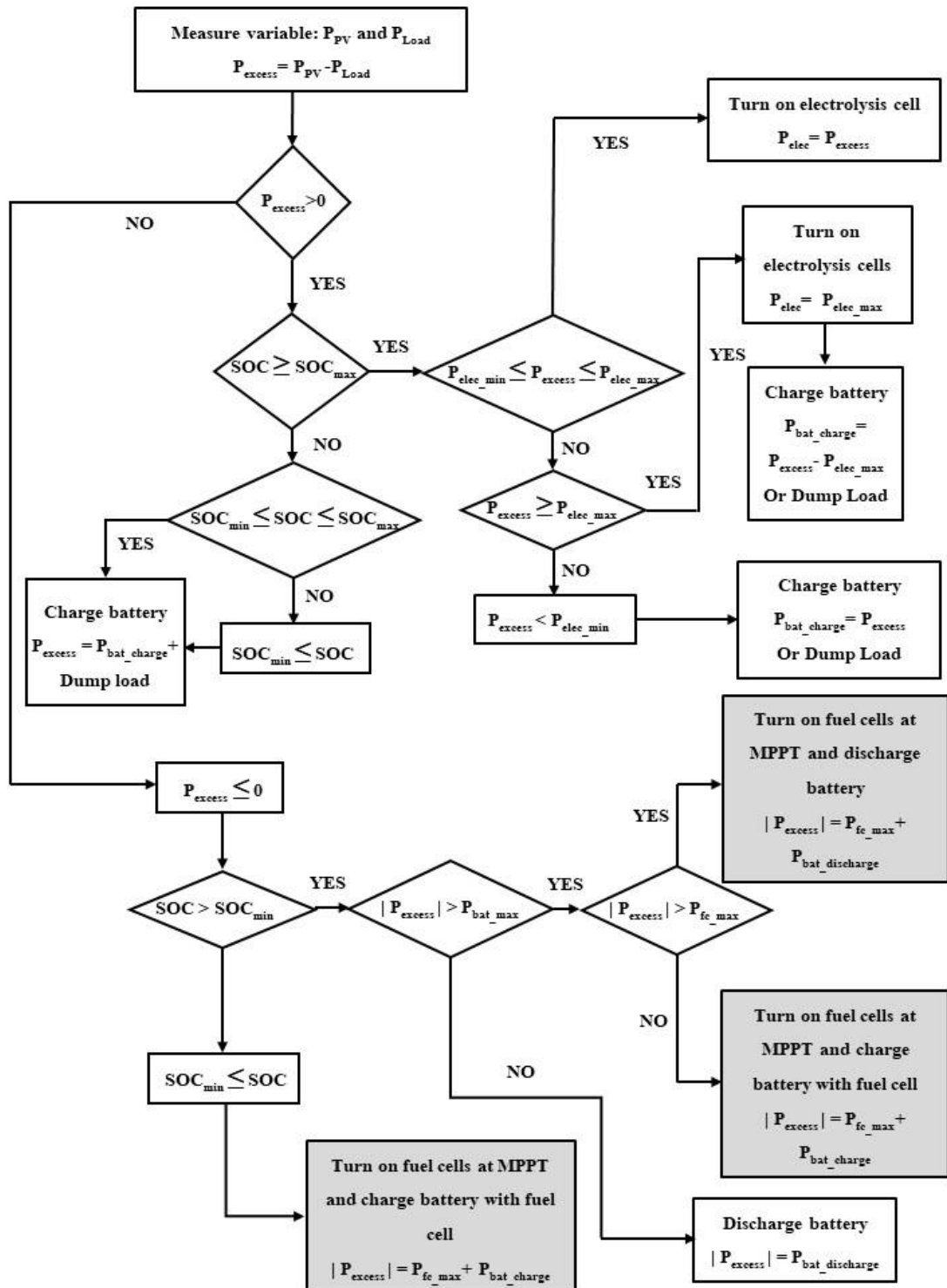
Fig. 6.5 Block diagram for EMS1
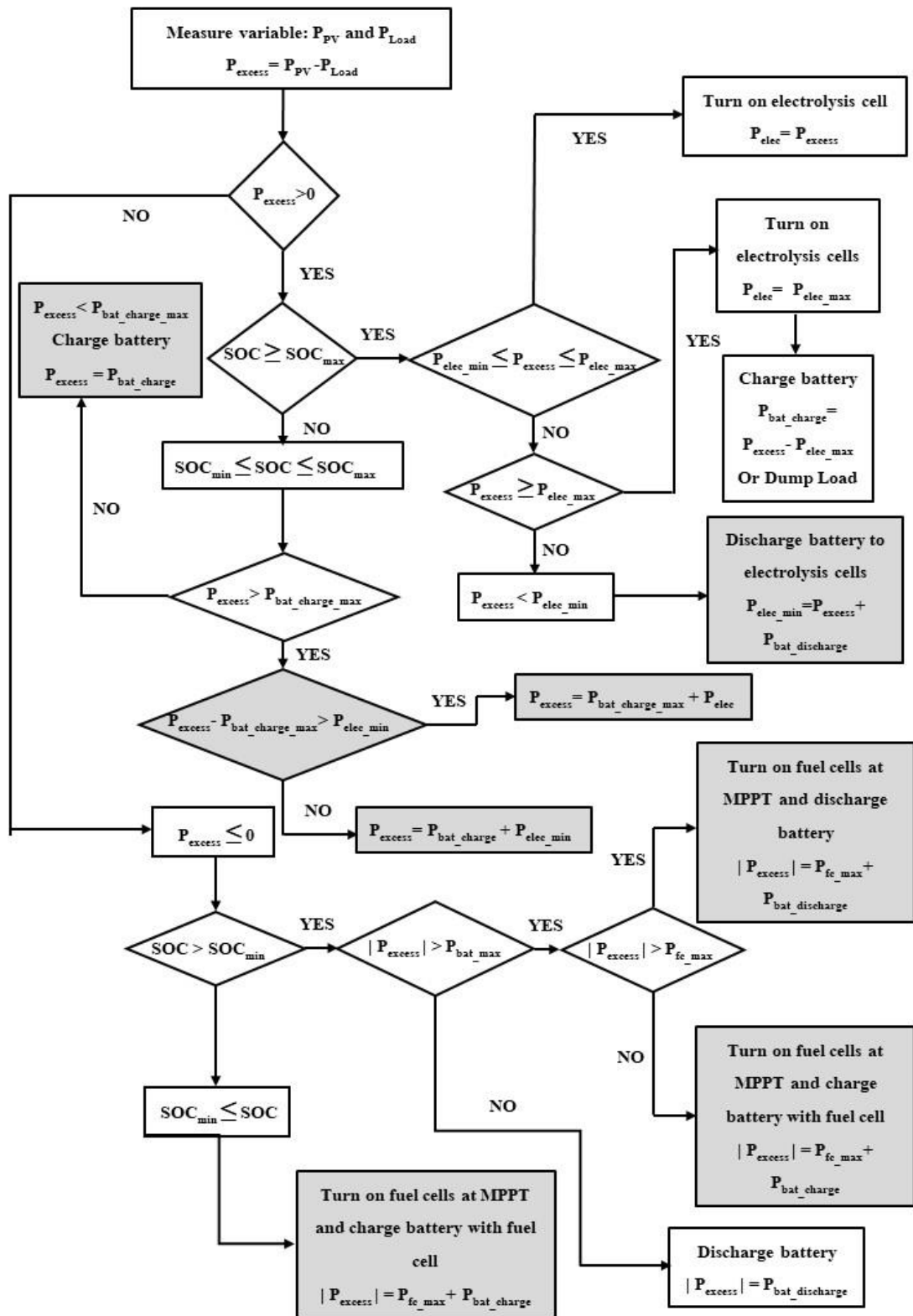
Fig. 6.6 Block diagram for EMS2

6.3 Solar irradiance profile

The solar irradiance profile in Thailand is used in this study, which has different solar irradiance forms in each season. In the summer, the maximum solar radiation is around $1000\,\mathrm{Wm}^{-2}$. In the winter, the maximum solar radiation is around $800\ \mathrm{Wm}^{-2}$. In the rainy season, there will be fluctuation in the pattern of solar irradiance. The solar profile in each scenario used in the simulations is shown in Figs. 6.7-6.9.
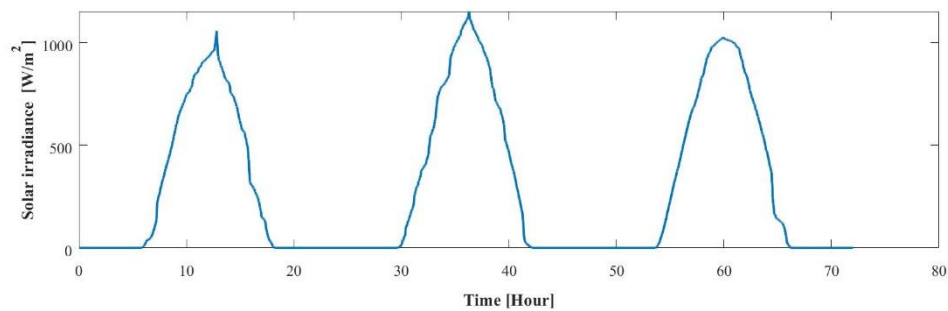
Fig. 6.7 Solar irradiance profile in a typical summer scenario
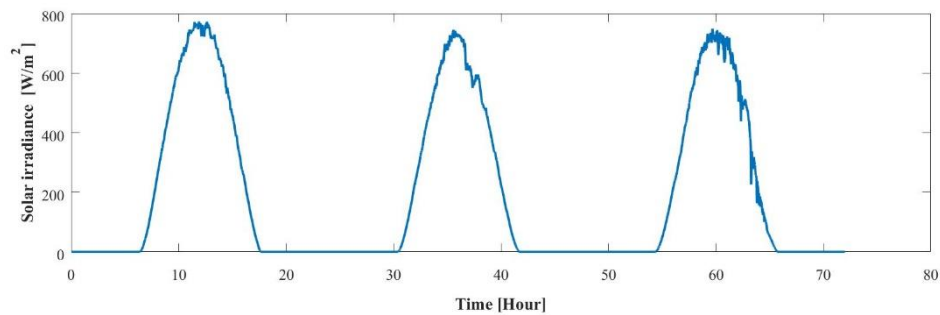
Fig. 6.8 Solar irradiance profile in a typical winter scenario
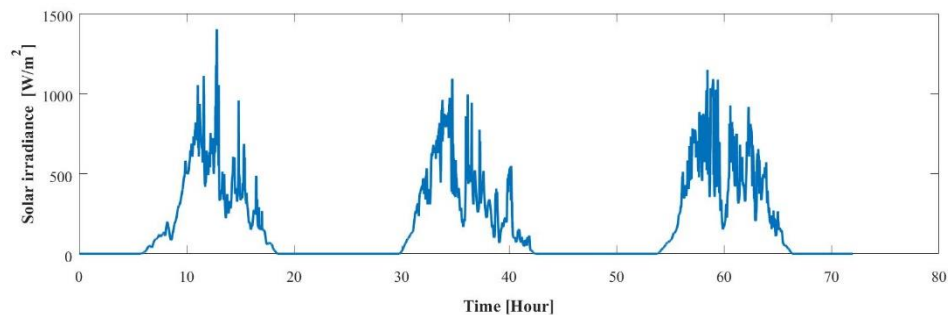
Fig. 6.9 Solar irradiance profile in arbitrarily varying weather scenario

6.4 Simulation results

The hybrid power system is simulated under two different energy management strategies and three scenarios. The simulation is considered for 72 hours to study the behavior of each unit and analyze the overall efficiency of the system which shows the following results.

Summer scenario:

The form of PV power has a similar form of power, which will increase gradually until midday to the highest value and will decrease to zero in the early hours. When calculating the deductions for load demand, it will be found that excess power is highest on the second day of operation at 5300 W and there is a maximum deficit power at 2400 W. From the simulation using the first proposed energy management strategy, the battery SOC is set at 72.5% or 80% of the maximum state of charge (90.6%). VRFB discharge in 0th -7.2th hours because PV arrays are unable to generate electricity during the night. When the sun is rising, the PV system can be produced electric power to meet the load demand. Until the power is more than the demand, then the battery is charged to store excess power. PEMEC will be used to produce hydrogen, which will be turned on when there is excess power remaining from battery charging or the battery SOC reach to the highest point at 7.2^{th}-14.8^{th} hours and 14.8^{th} – 17.3^{th} hour respectively. On the second day, there was more demand for electricity than the battery could afford. PEMFC is enabled by operating at the maximum power point at 24th – 31.3th hours. In the simulation of other times of the day, there is a behavior to the one mentioned above is shown in Fig. 6.10.
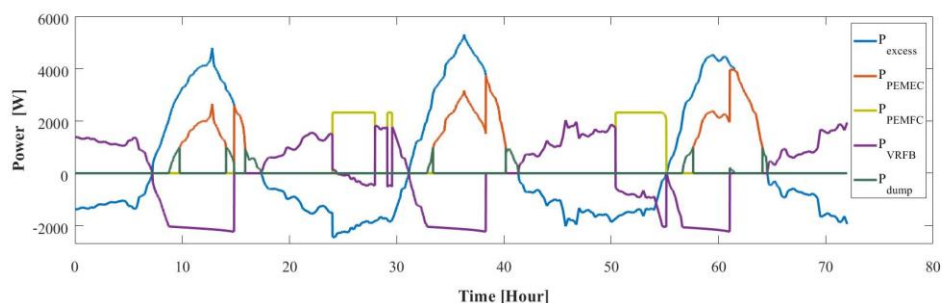
Fig. 6.10 System response for three-day simulation with EMS1 in summer scenario

When compared to the results of the second strategy simulation, the amount of excess energy that is not used (dump load) is reduced. The algorithm manages by supplying extra energy from the battery discharging providing enough power to reach the minimum power to enable PEMEC. The simulation result is shown in Fig. 6.11.
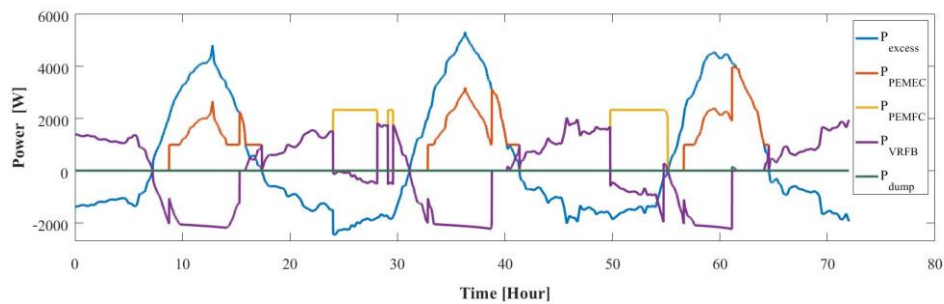
Fig. 6.11 System response for three-day simulation with EMS2 in summer scenario

Fig. 6.12 shows the state of charge in each strategy. It is found that the battery can store energy at full capacity every simulation day. The first strategy has a longer period of a state of charge at a maximum point than the second strategy, on the other hand, the second strategy has a longer battery operation time than the first. However, the simulation results show that the energy management strategy can handle the system with stability.
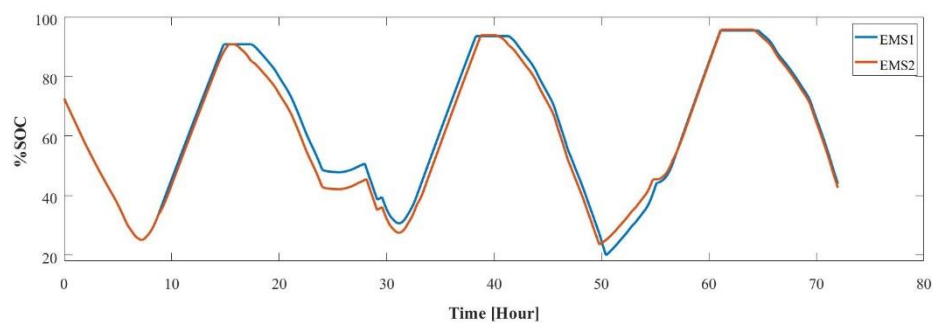
Fig. 6.12 State of charge of the battery in the summer scenario

Winters scenario:

Due to the reduction of solar irradiance, the power produced from PV also decreased. When considering the amount of excess power, it was found that the maximum power was 3300 W on the first day of the simulation and the use of fuel cells and battery in the winter scenario are longer than that in the summer scenario. In the first energy management strategy, there is a large amount of excess power which is not

being used because the power is too small to enable PEMEC. The simulation results of the first strategy are shown in Fig. 6.13.
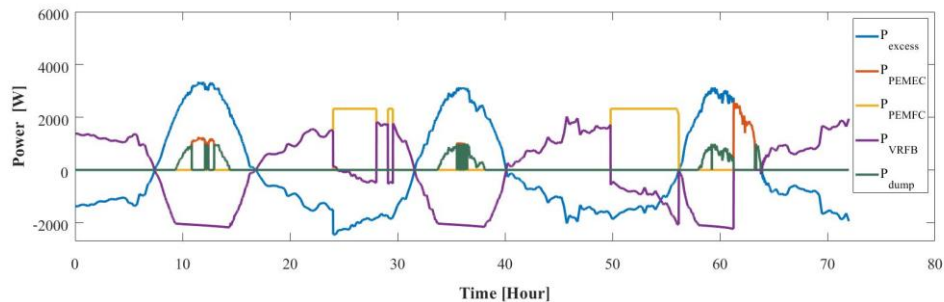
Fig. 6. 13System response for three-day simulation with EMS1 in winter scenario

In the second strategy, the dump load is completely eliminated by reducing the power for battery charging to provide sufficient power to enable PEMEC at the minimum point. The simulation results of the second strategy are shown in Fig. 6.14.
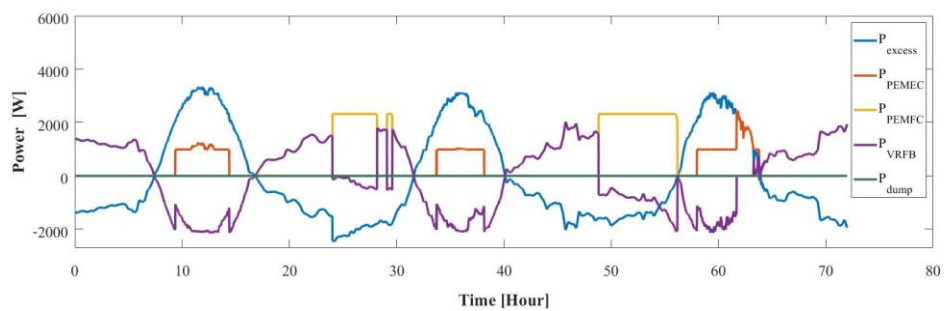
Fig. 6.14 System response for three-day simulation with EMS2 in winter scenario

The state of charge in winter is similar to summer but cannot reach a peak in the first two days, there is a maximum state of charge of more than 80%. However, on the third day of simulation, the battery was able to store energy at full capacity because the battery is discharged until the state of charge decrease to the minimum point at around the 50th hour, then the algorithm activates PEMFC to supply power to the system and charge battery until the right point to disable PEMFC (60% SOC). The SOC result is shown in Fig. 6.15.
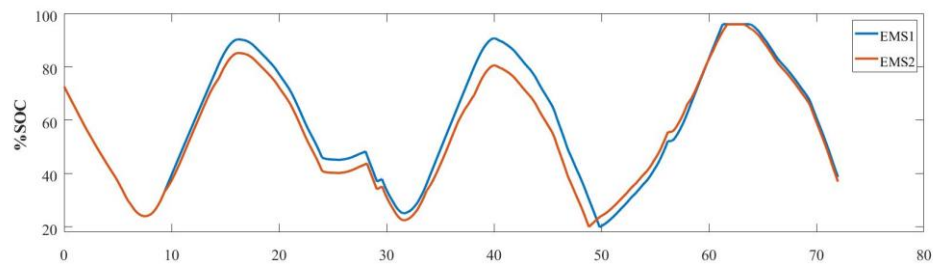
Fig. 6.15 State of charge of the battery in the winter scenario

Arbitrarily varying weather scenario:

In this scenario, the solar irradiance profile is highly inversion. This profile incorporates all possible formats of irradiance such as sudden changes, gradual rise, and fall, which illustrates the actual situation of solar radiation. The amount of excess energy varies with the electrical power from PV, causing some periods to have excess power, some periods lacking power. The vanadium redox flow batteries change the operating mode more often. In the 24th-30th hours, PEMFC stacks are frequently switched on/off, which can damage the long-term operation of fuel cells. In the first strategy, the behavior of each unit is shown in Fig. 6.16. The amount of dump load is low spread over many periods. In most cases, it is caused by insufficient energy to enable and frequent operations on/off of PEMEC.
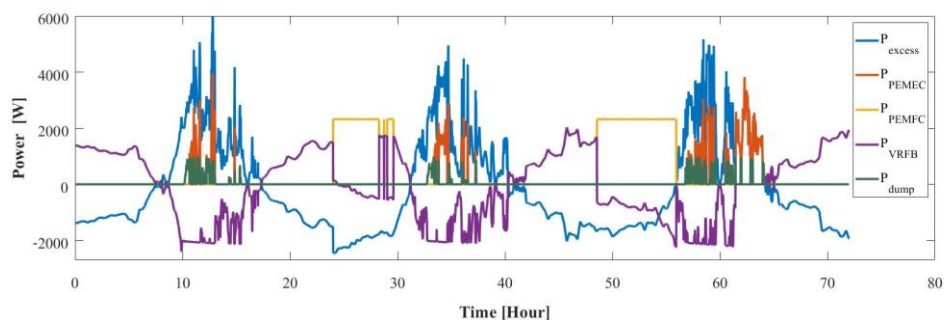
Fig. 6.16 System response for three-day simulation with EMS1 in arbitrarily varying weather scenario

In the second strategy, the algorithm can reduce the frequent on/off of PEMEC operation and the amount of dump load. The remaining dump load is caused by fluctuation in weather conditions causing the solar irradiance to be unusually high, which makes the capacity of PEMEC not enough to support. The simulation results of the second strategy can be shown in Fig. 6.17.
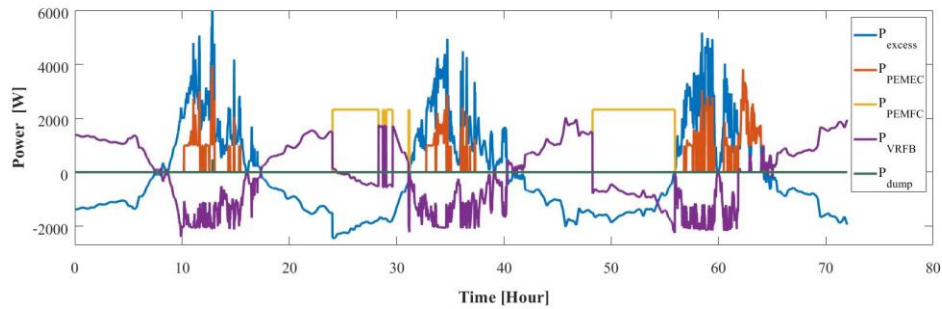
Fig. 6. 17System response for three-day simulation with EMS2 in arbitrarily varying weather scenario

In the operation of VRFB, the system manages at lower reliability than the previous two situations, there is a maximum state of charge of lower than 80% in the first two days. It will require more power for hydrogen production technology. However, the power supply to the load is still continuous by a combination of PV, PEMFC, and VRFB. The SOC result is shown in Fig. 6.18.
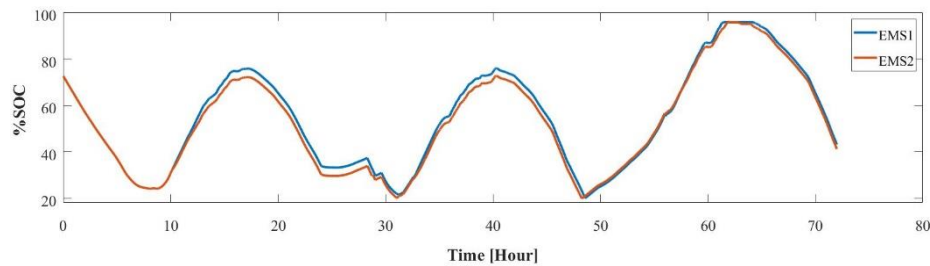
Fig. 6.18 State of charge of the battery in the arbitrarily varying weather scenario

Table 6.1 shows the analysis results of each subsystem in all energy management systems studied. When comparing the two strategies, it is found that the algorithm used in the second strategy allows every subsystem to have more operating time in every scenario which has advantages and disadvantages depending on each situation. In the summer scenario, VRFB usage is 87.36% in the first strategy and 93.13% in the second strategy. The operation increases by 7% while the hydrogen produced from PEMEC can increase slightly compared to the total amount of hydrogen produced. The amount of hydrogen used in PEMFC is less than hydrogen produced from PEM. Therefore, there is no need to take advantage of the dump load. In the winter scenario, VRFB is used almost all the time and a small increase in EMS2 but it can cause PEMEC to operate at its minimum point. The amount of hydrogen produced by

PEMEC increase 2.7 times in the second strategy and the dump load is completely eliminated. PEMFC energy consumption increases from 25.17 kWh to 27.88 kWh. From the amount of hydrogen deficit from PEMEC and PEMFC shows that the EMS 2 helps the system to be more stable and able to perform for longer. In arbitrarily varying weather scenarios, there is more excess energy in the winter but the energy changes suddenly. The amount of energy does not correspond to the behavior of all of each subsystem as described above. The results of the amount of hydrogen produced is a deficit when compared to the hydrogen consumed. PEMFC and PEMEC are frequently switched on and off. EMS2 can help solve PEMEC problems, but the problem still remains with PEMFC.

Two different energy management strategies for a hybrid renewable power system consisting of power generation from PV, hydrogen production technologies and vanadium redox flow batteries as an alternative to energy storage have been developed. EMS 1 resulted in less operation time than EMS 2. However, EMS 2 is considered an advantage in terms of the increase in hydrogen production. Moreover, the algorithm would guarantee the smooth operation with less frequent start-ups and shut-downs of PEMEC operation. EMS 1 would be sufficient for management in a situation of high excess energy as summer scenario which available for long-term operation. In contrast, in the situation where there is not enough excess power such as winter scenario, EMS 2 is a good choice to handle with high frequent start-ups and shut-downs problem. For the arbitrarily varying weather situation, both types of energy management strategies are not sufficient to deal with problems. It requires additional operating conditions, such as the minimum power setting to disable PEMFC once it has started or increased the battery capacity to support more operations.

Table 6.1 Power data for the operation of the subsystem for three-day simulation

	Summer		Winter		Arbitrarily varying weather	
	EMS1	EMS2	EMS1	EMS2	EMS1	EMS2
Battery						
Total charge time (hrs.)	29.43	31.23	33.47	35.05	35.45	36.37
Total battery charge power (kWh)	44.99	45.13	45.75	42.89	40.44	39.32
Total discharge time (hrs.)	33.47	35.82	36.02	35.37	33.77	33.78
Total battery discharge power (kWh)	37.50	37.43	38.45	36.71	33.93	36.71
Percentage of operating time	87.36%	93.13%	96.50%	97.80%	96.13%	97.43
PEMEC						
Total power (kWh)	40.85	45.56	9.81	25.10	14.76	21.45
H_2 production (m^3)	6.40	6.78	1.53	4.04	2.21	3.23
Percentage of operating time	25.86%	34.84%	6.1%	21.20%	7.5%	14.1%
PEMFC						
Total power (kWh)	21.21	23.07	25.17	27.88	28.48	29.68
H_2 consumption (m^3)	3.38	3.70	4.05	4.50	4.61	4.81
Percentage of operating time	12.71%	13.82%	15.07%	16.69%	17.04%	17.75%
Dump load						
Total power (kWh)	3.82	0.04	6.38	0	2.65	0.01

From suggestions to solve the toggle start-ups and shut-down problems, the algorithm that is used to solve this problem was developed. When PEMEC was enabled, the order of equipment selection has changed by requiring the PEMEC to be decided before the vanadium redox flow battery. Like the operation of PEMFC, once it was turned on, the fuel cell will be used until there was power left in the system. The simulation result of each subsystem was shown in Fig. 6.19.
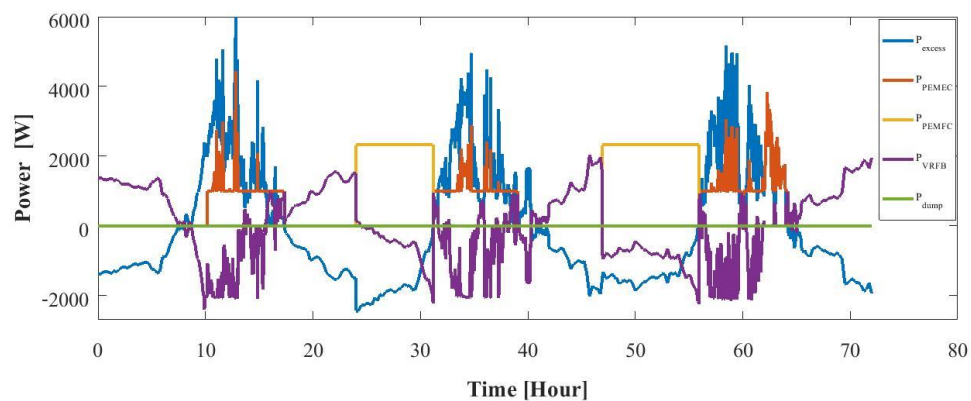

Fig. 6.19 System response for three-day simulation with suggested EMS in the arbitrarily varying weather scenario

From Fig. 6.19, it showed the smooth operation of PEMFC and PEMEC. However, the operation of the vanadium battery was volatile due to the operation of other devices. The capacity of the battery needs to be increased slightly to support more than normal use.

CHAPTER VII
CONCLUSIONS AND RECOMMENDATIONS

7.1 Conclusions

Vanadium redox flow batteries have been proposed for use in renewable energy management systems together with photovoltaic cell (PV), proton exchange membrane fuel cell (PEMFC) and proton exchange membrane electrolysis cell (PEMEC). The simulation was performed by comparing it with a conventional power system using lead-acid batteries in the same situation. The mathematical model of each subsystem is verified and validated with reference data before being used for energy management systems and get consistent results. The simulation of energy management systems with different types of batteries yields satisfactory results. Vanadium redox flow batteries have better performance and operating range, resulting in increased battery usage which reduces the use of other devices.

In a non-grid connected energy management system, there are three factors, consisting of the size of each unit in the system, the amount of incoming energy from renewable energy sources and the algorithm used in the energy management strategy. In unit-sizing design, we have used the method as Wang and Nehir's research [108]. The 5 kW PV arrays are set to support a peak load of 2.5 kW. Vanadium batteries, PEMFC and PEMEC is set to 400 Ah, 2.5 kW, and 4 kW respectively so that the system can operate without interruption. The input energy is produced from PV arrays based on solar irradiance which changes with the seasons. We divide the simulation into three situations according to the intensity of the radiation and climate in Thailand. In the first situation is the summer with the highest solar irradiance at 1000 W/m^2. In the second situation is the winter with the highest solar irradiance around 800-900 W/m^2. In the final situation is rainy which the irradiance profile is unstable and there is a sudden change. The energy management strategies proposed in the research are two different forms based on the operating requirement of PEMEC. In the second EMS, it is determined that there is enough power to operate at the minimum point of PEMEC by supplying from the battery discharging. The simulations of two strategies and three situations were analyzed for stability and possibility to find suitable strategies.

The simulation results are satisfactory, with appropriate strategies in the summer and winter scenarios. The different strategies result in changing operation times, which the second strategy will increase each subsystem's operation. In the summer, there is a lot of excess energy to make the system stable, so there is no need to use a second strategy while in the winter there is low excess energy causing a lot of dump load in each period that is not enough to enable PEMEC. The use of the second strategy helps to produce more hydrogen and eliminate excess energy that is not being consumed and helps the operation smoothly. For the rainy season, the proposed energy management strategies can be managed but not as good as it should due to frequent switching on and off problem in PEMFC and PEMEC. The second strategy can be solved in the PEMEC operation but in PEMFC, the additional conditions must be established in order to improve system stability.

7.2 Recommendations

7.2.1 In order to make the system more efficient in terms of energy and lifespan of the equipment, the optimization problems needs to be developed   to find operating conditions that can lead to optimal energy use for each device and increase the equipment life time.

7.2.2 The converter and flow delay should be calculated in the system so that the energy can be tracked accurately.

7.2.3. The simulation of long-term operations should be further studied to show the deterioration of each equipment, including economic aspect to select the most suitable device for operate in hybrid power system.

REFERENCES

[1]. Massoud Amin S. Smart Grid: Overview, Issues and Opportunities. Advances and Challenges in Sensing, Modeling, Simulation, Optimization and Control. European Journal of Control. 2011;17(5-6):547-67.

[2]. Hossain MS, Madlool NA, Rahim NA, Selvaraj J, Pandey AK, Khan AF. Role of smart grid in renewable energy: An overview. Renewable and Sustainable Energy Reviews. 2016;60:1168-84.

[3]. BP p.l.c. [online]. 2018 Jun 1st [cited 26 Jan 2019];Available from: URL: https://www.bp.com/content/dam/bp/business-sites/en/global/corporate/pdfs/energy-economics/statistical-review/bp-stats-review-2018-full-report.pdf.

[4]. Guinot B, Champel B, Montignac F, Lemaire E, Vannucci D, Sailler S, et al. Techno-economic study of a PV-hydrogen-battery hybrid system for off-grid power supply: Impact of performances' ageing on optimal system sizing and competitiveness. International Journal of Hydrogen Energy. 2015;40(1):623-32.

[5]. Karami N, Moubayed N, Outbib R. Energy management for a PEMFC–PV hybrid system. Energy Conversion and Management. 2014;82:154-68.

[6]. Garcia P, Garcia CA, Fernandez LM, Llorens F, Jurado F. ANFIS-Based Control of a Grid-Connected Hybrid System Integrating Renewable Energies, Hydrogen and Batteries. IEEE Transactions on Industrial Informatics. 2014;10(2):1107-17.

[7]. Zervas PL, Sarimveis H, Palyvos JA, Markatos NCG. Model-based optimal control of a hybrid power generation system consisting of photovoltaic arrays and fuel cells. Journal of Power Sources. 2008;181(2):327-38.

[8]. Wu W, Christiana VI, Chen S-A, Hwang J-J. Design and techno-economic optimization of a stand-alone PV (photovoltaic)/FC (fuel cell)/battery hybrid power system connected to a wastewater-to-hydrogen processor. Energy. 2015;84:462-72.

[9]. Behzadi MS, Niasati M. Comparative performance analysis of a hybrid PV/FC/battery stand-alone system using different power management strategies and sizing approaches. International Journal of Hydrogen Energy. 2015;40(1):538-48.

[10]. Torreglosa JP, García P, Fernández LM, Jurado F. Energy dispatching based on predictive controller of an off-grid wind turbine/photovoltaic/hydrogen/battery hybrid system. Renewable Energy. 2015;74:326-36.

[11]. Zhang F, Thanapalan K, Procter A, Carr S, Maddy J, Premier G. Power management control for off-grid solar hydrogen production and utilisation system. International Journal of Hydrogen Energy. 2013;38(11):4334-41.

[12]. Kaundinya DP, Balachandra P, Ravindranath NH. Grid-connected versus stand-alone energy systems for decentralized power—A review of literature. Renewable and Sustainable Energy Reviews. 2009;13(8):2041-50.

[13]. Singh GK. Solar power generation by PV (photovoltaic) technology: A review. Energy. 2013;53:1-13.

[14]. Joshi P, Arora S. Maximum power point tracking methodologies for solar PV systems – A review. Renewable and Sustainable Energy Reviews. 2017;70:1154-77.

[15]. Trifkovic M, Sheikhzadeh M, Nigim K, Daoutidis P. Modeling and Control of a Renewable Hybrid Energy System With Hydrogen Storage. IEEE Transactions on Control Systems Technology. 2014;22(1):169-79.

[16]. Diouf B, Pode R. Potential of lithium-ion batteries in renewable energy. Renewable Energy. 2015;76:375-80.

[17]. Berrueta A, Heck M, Jantsch M, Ursúa A, Sanchis P. Combined dynamic programming and region-elimination technique algorithm for optimal sizing and management of lithium-ion batteries for photovoltaic plants. Applied Energy. 2018;228:1-11.

[18.] Chang Y, Mao X, Zhao Y, Feng S, Chen H, Finlow D. Lead-acid battery use in the development of renewable energy systems in China. J POWER SOURCES. 2009;191(1):176-83.

[19]. Zimmerman N. Vanadium redox flow battery sizing of VRB in electrified heavy consturction equipment [Internet]. Mälardalen University; 2014 [cited 2019 Jan 24]. 68 p. Availablefrom:URL:http://www.diva-portal.org/smash/get/diva2:772090/FULLTEXT01.pdf

[20]. Akinyele DO, Rayudu RK. Review of energy storage technologies for sustainable power networks. Sustainable Energy Technologies and Assessments. 2014;8:74-91.

[21]. Weber S, Peters JF, Baumann M, Weil M. Life Cycle Assessment of a Vanadium Redox Flow Battery. Environ Sci Technol. 2018;52(18):10864-73.

[22]. Uhrig M, Koenig S, Suriyah MR, Leibfried T. Lithium-based vs. Vanadium Redox Flow Batteries – A Comparison for Home Storage Systems. ENRGY PROCED. 2016;99:35-43.

[23]. Ipsakis D, Voutetakis S, Seferlis P, Stergiopoulos F, Elmasides C. Power management strategies for a stand-alone power system using renewable energy sources and hydrogen storage. International Journal of Hydrogen Energy. 2009;34(16):7081-95.

[24]. Dash V, Bajpai P. Power management control strategy for a stand-alone solar photovoltaic-fuel cell–battery hybrid system. Sustainable Energy Technologies and Assessments. 2015;9:68-80.

[25]. Cozzolino R, Tribioli L, Bella G. Power management of a hybrid renewable system for artificial islands: A case study. Energy. 2016;106:774-89.

[26]. Shongwe S, Hanif M. Comparative Analysis of Different Single-Diode PV Modeling Methods. IEEE Journal of Photovoltaics. 2015;5(3):938-46.

[27]. Wang C. Modeling and control of hybrid wind/photovoltaic/fuel cell distributed generation systems. Bozeman, Montana: Montana state university; 2006.

[28]. Khan MJ, Iqbal MT. Modelling and Analysis of Electro-chemical, Thermal, and Reactant Flow Dynamics for a PEM Fuel Cell System. Fuel Cells. 2005;5(4):463-75.

[29]. Biaku C, Dale N, Mann M, Salehfar H, Peters A, Han T. A semiempirical study of the temperature dependence of the anode charge transfer coefficient of a 6kW PEM electrolyzer. International Journal of Hydrogen Energy. 2008;33(16):4247-54.

[30]. Tang A, Bao J, Skyllas-Kazacos M. Dynamic modelling of the effects of ion diffusion and side reactions on the capacity loss for vanadium redox flow battery. Journal of Power Sources. 2011;196(24):10737-47.

[31]. Load profile. In: Authority PE, editor. 2014 [Available from: http://peaoc.pea.co.th/loadprofile/].

[32]. Giles DM. Solar Flux: AERONET. 2018 [Available from: https://solrad-net.gsfc.nasa.gov/cgi-bin/type_one_station_flux?site=Silpakorn_Univ&nachal=2&level=1&place_code=10&data_type=flux&shef_code=P.

[33]. Chatrattanawet N, Hakhen T, Kheawhom S, Arpornwichanop A. Control structure design and robust model predictive control for controlling a proton exchange membrane fuel cell. J CLEAN PROD. 2017;148:934-47.

[34]. NIST. Energy Storage & Delivery. [cited 26 Jan 2019];Available from: URL: https://www.nist.gov/programs-projects/energy-storage-delivery.

[35]. Vanadium Redox Flow Battery (VFB). [cited 26 Jan 2019];Available from: URL:http://www.uetechnologies.com/technology.

[36]. Vivas FJ, De las Heras A, Segura F, Andújar JM. A review of energy management strategies for renewable hybrid energy systems with hydrogen backup. Renewable and Sustainable Energy Reviews. 2018;82:126-55.

[37]. Chauhan A, Saini RP. A review on Integrated Renewable Energy System based power generation for stand-alone applications: Configurations, storage options, sizing methodologies and control. Renewable and Sustainable Energy Reviews. 2014;38:99-120.

[38]. Hatti M, Meharrar A, Tioursi M. Power management strategy in the alternative energy photovoltaic/PEM Fuel Cell hybrid system. Renewable and Sustainable Energy Reviews. 2011;15(9):5104-10.

[39]. Uzunoglu M, Onar OC, Alam MS. Modeling, control and simulation of a PV/FC/UC based hybrid power generation system for stand-alone applications. Renewable Energy. 2009;34(3):509-20.

[40]. Dagdougui H, Minciardi R, Ouammi A, Robba M, Sacile R. A Dynamic Decision Model for the Real-Time Control of Hybrid Renewable Energy Production Systems. IEEE Systems Journal. 2010;4(3):323-33.

[41]. Talebian ME, Sobhani S, Borzooi A, editors. New hybrid system of fuel cell power plant and wind turbine for household consumption. 2013 3rd International Conference on Electric Power and Energy Conversion Systems; 2013 2-4 Oct. 2013.

[42]. Das D, Esmaili R, Xu L, Nichols D, editors. An optimal design of a grid connected hybrid wind/photovoltaic/fuel cell system for distributed energy production. 31st Annual Conference of IEEE Industrial Electronics Society, 2005 IECON 2005; 2005 6-10 Nov. 2005.

[43]. Thounthong P, Sikkabut S, Mungporn P, Sethakul P, Pierfederici s, Davat B. Differential flatness based-control of fuel cell/photovoltaic/wind turbine/supercapacitor hybrid power plant2013. 298-305 p.

[44]. Stewart EM, Lutz AE, Schoenung S, Chiesa M, Keller JO, Fletcher J, et al. Modeling, analysis and control system development for the Italian hydrogen house. International Journal of Hydrogen Energy. 2009;34(4):1638-46.

[45]. Moghaddam AA, Seifi A, Niknam T, Alizadeh Pahlavani MR. Multi-objective operation management of a renewable MG (micro-grid) with back-up micro-turbine/fuel cell/battery hybrid power source. Energy. 2011;36(11):6490-507.

[46]. Kato N, Kurozumi K, Susuld N, Muroyama S, editors. Hybrid power-supply system composed of photovoltaic and fuel-cell systems. 2001 Twenty-Third International Telecommunications Energy Conference INTELEC 2001; 2001 18-18 Oct. 2001.

[47]. Samson GT, Undeland TM, Ulleberg O, Vie PJS. Optimal load sharing strategy in a hybrid power system based on PV/Fuel Cell/ Battery/Supercapacitor. 2009 International Conference on Clean Electrical Power2009. p. 141-6.

[48]. Mohammadi M, Nafar M. Fuzzy sliding-mode based control (FSMC) approach of hybrid micro-grid in power distribution systems. International Journal of Electrical Power & Energy Systems. 2013;51:232-42.

[49]. Ramos J, Martín JJ, Belver I, Larrañaga Lesaca JM, Guerrero E, Pérez E. Modelling of Photovoltaic Module. Renewable Energy and Power Quality Journal. 2010;1:1186-90.

[50]. Kumari J, Ch SB. Mathematical Modeling and Simulation of Photovoltaic Cell using Matlab-Simulink Environment. International Journal of Electrical and Computer Engineering. 2012;2:26-34.

[51]. Walker G. Evaluating MPPT converter topologies using a matlab PV model. Journal of Electrical and Electronics Engineering, Australia. 2001;21(1):49-55.

[52]. Weidong X, Dunford WG, Capel A, editors. A novel modeling method for photovoltaic cells. 2004 IEEE 35th Annual Power Electronics Specialists Conference (IEEE Cat No04CH37551); 2004 20-25 June 2004.

[53]. Ulapane N, Dhanapala C, Wickramasinghe S, Abeyratne S, Ratnayake KRMN, Binduhewa P. Extraction of parameters for simulating photovoltaic panels2011. 539-44 p.

[54]. Bellini A, Bifaretti S, Iacovone V, Cornaro C. Simplified model of a photovoltaic module2009. 47-51 p.

[55]. Hadj Arab A, Chenlo F, Benghanem M. Loss-of-load probability of photovoltaic water pumping systems. Solar Energy. 2004;76(6):713-23.

[56]. de Blas MA, Torres JL, Prieto E, García A. Selecting a suitable model for characterizing photovoltaic devices. Renewable Energy. 2002;25(3):371-80.

[57]. Lineykin S, Averbukh M, Kuperman A. An improved approach to extract the single-diode equivalent circuit parameters of a photovoltaic cell/panel. Renewable and Sustainable Energy Reviews. 2014;30:282-9.

[58]. Zhang Y, Gao S, Gu T. Prediction of I-V characteristics for a PV panel by combining single diode model and explicit analytical model. Solar Energy. 2017;144:349-55.

[59]. Standaert F, Hemmes K, Woudstra N. Analytical fuel cell modeling. J POWER SOURCES. 1996;63(2):221-34.

[60]. Standaert F, Hemmes K, Woudstra N. Analytical fuel cell modeling; non-isothermal fuel cells. J POWER SOURCES. 1998;70(2):181-99.

[61]. Amphlett J, Mann RF, Peppley B, Roberge P, Rodrigues A. A model predicting transient response of proton exchange membrane fuel cells1996. 183-8 p.

[62]. Maggio G, Recupero V, Pino L. Modeling polymer electrolyte fuel cells: an innovative approach. Journal of Power Sources. 2001;101(2):275-86.

[63]. Gurau V, Liu H, Kakaç S. Two-Dimensional Model for Proton Exchange Membrane Fuel Cells. AIChE Journal. 1998;44:2410-22.

[64]. Awasthi A, Scott K, Basu S. Dynamic modeling and simulation of a proton exchange membrane electrolyzer for hydrogen production. International Journal of Hydrogen Energy. 2011;36(22):14779-86.

[65]. Dale NV, Mann MD, Salehfar H. Semiempirical model based on thermodynamic principles for determining 6kW proton exchange membrane electrolyzer stack characteristics. J POWER SOURCES. 2008;185(2):1348-53.

[66]. García-Valverde R, Espinosa N, Urbina A. Simple PEM water electrolyser model and experimental validation. International Journal of Hydrogen Energy. 2012;37(2):1927-38.

[67]. Marangio F, Santarelli M, Calì M. Theoretical model and experimental analysis of a high pressure PEM water electrolyser for hydrogen production. International Journal of Hydrogen Energy. 2009;34(3):1143-58.

[68]. Carmo M, Fritz DL, Mergel J, Stolten D. A comprehensive review on PEM water electrolysis. International Journal of Hydrogen Energy. 2013;38(12):4901-34.

[69]. Bass M, Freger V. Hydration of Nafion and Dowex in liquid and vapor environment: Schroeder's paradox and microstructure. Polymer. 2008;49:497-506.

[70]. Onishi L, Prausnitz J, Newman J. Water−Nafion Equilibria. Absence of Schroeder's Paradox. The journal of physical chemistry B. 2007;111:10166-73.

[71]. Choi P, Bessarabov DG, Datta R. A simple model for solid polymer electrolyte (SPE) water electrolysis. Solid State Ionics. 2004;175(1):535-9.

[72]. You D, Zhang H, Chen J. A simple model for the vanadium redox battery. Electrochimica Acta. 2009;54(27):6827-36.

[73]. Al-Fetlawi H, Shah AA, Walsh FC. Non-isothermal modelling of the all-vanadium redox flow battery. Electrochimica Acta. 2009;55(1):78-89.

[74]. Ma X, Zhang H, Xing F. A three-dimensional model for negative half cell of the vanadium redox flow battery. Electrochimica Acta. 2011;58:238-46.

[75]. Bhattacharjee A, Saha H. Design and experimental validation of a generalised electrical equivalent model of Vanadium Redox Flow Battery for interfacing with renewable energy sources. Journal of Energy Storage. 2017;13:220-32.

[76]. Husain MA, Tariq A, Hameed S, Arif MSB, Jain A. Comparative assessment of maximum power point tracking procedures for photovoltaic systems. Green Energy & Environment. 2017;2(1):5-17.

[77]. Faisal M, Husain M, Tabish M, Beg S, Tariq A. MATLAB Based Modeling of PV Array and its Study for Different Conditions2012.

[78]. Ahmed NA, editor On-grid hybrid wind/photovoltaic/fuel cell energy system. 2012 10th International Power & Energy Conference (IPEC); 2012 12-14 Dec. 2012.

[79]. Ahmed J, Salam Z. An improved perturb and observe (P&O) maximum power point tracking (MPPT) algorithm for higher efficiency. Applied Energy. 2015;150:97-108.

[80]. Scarpa VVR, Buso S, Spiazzi G. Low-Complexity MPPT Technique Exploiting the PV Module MPP Locus Characterization. IEEE Transactions on Industrial Electronics. 2009;56(5):1531-8.

[81]. Lin R, Cui X, Shan J, Técher L, Xiong F, Zhang Q. Investigating the effect of start-up and shut-down cycles on the performance of the proton exchange membrane fuel cell by segmented cell technology. International Journal of Hydrogen Energy. 2015;40(43):14952-62.

[82]. Haruni AMO, Negnevitsky M, Haque ME, Gargoom A. A Novel Operation and Control Strategy for a Standalone Hybrid Renewable Power System. IEEE Transactions on Sustainable Energy. 2013;4(2):402-13.

[83]. Bizon N, Oproescu M, Raceanu M. Efficient energy control strategies for a Standalone Renewable/Fuel Cell Hybrid Power Source. Energy Conversion and Management. 2015;90:93-110.

[84]. Rashid M, Al Mesfer M, Naseem H, Danish M. Hydrogen Production by Water Electrolysis: A Review of Alkaline Water Electrolysis, PEM Water Electrolysis and High Temperature Water Electrolysis. International Journal of Engineering and Advanced Technology. 2015;ISSN:2249-8958.

[85]. Zeng K, Zhang D. Recent progress in alkaline water electrolysis for hydrogen production and applications. Progress in Energy and Combustion Science. 2010;36(3):307-26.

[86]. Ulleberg Ø. The importance of control strategies in PV–hydrogen systems. Solar Energy. 2004;76(1):323-9.

[87]. Dufo-López R, Lujano-Rojas JM, Bernal-Agustín JL. Comparison of different lead–acid battery lifetime prediction models for use in simulation of stand-alone photovoltaic systems. Applied Energy. 2014;115:242-53.

[88]. Crossland AF, Anuta OH, Wade NS. A socio-technical approach to increasing the battery lifetime of off-grid photovoltaic systems applied to a case study in Rwanda. Renewable Energy. 2015;83:30-40.

[89]. Horkos PG, Yammine E, Karami N, editors. Review on different charging techniques of lead-acid batteries. 2015 Third International Conference on Technological Advances in Electrical, Electronics and Computer Engineering (TAEECE); 2015 29 April-1 May 2015.

[90]. Jirabovornwisut T. Analysis and design of vanadium redox flow battery: Chulalongkorn University; 2018.

[91]. Xiaofeng S, Zhizhen L, Baocheng W, Xin L, editors. A Hybrid renewable DC microgrid voltage control. 2009 IEEE 6th International Power Electronics and Motion Control Conference; 2009 17-20 May 2009.

[92]. Zhou K, Ferreira JA, de Haan SWH. Optimal energy management strategy and system sizing method for stand-alone photovoltaic-hydrogen systems. International Journal of Hydrogen Energy. 2008;33(2):477-89.

[93]. Tesfahunegn SG, Ulleberg Ø, Vie PJS, Undeland TM. Optimal shifting of Photovoltaic and load fluctuations from fuel cell and electrolyzer to lead acid battery in a Photovoltaic/hydrogen standalone power system for improved performance and life time. J POWER SOURCES. 2011;196(23):10401-14.

[94]. Carapellucci R, Giordano L. Modeling and optimization of an energy generation island based on renewable technologies and hydrogen storage systems. International Journal of Hydrogen Energy. 2012;37(3):2081-93.

[95]. Ziogou C, Ipsakis D, Elmasides C, Stergiopoulos F, Papadopoulou S, Seferlis P, et al. Automation infrastructure and operation control strategy in a stand-alone power system based on renewable energy sources. J POWER SOURCES. 2011;196(22):9488-99.

[96]. Giannakoudis G, Papadopoulos AI, Seferlis P, Voutetakis S. Optimum design and operation under uncertainty of power systems using renewable energy sources and hydrogen storage. International Journal of Hydrogen Energy. 2010;35(3):872-91.

[97]. Brka A, Kothapalli G, Al-Abdeli YM. Predictive power management strategies for stand-alone hydrogen systems: Lab-scale validation. International Journal of Hydrogen Energy. 2015;40(32):9907-16.

[98]. Miland H, Ulleberg Ø. Testing of a small-scale stand-alone power system based on solar energy and hydrogen. Solar Energy. 2012;86(1):666-80.

[99]. García-Triviño P, Fernández-Ramírez LM, Gil-Mena AJ, Llorens-Iborra F, García-Vázquez CA, Jurado F. Optimized operation combining costs, efficiency and lifetime of a hybrid renewable energy system with energy storage by battery and hydrogen in grid-connected applications. International Journal of Hydrogen Energy. 2016;41(48):23132-44.

[100]. García-Triviño P, Llorens-Iborra F, García-Vázquez CA, Gil-Mena AJ, Fernández-Ramírez LM, Jurado F. Long-term optimization based on PSO of a grid-connected renewable energy/battery/hydrogen hybrid system. International Journal of Hydrogen Energy. 2014;39(21):10805-16.

[101]. Gorgun H. Dynamic modelling of a proton exchange membrane (PEM) electrolyzer. International Journal of Hydrogen Energy. 2006;31(1):29-38.

[102]. A. Duffie J, Beckman WA. Solar Engineering of Thermal Processes Second Edition1980. 16591 p.

[103]. Mueller F, Brouwer J, Kang S, Kim H-S, Min K. Quasi-three dimensional dynamic model of a proton exchange membrane fuel cell for system and controls development. J POWER SOURCES. 2007;163(2):814-29.

[104]. Aouali FZ, Becherif M, Tabanjat A, Emziane M, Mohammedi K, Krehi S, et al. Modelling and Experimental Analysis of a PEM Electrolyser Powered by a Solar Photovoltaic Panel. ENRGY PROCED. 2014;62:714-22.

[105]. Yang WW, He YL, Li YS. Performance Modeling of a Vanadium Redox Flow Battery during Discharging. Electrochimica Acta. 2015;155:279-87.

[106]. Ngamsai K, Arpornwichanop A. Analysis and measurement of the electrolyte imbalance in a vanadium redox flow battery. J POWER SOURCES. 2015;282:534-43.

[107]. Blaifi S, Moulahoum S, Colak I, Merrouche W. Monitoring and enhanced dynamic modeling of battery by genetic algorithm using LabVIEW applied in photovoltaic system. Electrical Engineering. 2017;100(2):1021-38.

[108]. Wang C, Nehrir MH. Power Management of a Stand-Alone Wind/Photovoltaic/Fuel Cell Energy System. IEEE Transactions on Energy Conversion. 2008;23(3):957-67.

จุฬาลงกรณ์มหาวิทยาลัย

CHULALONGKORN UNIVERSITY

APPENDIX A
MATHEMATICAL CALCULATION

A.1 Power over a period of time

The calculations in this section begin with the sum of the total energy throughout the simulation period. For example, the sum of the power used to charge the vanadium redox flow battery of EMS 1 in the summer scenario is 2,699,922.712 watt. The power consumed will be averaged over all simulated time (4320 minutes).

$$\text{Average power} = \frac{2699922.712}{4320} = 624.9821 \frac{\text{W}}{\text{min}}$$

In fact, the measured power is in watts per hour, so it is assumed that the average energy calculated is the power consumed per hour.

$$\text{Average power} = 624.9821 \text{W}$$

The total energy consumed can be calculated from the product of the average power of the total simulation time (72 hours).

$$\text{Total energy consumed} = \frac{624.9821 \times 72}{1000} = 44.9987 \text{kWh}$$

A.2 Hydrogen production and consumption

The amount of hydrogen used in the PEMFC or the amount of hydrogen produced from PEMEC is given by Faraday's law, which can be expressed as Eq. A.1 and Eq. A.2 respectively.

$$mol_{H_{2\_PEMFC}} = \frac{n_c I_{PEMFC}}{V_e F} \tag{A.1}$$

$$mol_{H_{2\_PEMEC}} = \eta_F \frac{n_c I_{PEMEC}}{V_e F} \tag{A.2}$$

where $mol_{H_{2\_PEMFC}}$ and $mol_{H_{2\_PEMEC}}$ (mol s^{-1}) are total molar flowrate throughout the simulation period. n_c is a number of cells in the stack. η_F is the Faraday's efficiency which means the ratio between the actual and theoretical amount of hydrogen produced. It is usually around 80-100%. In this work, it is set the value to 80%.

From Eq. A.1 and A.2, it can be able to calculate the moles of the hydrogen used throughout the simulation period. For example, the total mole consumption from PEMEC of EMS 1 in summer scenario equal to 285.91 moles. The amount of moles production or consumption is measured in terms of volume for use in the design of storage tanks, which can be calculated by ideal gas laws Eq. (A.3).

$$V = \frac{nRT}{P} \tag{A.3}$$

$$= \frac{285.91 \times 8.314 \times 273.15}{101300} \; mol \times \frac{m^3 \times Pa}{mol \times K} \times K \times \frac{1}{Pa}$$

$$= 6.41 \; m^3$$

APPENDIX B

SIMULATION DATA

B.1 Simulation results compare the use between lead-acid battery and vanadium redox flow battery

The simulation results compare the behavior of each subsystem of the energy management system using lead-acid and vanadium redox flow batteries at the same condition are shown in Fig. B.1-B.6 and Power data for the operation of the comparison energy management system between using lead-acid and vanadium redox flow battery is shown in Table. B.1 respectively
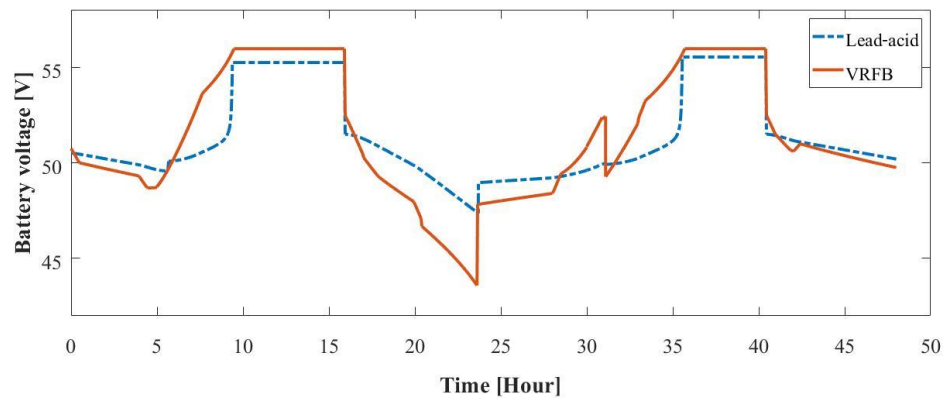
Fig. B.1 Battery voltage comparison between lead-acid and VRFB
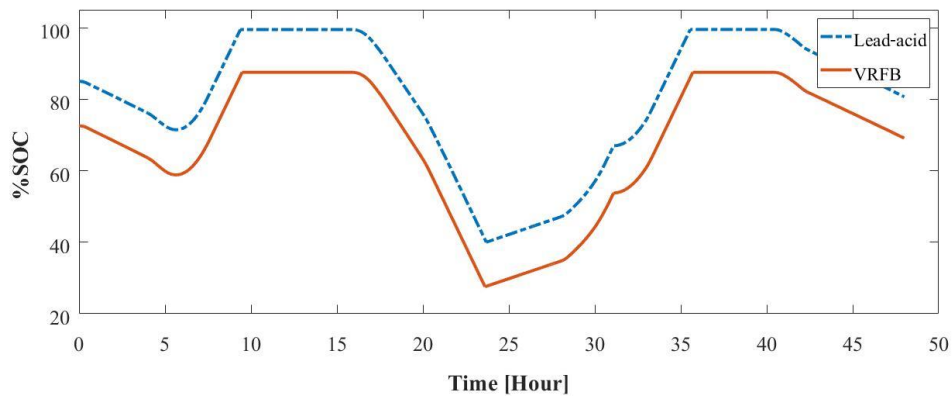
Fig. B.2 Battery current comparison between lead-acid and VRFB
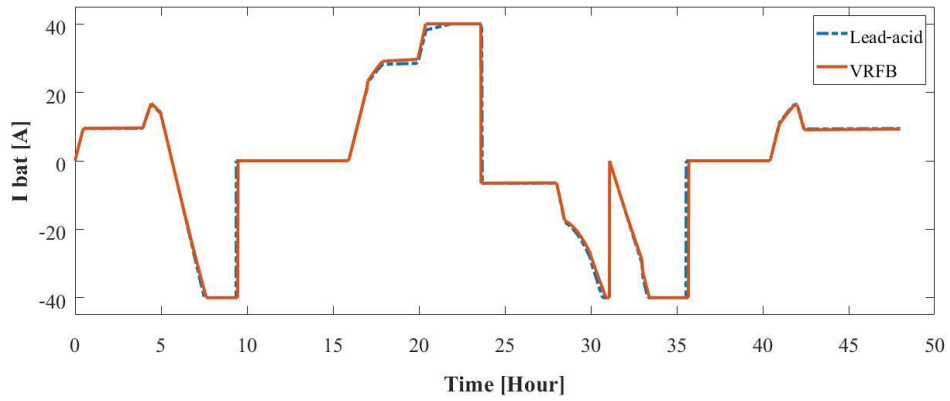
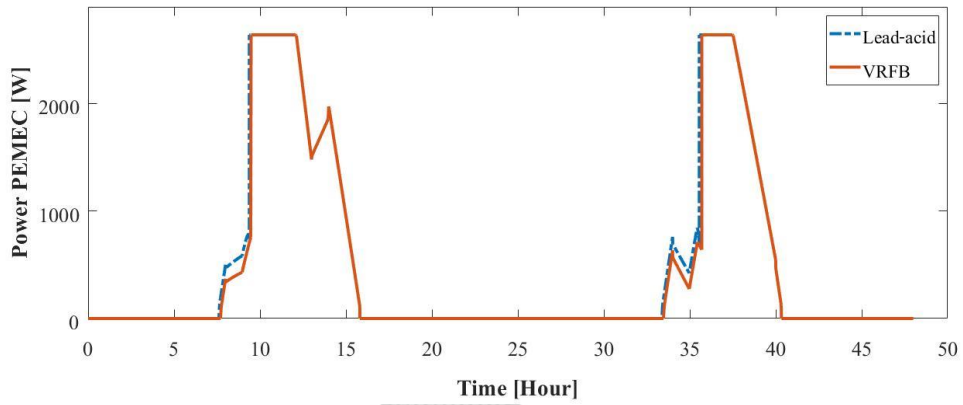Fig. B.3 Battery SOC comparison between lead-acid and VRFB

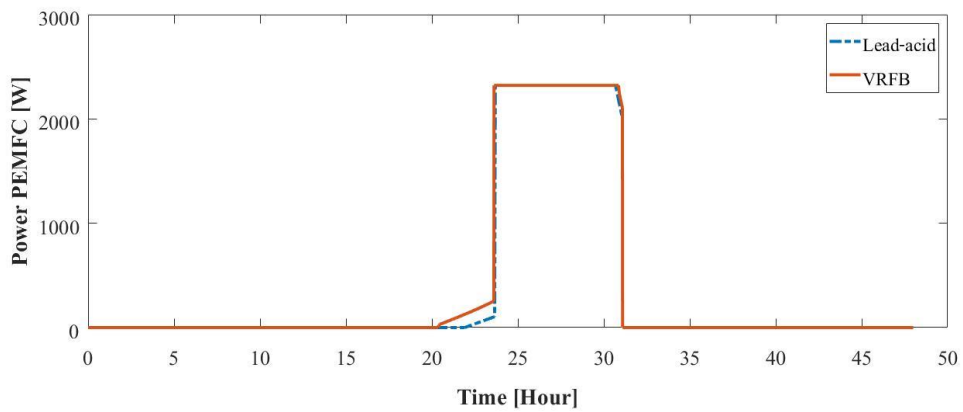Fig. B.4 Power consumed from PEMEC comparison between lead-acid and VRFB

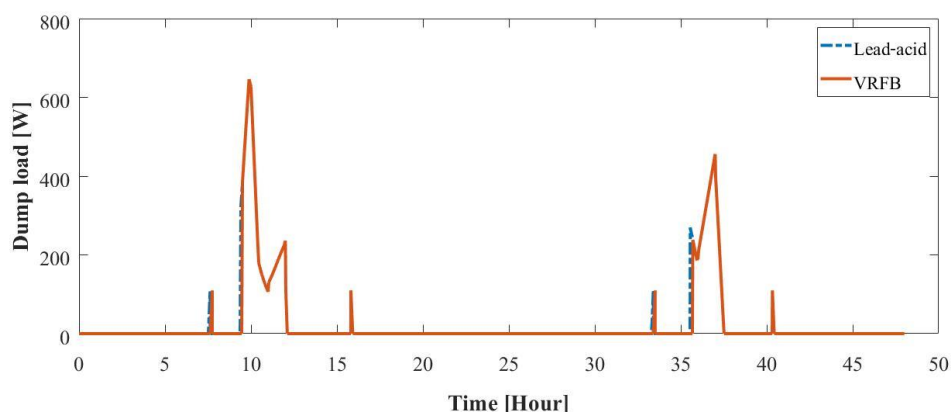Fig. B.5 Power produced from PEMFC comparison between lead-acid and VRFB

Fig. B.6 Dump load comparison between lead-acid and VRFB

Table B.1 Power data for the operation of the comparison energy management system between using lead-acid and vanadium redox flow battery

	Lead-acid system	VRFB system
Battery		
Total charge time (hrs.)	15.61	15.93
Total battery charge power (kWh)	17.64	18.65
Total discharge time (hrs.)	20.98	20.91
Total battery discharge power (kWh)	18.29	17.70
Percentage of operating time	76.22%	76.74%
PEMEC		
Total power (kWh)	23.99	22.96
H_2 production (m^3)	3.58	3.4
PEMFC		
Total power (kWh)	17.22	17.76
H_2 consumption (m^3)	2.86	2.93
Dump load		
Total power (kWh)	1.31	1.24

B.2 Simulation result in summer scenario

The simulation results compare the behavior of each subsystem of the energy management system with EMS 1 and EMS 2 in the summer scenario are shown in Fig. B.7-B.12.
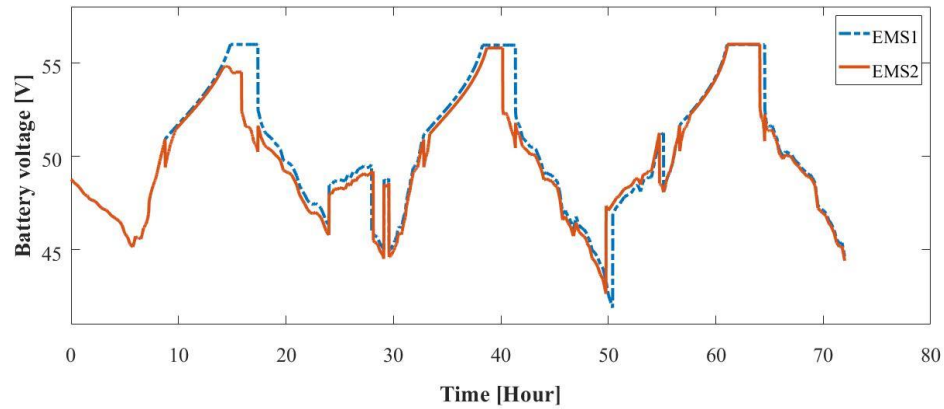

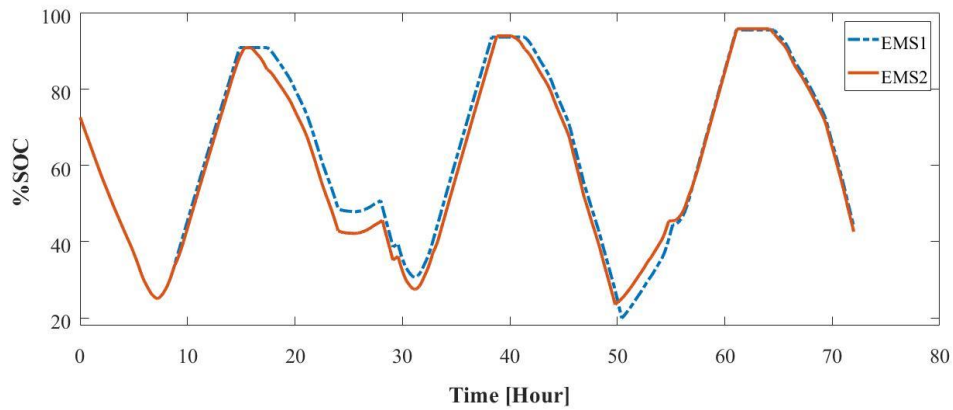Fig. B.7 Battery voltage comparison between EMS 1 and EMS 2 in summer scenario

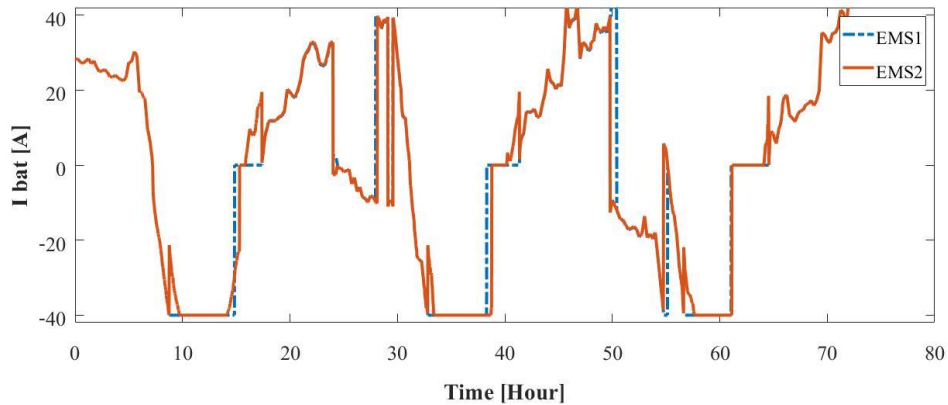Fig. B.8 Battery SOC comparison between EMS 1 and EMS 2 in summer scenario

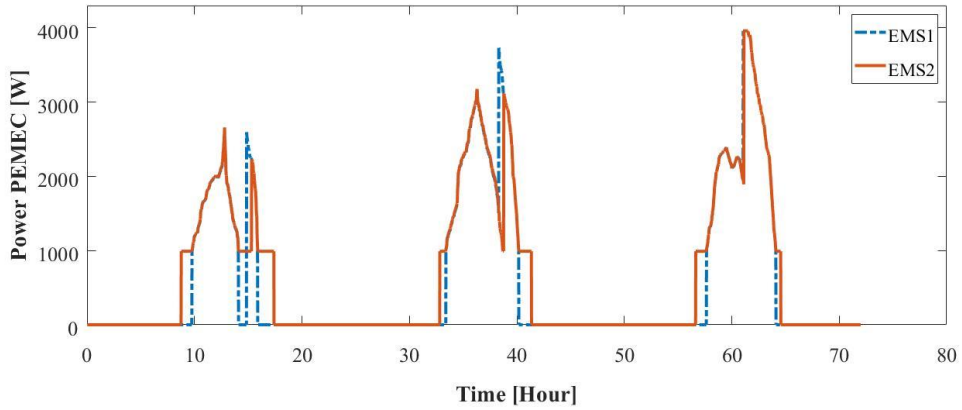Fig. B.9 Battery current comparison between EMS 1 and EMS 2 in summer scenario

Fig. B.10 Power consumed from PEMEC comparison between EMS 1 and EMS 2 in summer scenario
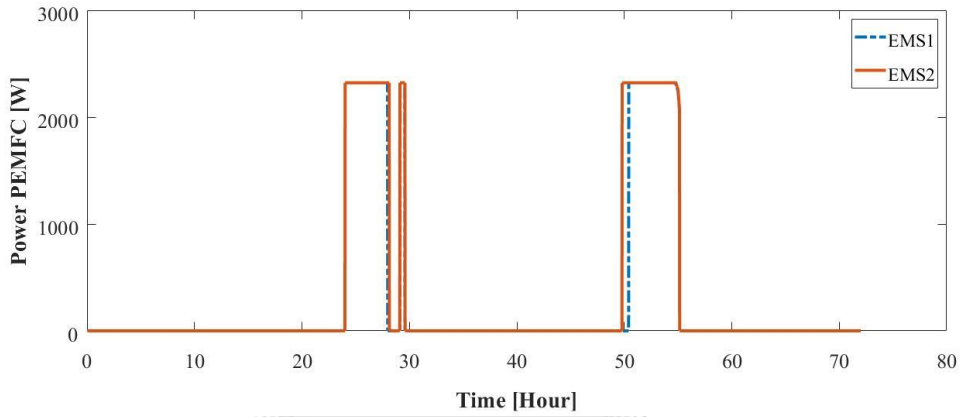

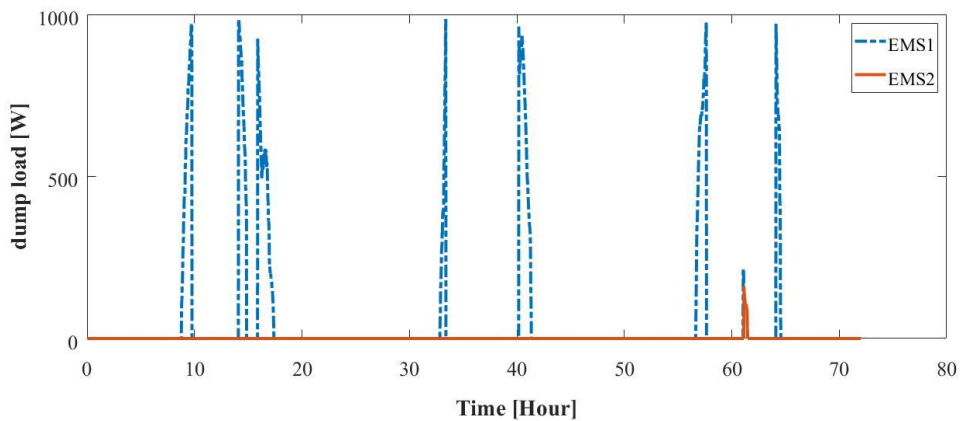Fig. B.11 Power produced from PEMFC comparison between EMS 1 and EMS 2 in summer scenario

Fig. B.12 Dump load comparison between EMS 1 and EMS 2 in summer scenario

B.3 Simulation results in winter scenario

The simulation results compare the behavior of each subsystem of the energy management system with EMS 1 and EMS 2 in the winter scenario are shown in Fig. B.13-B.18.
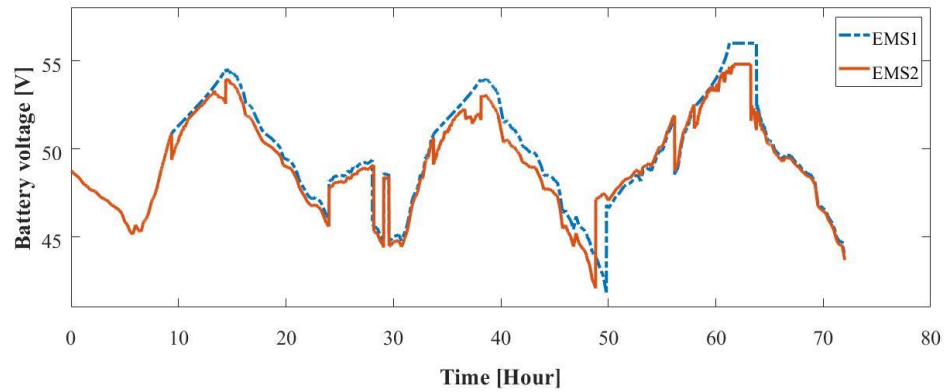

Fig. B.13 Battery voltage comparison between EMS 1 and EMS 2 in winter scenario

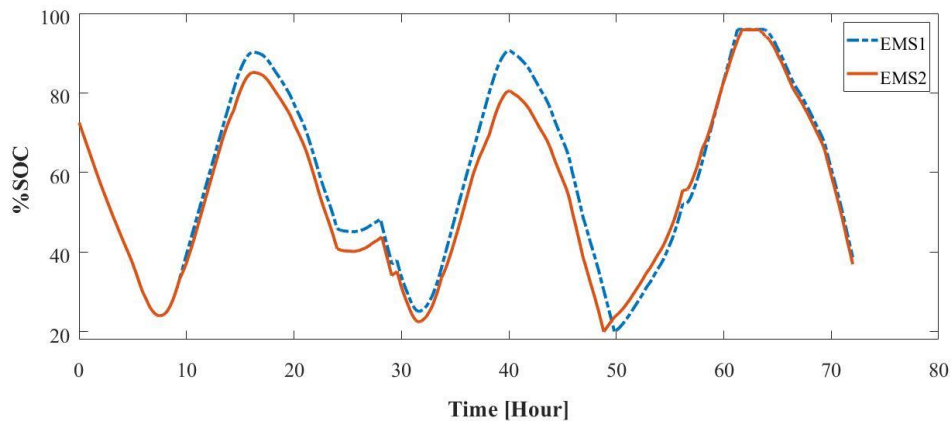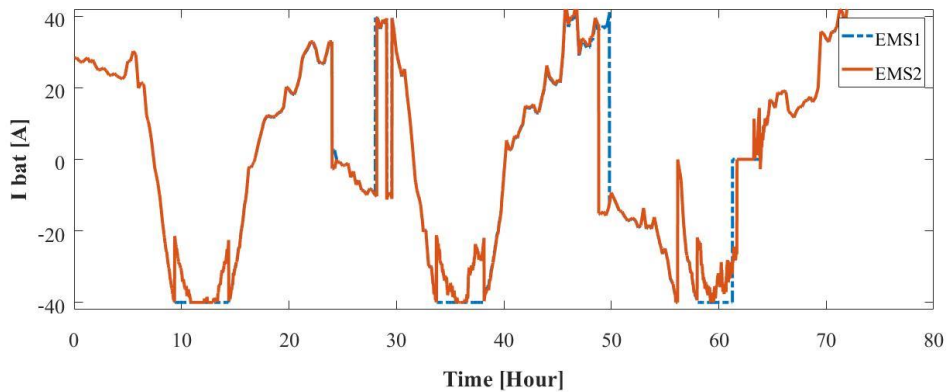Fig. B.14 Battery SOC comparison between EMS 1 and EMS 2 in winter scenario

Fig. B.15 Battery current comparison between EMS 1 and EMS 2 in winter scenario
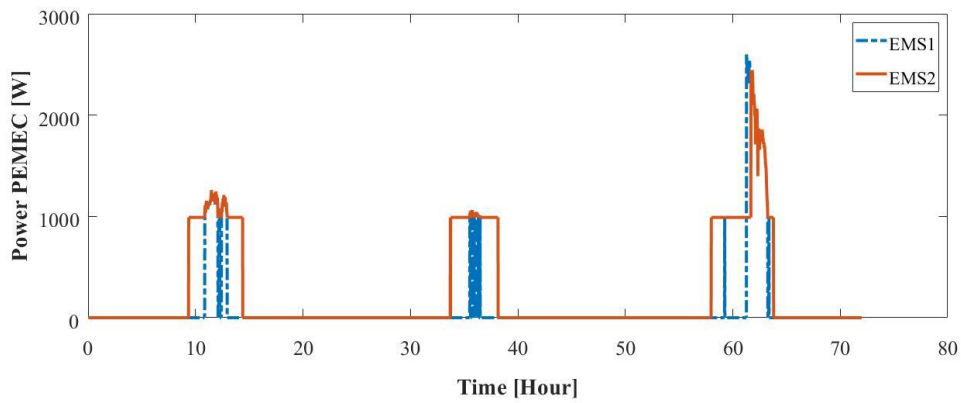
Fig. B.16 Power consumed from PEMEC comparison between EMS 1 and EMS 2 in winter scenario
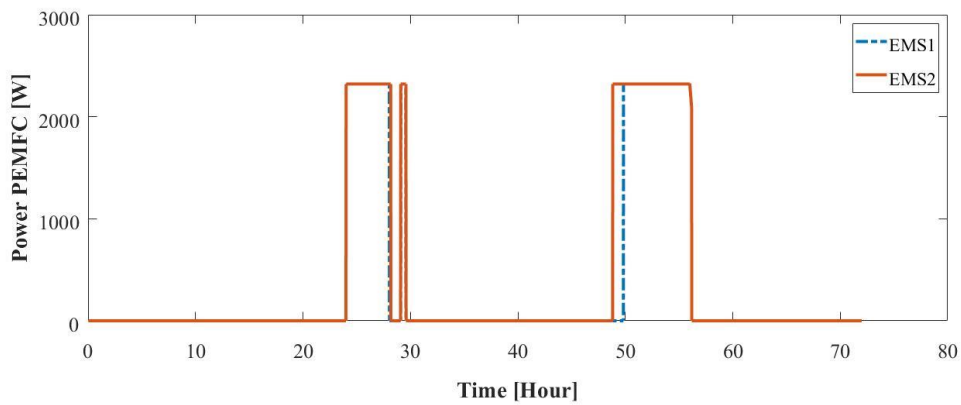
Fig. B.17 Power produced from PEMFC comparison between EMS 1 and EMS 2 in winter scenario
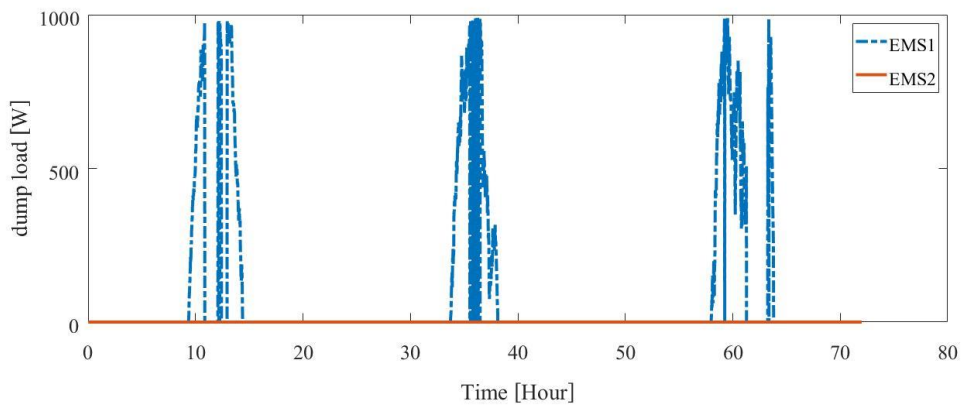
Fig. B.18 Dump load comparison between EMS 1 and EMS 2 in winter scenario

B.4 Simulation results in arbitrarily varying weather scenario

The simulation results compare the behavior of each subsystem of the energy management system with EMS 1 and EMS 2 in the summer scenario are shown in Fig. B.19-B.24.
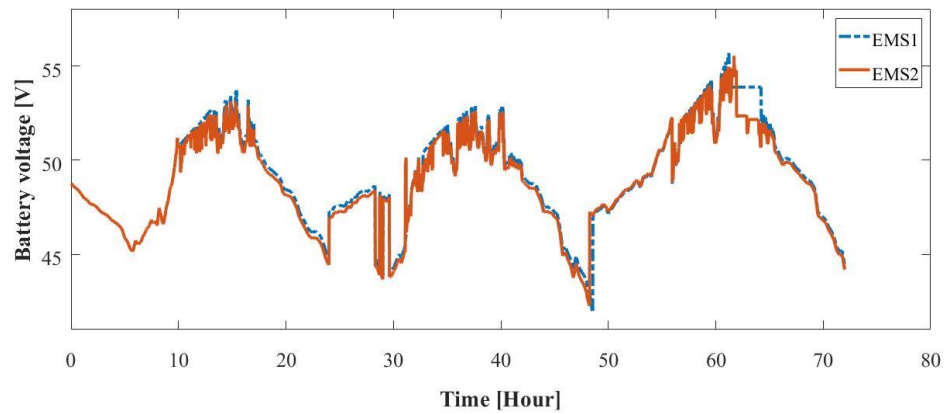
Fig. B.19 Battery voltage comparison between EMS 1 and EMS 2 in arbitrarily varying weather scenario
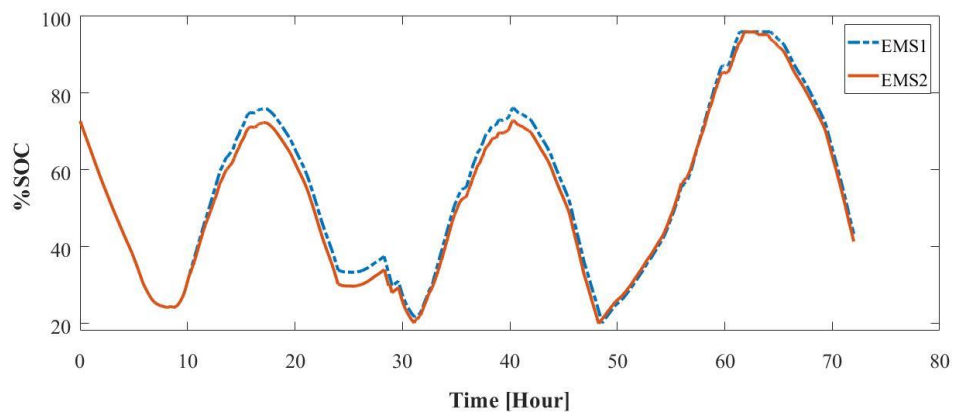
Fig. B.20 Battery SOC comparison between EMS 1 and EMS 2 in arbitrarily varying weather scenario

Fig. B.21 Battery current comparison between EMS 1 and EMS 2 in arbitrarily varying weather scenario
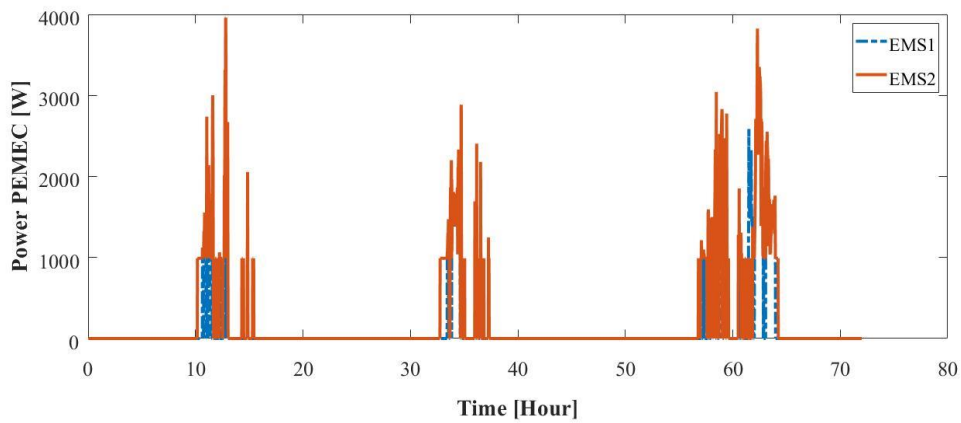
Fig. B.22 Power consumed from PEMEC comparison between EMS 1 and EMS 2 in arbitrarily varying weather scenario
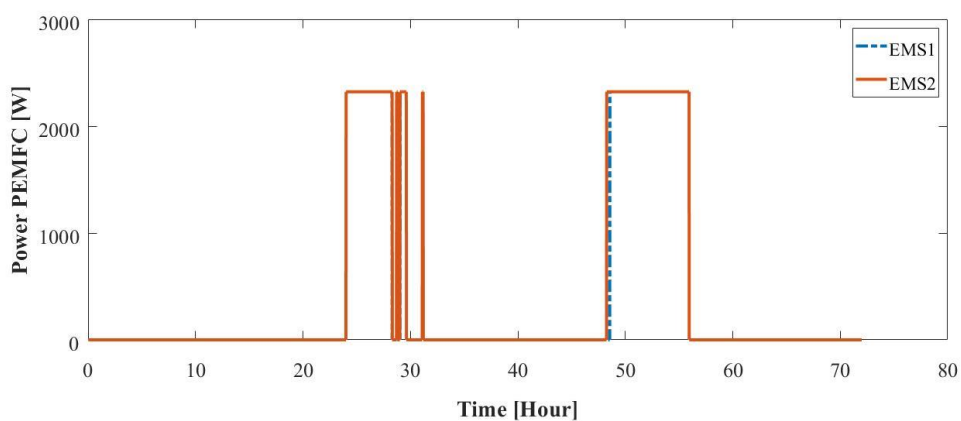
Fig. B.23 Power produced from PEMFC comparison between EMS 1 and EMS 2 in arbitrarily varying weather scenario

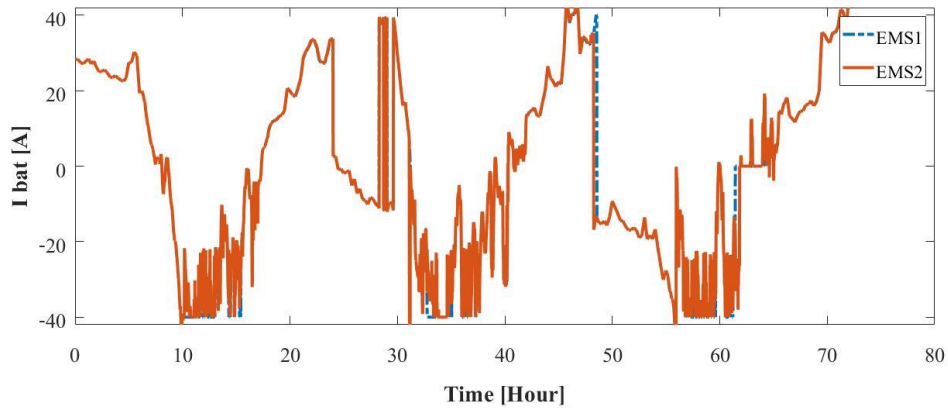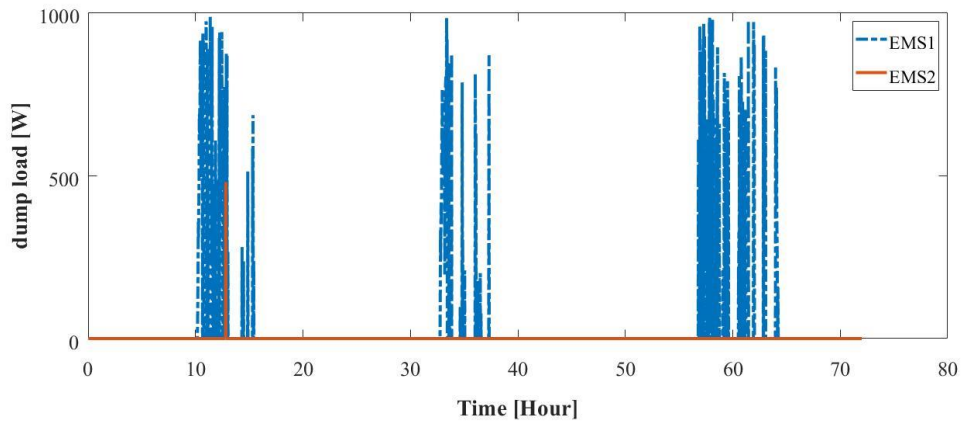Fig. B.24 Dump load comparison between EMS 1 and EMS 2 in arbitrarily varying weather scenario

B.5 Solar irradiance data

B.5.1 Summer scenario

Table B.2 Solar irradiance data in summer scenario

Time (Hr.)	Irradiance (Wm^{-2})	Time (Hr.)	Irradiance (Wm^{-2})	Time (Hr.)	Irradiance (Wm^{-2})
1	0	25	0	49	0
2	0	26	0	50	0
3	0	27	0	51	0
4	0	28	0	52	0
5	0	29	0	53	0
6	7.88	30	15.76	54	28.65
7	93.84	31	189.11	55	229.94
8	371.78	32	388.25	56	446.28
9	585.96	33	585.96	57	661.89
10	746.42	34	800.14	58	834.53
11	854.58	35	990.69	59	983.52
12	929.80	36	1105.30	60	1021.49
13	919.05	37	1038.68	61	996.42
14	792.98	38	917.62	62	851.00
15	609.60	39	690.54	63	671.92
16	310.17	40	464.90	64	469.20
17	151.86	41	235.67	65	138.97
18	12.18	42	5.73	66	13.61
19	0	43	0	67	0
20	0	44	0	68	0
21	0	45	0	69	0
22	0	46	0	70	0
23	0	47	0	71	0
24	0	48	0	72	0

B.5.2 Winter scenario

Table B.3 Solar irradiance data in winter scenario

Time (Hr.)	Irradiance (Wm^{-2})	Time (Hr.)	Irradiance (Wm^{-2})	Time (Hr.)	Irradiance (Wm^{-2})
1	0	25	0	49	0
2	0	26	0	50	0
3	0	27	0	51	0
4	0	28	0	52	0
5	0	29	0	53	0
6	0	30	0	54	0
7	58.74	31	53.72	55	47.99
8	251.43	32	231.38	56	209.17
9	446.99	33	416.190	57	391.83
10	614.61	34	560.89	58	577.36
11	742.84	35	694.13	59	702.01
12	751.43	36	728.51	60	724.93
13	717.05	37	616.76	61	706.30
14	624.64	38	568.77	62	580.95
15	456.30	39	406.88	63	459.88
16	261.46	40	225.64	64	189.83
17	75.93	41	63.75	65	53.01
18	0	42	0	66	0
19	0	43	0	67	0
20	0	44	0	68	0
21	0	45	0	69	0
22	0	46	0	70	0
23	0	47	0	71	0
24	0	48	0	72	0

B.5.3 arbitrarily varying weather scenario

Table B.4 Solar irradiance data in arbitrarily varying weather scenario

Time (Hr.)	Irradiance (Wm^{-2})	Time (Hr.)	Irradiance (Wm^{-2})	Time (Hr.)	Irradiance (Wm^{-2})
1	0	25	0	49	0
2	0	26	0	50	0
3	0	27	0	51	0
4	0	28	0	52	0
5	0	29	0	53	0
6	8.60	30	14.33	54	10.75
7	81.66	31	133.95	55	83.09
8	112.46	32	465.62	56	297.99
9	207.74	33	647.56	57	570.20
10	500	34	859.60	58	684.10
11	707.74	35	358.88	59	1090.97
12	515.76	36	858.88	60	167.62
13	1053.72	37	326.65	61	442.69
14	319.48	38	276.50	62	340.26
15	350.29	39	172.64	63	251.43
16	152.58	40	470.63	64	347.42
17	165.47	41	126.79	65	204.87
18	45.13	42	23.64	66	33.67
19	0	43	0	67	0
20	0	44	0	68	0
21	0	45	0	69	0
22	0	46	0	70	0
23	0	47	0	71	0
24	0	48	0	72	0

B.6 Load profile

Table B.5 Load profile

Time (Hr.)	Power (W)	Time (Hr.)	Power (W)	Time (Hr.)	Power (W)
1	1336.51	25	2231.46	49	1574.95
2	1245.62	26	2155.37	50	1871.68
3	1168.99	27	1871.68	51	1603.21
4	1087.47	28	1818.42	52	1507.56
5	1257.84	29	1705.38	53	1644.52
6	907.31	30	1345.61	54	1508.65
7	652.15	31	1006.49	55	1213.01
8	608.95	32	564.11	56	1171.70
9	396.59	33	471.72	57	473.90
10	368.87	34	415.21	58	653.24
11	399.04	35	508.68	59	402.16
12	429.20	36	427.16	60	747.80
13	422.09	37	397.81	61	694.54
14	482.59	38	365.21	62	660.31
15	530.42	39	373.90	63	542.92
16	615.56	40	771.72	64	1023.88
17	411.94	41	569.55	65	999.43
18	619.55	42	735.85	66	950.52
19	651.07	43	648.89	67	578.79
20	962.29	44	1252.14	68	795.63
21	1109.39	45	1053.23	69	833.13
22	1545.97	46	1720.60	70	1568.43
23	1254.67	47	1324.96	71	1690.72
24	1499.59	48	1415.178	72	1941.79

VITA

NAME	Chacrit Lerdwithayaprasit
DATE OF BIRTH	23 July 1995
PLACE OF BIRTH	Bangkok
INSTITUTIONS ATTENDED	Bachelor Degree of Chemical Engineering from Faculty of Engineering, Mahidol University, Thailand in 2017 Master Study in the major in Chemical Engineering at Chulalongkorn University, Thailand in August 2017.
HOME ADDRESS	14 Soi Bangwaek 69, Bangwaek, Phasi Charoen, Bangkok 10160.
PUBLICATION	Pure and Applied Chemistry International Conference 2019:Power Management of Hybrid Renewable Energy System for Stand-Alone Applications

จุฬาลงกรณ์มหาวิทยาลัย
CHULALONGKORN UNIVERSITY